ACTIVITY REPORT OF THE PROFESSIONAL GROUP OF THE TERNARY AND MULTINARY COMPOUNDS, JAPAN SOCIETY OF APPLIED PHYSICS

1990

Proc. 8th Int. Conf. Ternary and Multinary Compounds,
(ICTMC-8, Kishinev, Moldova 1990) p. 17
P.93

TERNARY AND MULTINARY COMPOUNDS

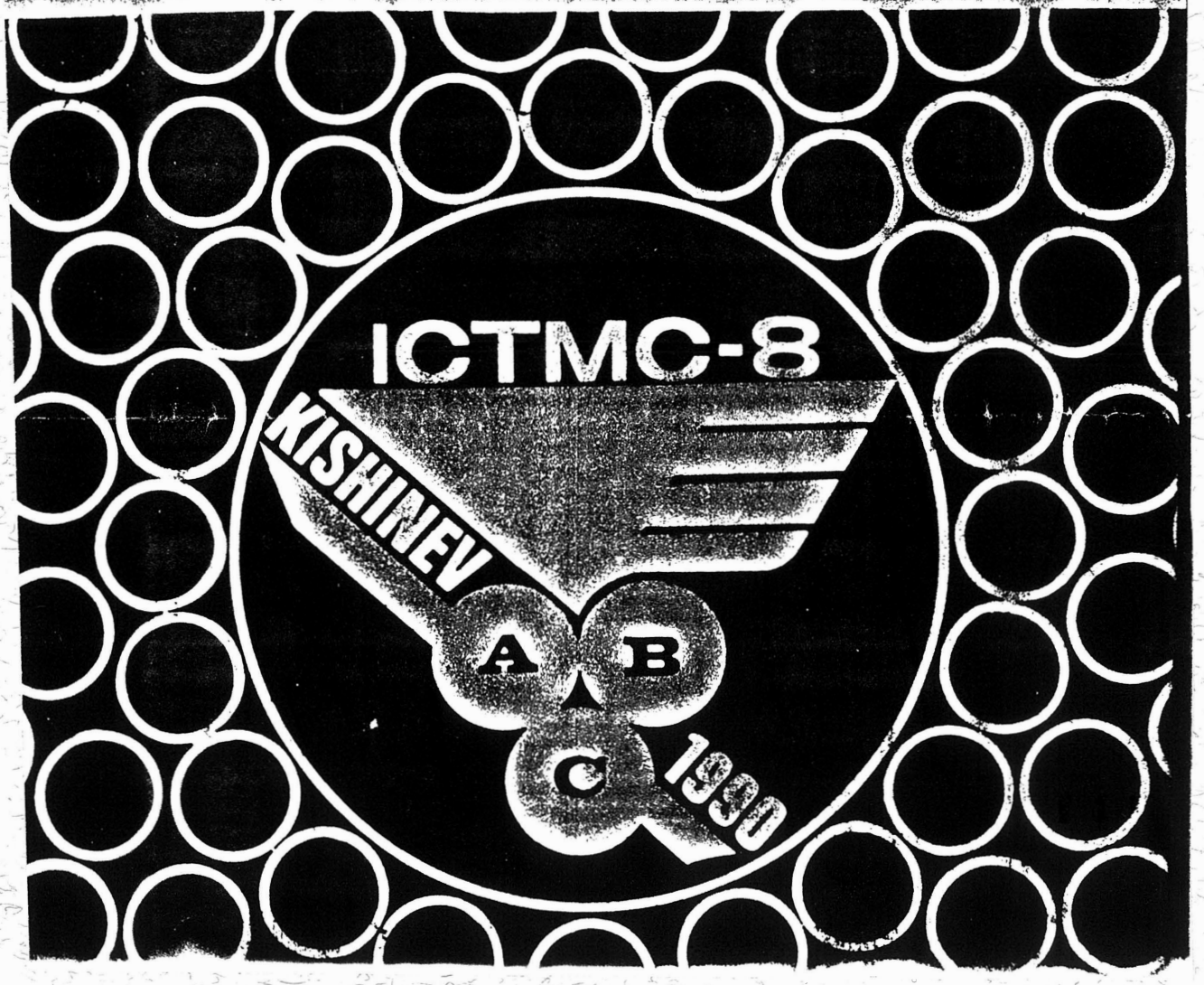

Contents

Vol-1

Crystal Growth

Crystal Growth and Characterization of $AgGaS_2$
K.Masumoto and K.Mochizuki 1 93-100

Solution Growth of Bulk $CuGaS_2$ Crystals
H.Miyake and K.Sugiyama 9 117-120

Stoichiometric Control for $CuInSe_2$ Bulk single Crystals
S.Nomura, M.Sugiyama and T.Takizawa 13 113-116

(C) Growth of $CuGaS_2$ by Travelling Heater Method
N.Yamamoto, Y.Kimura and H.Horinaka 17 244 184-187

Electrical and Optical Characterization of I-III-VI_2 Crystals

Anomalous Temperature Dependence of the Electrical Resistivity of $CuGa(S_{1-x}Se_x)_2$ System
S.Endo, H.Matsushita, H.Nakanishi, T.Irie and S.Nomura 21 125-128

Photoluminescence and Raman Spectra of $CuInSe_2$ Single Crystals
H.Nakanishi, T.Maeda, S.Ando, S.Endo, T.Irie, H.Tanino and T.Yao 25 152-155

Behavior of Amphoteric Impurities of Zn and Cd in $CuGaS_2$ Crystals
A.Ooe, N.Tsuboi, H.Kinto, S.Iida and H.Furusaki ...29 160-163

Optical Characterization of Fe Atoms in $CuMS_2$(M=Al,Ga and In) Crystals
K.Sato 33 50-57

Optical Properties of Mn-doped Crystals of $CuAlS_2$ and $CuAlSe_2$
K.Sato, K.Ishii, K.Ohe, K.Watanabe and Y.Kudo 41 137-140

Electroreflectance and Photoluminescence in $CuAl_xGa_{1-x}S_2$
S. Shirakata, K.Saiki and S.Isomura 45 156-159

Photoluminescence in Yb-doped I-III-VI_2 Compounds
S. Shirakata, K.Ishii and S.Isomura 49 164-167

Spinel Type Compound

EPR Studies of Electron-Irradiated $CdIn_2S_4$ Single Crystals
T.Takizawa, E.Christoffel, A.Goltzene and C.Schwab 53 292-295

$CdInGaS_4$

Optical Properties of Layered Semiconductor $CdInGaS_4$ and Related Phenomena
T.Irie, S.Endo and H.Nakanishi 57 33-40

The Dependence of Optical Absorption in $CdInGaS_4$ on Temperature and Hydrostatic Pressure

T.Toyoda, H.Nakanishi, S.Endo and T.Irie 65 401-404

The Refractive Indices and the Optical Dispersion Parameters in $CdInGaS_4$

T.Toyoda, H.Nakanishi, S.Endo and T.Irie 69 429-432

Application Oriented Works

Application of $AgGaS_2$ e Filter to Easy Raman Spectroscopy

N.Yamamoto, H,Horinaka and H.Mineguchi 73

Characterization of $CuInSe_2$ Thin Films Prepared by ICB(Ionized Cluster Beam) Technique

K.Sato, S.Matsuda and Y.Kudo 77 205-208

CRYSTAL GROWTH AND CHARACTERIZATION OF $AgGaS_2$

K.Masumoto[a,b] and K.Mochizuki[a]
[a]Department of Electronic Materials Faculty of Science and Technology, Ishinomaki Senshu University, Ishinomaki 986 Japan
[b]The Research Institute for Electric and Magnetic Materials, Yagiyama-minami Sendai 982 Japan

Phase diagram, crystal growth and lattice defect control of $AgGaS_2$ were investigated. Optimum growth conditions were examined for both vapor and melt growths. The origin of PL was discussed in connection with the controlled lattice defects.

$AgGaS_2$, a I-III-VI_2 chalcopyrite type semiconductor, is expected to be one of the candidate materials for a nonlinear optics and a blue emitting diode. In this study, an attention has been paid to some of the important and basic problems and they are as follows : (1) To clarify the pressure-temperature diagram which is indispensable for compound semiconductors. (2) Examination of growth conditions in obtaining high quality single crystals for both vapor and melt growths. (3) Assignment of native lattice defects responsible for the obvious emissions observed in PL spectra. The emission mechanisms of the lines newly observed in the band-edge region are also discussed. (4) Attempt of intentional Zn-doping which aims at selective substitution of Zn for Ga site and p-type conductivity.

(1) P-T diagram of $AgGaS_2$

To the author's knowledge, so far, a P-T diagram of $AgGaS_2$ has not been published, therefore in the present experiments, the diagram was made by the visual observation of surface melting /1/. Solid and broken lines in Fig.1 shows the lquidus of $AgGaS_2$ as a function of the controlled vapor pressures of sulfur (Ps_2). The liquidus temperature decreased gradually over the temperature range of more than 100 K with decreasing Ps_2. This is the reason why the melting point data reported so far /2,3/ is so scattered. From the figure, stable range of solid phase became clear.

(2) Growth conditions and characteristics of grown crystals

(i) Chemical vapor growth by iodine transport method /4/

Fig.2 shows a typical growth rate as a function of the amount of iodine as a transport agent. The behavior is quantitatively explained by vapor diffusion of gaseous molecules which limit the growth rate /5/. The as-grown crystals were transparent yellow and in two forms. A relation between crystal form and growth condition is shown in Fig.3, and good single crystals in rod form were obtained at the transport rate less than 10 mg/day and at the growth temperature higher than 1150 K. The dimensions of the biggest plate crystal were $6 \times 5 \times 2$ mm^3. As shown in Fig.4, the PL spectra of the crystals were dependent on the amount of iodine and they consisted of red band (2.02 eV), green band (2.48 eV) and blue peak (2.63 eV). Band edge-emissions with the energy close to 2.7 eV were observed only for the crystals with the iodine less than 0.18 mg/cm^3. From the fact that the emission intensity of the free excitonic line for the grown crystals decreases with increasing the quantity of iodine, it was suggested that unidentified non-radiative center was created in the crystal by the incorporation of iodine.

(ii) Growth from the melt

Bridgman and G.F.(Gradient Freezing) methods were used from the melt growth of $AgGaS_2$. Growth parameters such as growth rate, temperature gradient at growing interface and source composition were changed to obtain a good quality single crystals. Transparency and the sizes of the grown crystals depended effectively on the growth conditions. Growth rate less than 11 mm/day is required to obtain single crystals of the size larger than

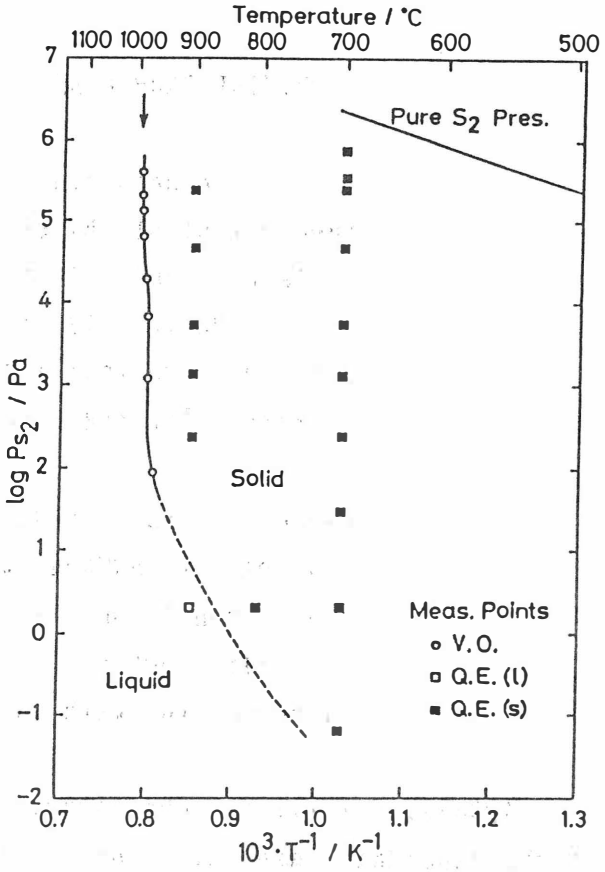

Fig.1 Temperature at which the liquid phase appears on the surface as a function of controlled Ps_2. V.O. : visual observation method, Q.E. : quenching method.

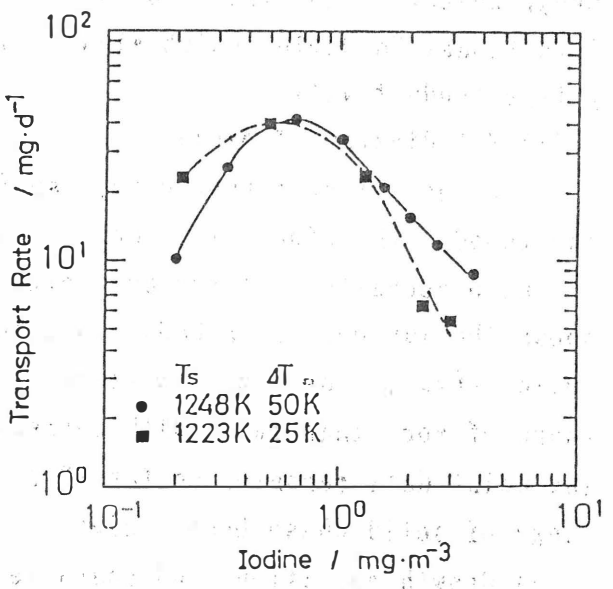

Fig.2 Relation between growth rate and the amount of iodine.

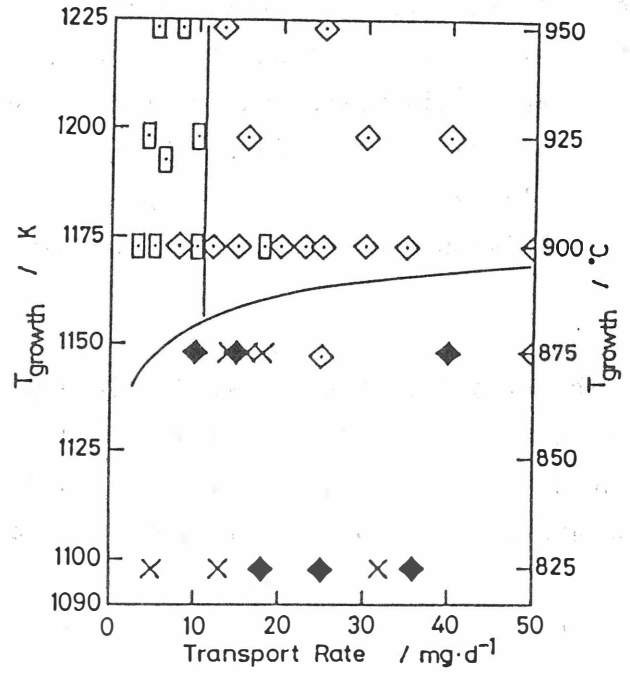

Fig.3 Crystal forms. Rectangles: rods, diamonds: plates, stripped diamonds: polycrystals, crossed line: fine crystals.

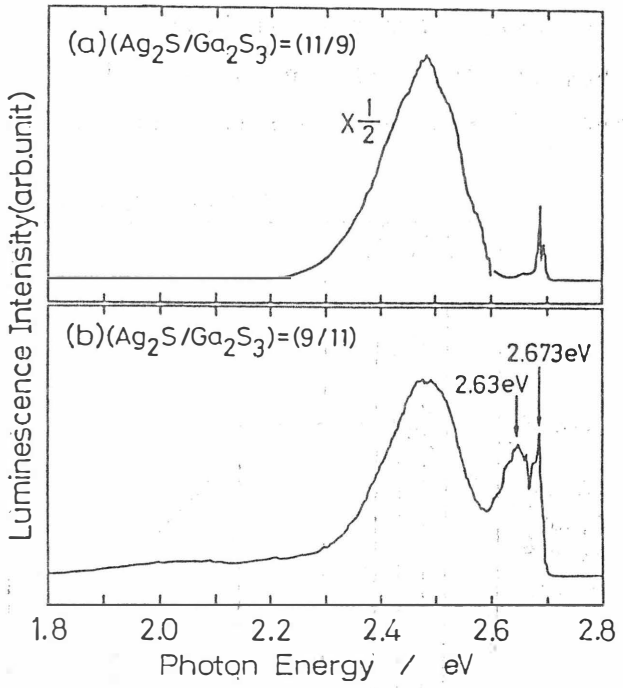

Fig.5 Photoluminescence spectra at 4.2K of $AgGaS_2$ single crystals grown from the melt with the following composition : ratio of (Ag_2S/Ga_2S_3); (a)11/9, (b)9/11.

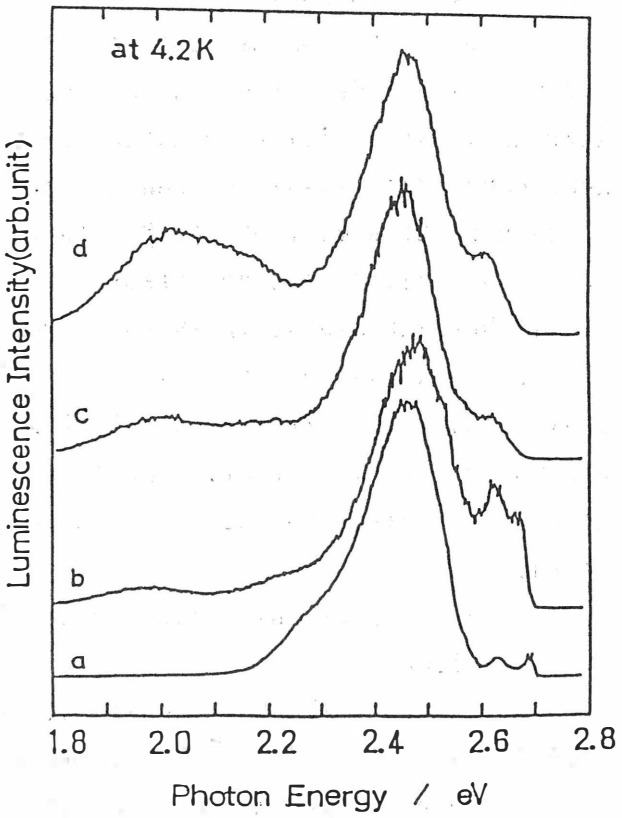

Fig.4 Photoluminescence spectra of $AgGaS_2$ single crystals. The amounts of iodine were (a)0.18, (b)0.79, (c)2.09 and (d)3.53 mg/cm^3, respectively.

10×5×3 mm^3. When the source composition is excess with Ga_2S_3 (Ag_2S/Ga_2S_3 < 1), untransparent yellow crystals were usually grown. Transparent clear crystals were grown from the source with stoichiometric or Ag_2S excess composition.

Fig.5 shows PL specra at 4.2 K of the crystals grown from different source compositions. Clear band-edge emissions were observed for the crystals grown from the melt with the source composition ratio (Ag_2S/Ga_2S_3) = 11/9 (Ag_2S excess composition). On the other hand, near band-edge emissions at 2.63 and 2.673 eV were newly observed for the crystals grown from the melt with the source composition ratio (Ag_2S/Ga_2S_3) = 9/11

(Ga_2S_3 excess composition). In the case that the source composition is excess with Ga_2S_3, the composition of the grown crystal should deviate from stoichiometry to the side of Ga and S excess region and this means that native defect like Ag vacancy will be created in the grown crystal. Therefore, the observed near band-edge emissions seem to be related to Ag vacancy.

(3) Heat-treatment of $AgGaS_2$ and a relation between the origin of PL and the controlled lattice defect

(i) Heat-treatment in sulfur vapor

Fig.6 shows PL spectra at 4.2 K of the crystals heat-treated only under controlled Ps_2. It is known that near band-edge emissions at 2.63 and 2.673 eV disappear for the crystals heat-treated under low Ps_2 and appear again under high Ps_2. This supports that the emissions are related to the defect like metal vacancy.

(ii) Heat-treatment under controlled vapor pressures of two constituent elements

Fig.7 shows the heat-treatment apparatus for specifying the two component activities of $AgGaS_2$. The sample was put in the sample chamber together with Ga_2S_3 powder or $AgGaS_2$ powder having 5 % Ag_2S excess composition and heat-treated under controlled Ps_2. Fig.8 shows the PL spectra at 4.2 K of the crystals heat-treated with Ga_2S_3 powder under controlled Ps_2. As seen in the figure, the intensity of the near band-edge emissions observed at 2.63 and 2.673 eV increases with increasing Ps_2. This suggests that the emissions relate Ag vacancy or sulfur interstitial (S_i), because Ga element is saturated on the

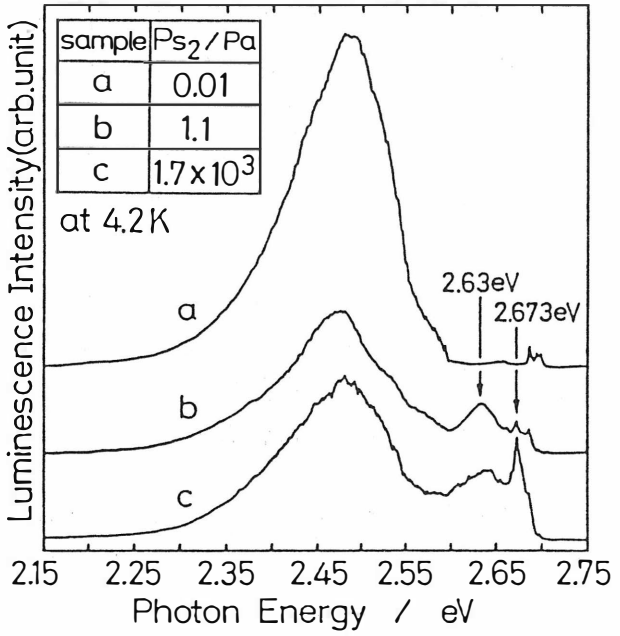

Fig.6 Photoluminescence spectra at 4.2K of the samples heat-treated under controlled Ps_2.

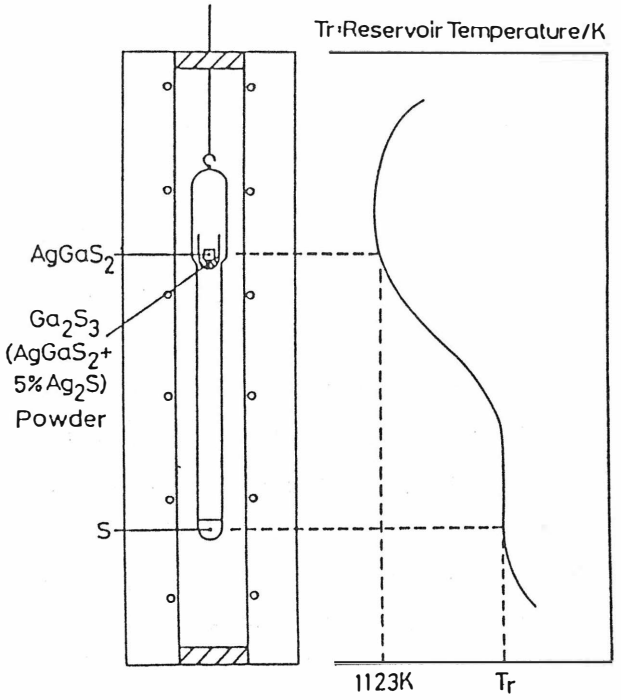

Fig.7 Heat-treatment apparatus for controlling two component activities.

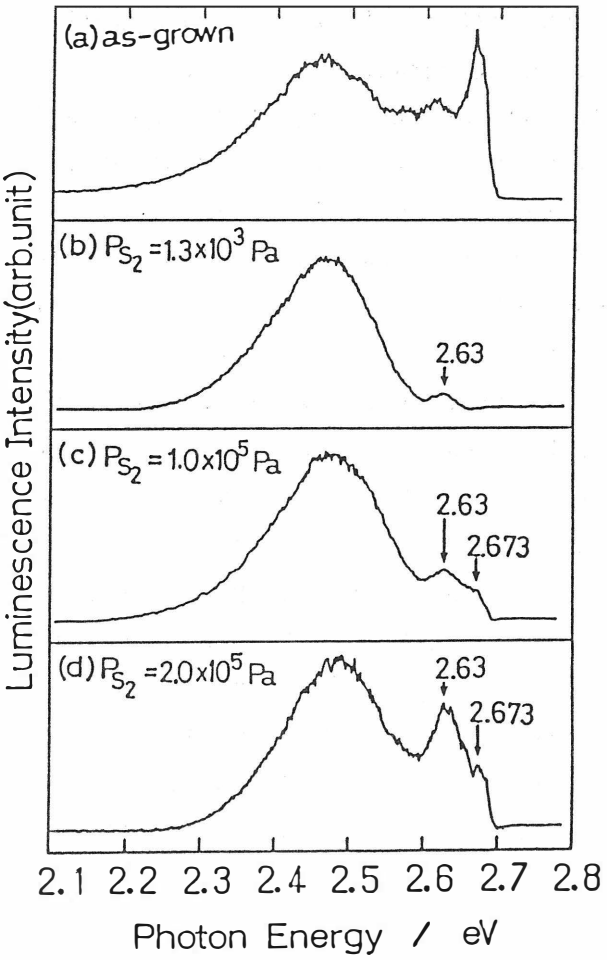

Fig.8 Photoluminescence spectra at 4.2K of crystals heat-treated with Ga_2S_3 powder under controlled Ps_2.

(iv) Emission mechanism of PL in the band-edge region

Band-edge emissions close to 2.7 eV were clearly seen for the samples with metal excess composition and the typical PL (solid line) and reflection (dashed line) spectra are shown in Fig. 10. Three lines with the symbols of E_x, I_2 and I_1 were commonly observed at 2.699, 2.695 and 2.688 eV. Based on the previous results /6-9/, these emission lines were already assigned as the radiative recombination of free excitons (E_x), excitons bound to a neutral donor and acceptor (I_2 and I_1), heat-treated sample. On the contrary, when the crystal was heat-treated with the powders of Ag_2S excess composition under controlled Ps_2, the corresponding near band-edge emissions were not seen. This fact eliminates S_i as a possible defect responsible for the emissions. Accordingly, as was stated in the section of (2)-(ii), V_{Ag} is related to the emissions observed at 2.63 and 2.673 eV.

(iii) Ga-dipping

Fig.9 shows the Ga-dipping effect on the PL spectra. It is known that a broad and dominant emission at about 2.48 eV disappears after dipping. The origin of this emission is not clear now, but Ga vacancy might relate to this emission.

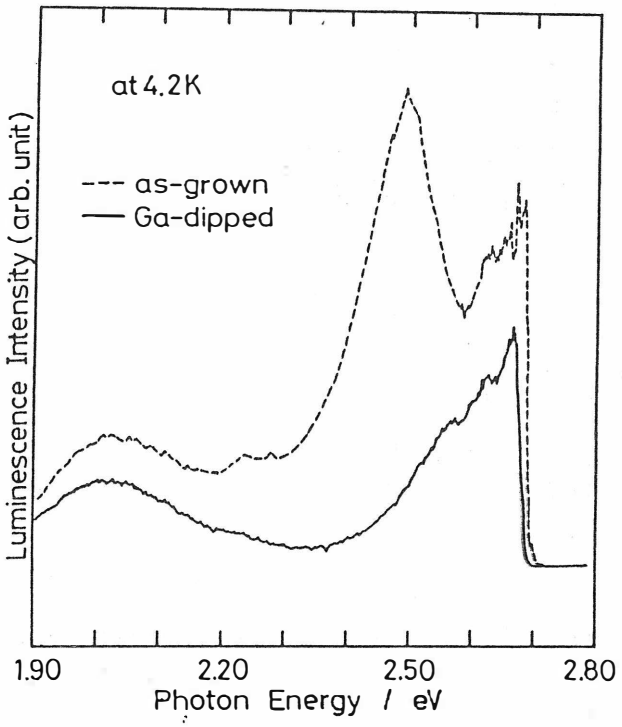

Fig.9 Ga-dipping effect on the photoluminescence spectra at 4.2K of $AgGaS_2$ single crystals. Solid line : PL spectrum of the crystal heat-treated in Ga solvent, dashed line : typical PL spectrum of the as-grown crystal.

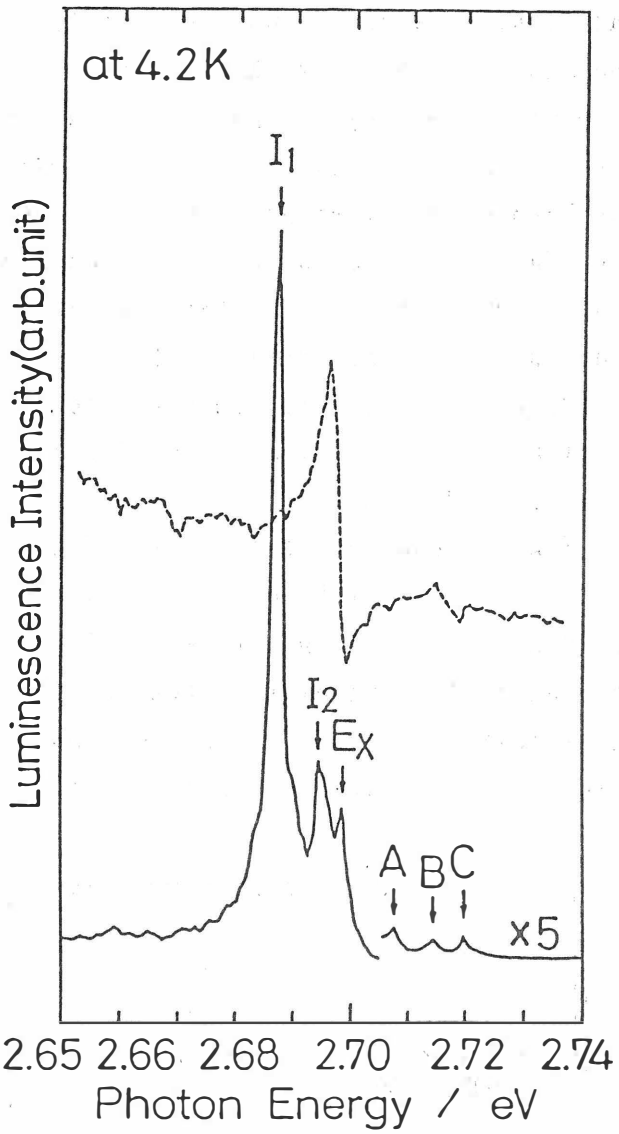

Fig.10 photoluminescence (solid line) and reflection (dashed line) spectrum at 4.2K in the band-edge region of a crystal grown by the Bridgman method, source composition (Ag_2S/Ga_2S_3) = 11/9.

Where, $E_x(n)$ is the photon energy due to radiative recombination of free excitons in the nth excited state, E_g the energy gap of the material, R_x binding energy of ground state free excitons. If the energies of ground (n=1) and excited (n=2) states of free exciton correspond to 2.699 and 2.720 eV, as was confirmed from reflection spectra, the unknown respectively. It was found that the emission intensity of I_1, related to an acceptor defect, increases and that of I_2 line, related to a donor one, decreases respectively with increasing Ps_2. The dependence was the same with those observed in II-VI compounds /10/. However, the relative intensity change of (I_1/I_2) is very small. New emission A to D lines, not reported so far, were observed in the region with the energy higher than that of a free excitonic line and the detailed spectra are shown in Fig.11. Their emission energies are 2.708, 2.715, 2.720 and 2.728 eV, respectively. The C line seems to be related to the excited state of free excitons (n=2) from the agreement of the emission energy with that of 2nd structure in reflection spectra /6,7/. Concerning to D line, there is a possibility that the emission is related to the 3rd or 4th excited state of a free exciton. Then, the energy was estimated by a well-known eq.(1) /11/,

$$E_x(n) = E_g - R_x / n^2 \qquad (1).$$

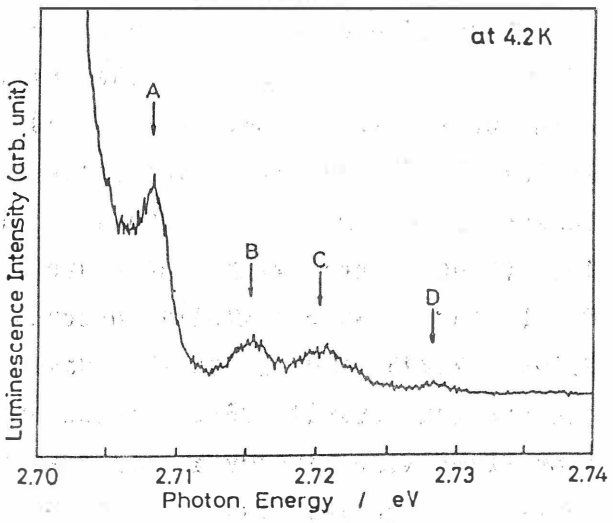

Fig.11 Detailed photoluminescence spectra at 4.2K of A to D lines.

values of E_g and R_x are estimated from eq.(1) as 2.727 eV and 28 meV, respectively. By using these values of E_g and R_x, the emission energies $E_x(n)$ in the 3rd and 4th excited states of free excitons are estimated at 2.724 and 2.725 eV, respectively. The emission energy of D line rather agrees with the band-gap energy at 4.2 K. This suggests that D line is due to the optical transition between bands. To speculate the emission mechanism on A and B lines, the one method is to compare the emission intensity of A to B to C lines with that of I_1 to I_2 to E_x lines. Intensity ratio of each emission in the former group is similar to that of the latter group. This suggests a possibility that the relation of A and B lines to the C line might be the same with that of the I_1 and I_2 lines to E_x line. In other words, A and B lines might be due to the radiative recombination of bound excitons in the first excited state (n=2). Kasuya et al. /12/ proposed eq. (2) which estimates the energy levels of the excited states of bound excitons for the study of ZnSe.

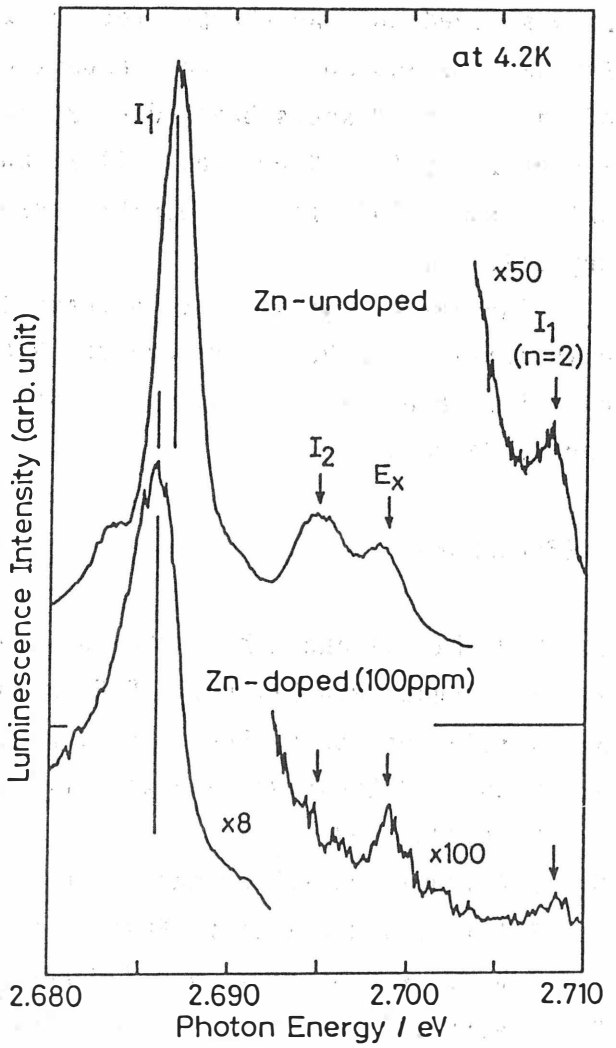

Fig.12 Photoluminescence spectra at 4.2K in the band-edge region of the crystal doped with Zn.

$$E(X_{2s},D_{1s}) = E(X_{1s},D_{1s}) + \{E(X_{2s}) - E(X_{1s})\} \qquad (2).$$

Where, $E(X_{ns})$ is the emission energy due to the free excitons in the ground (n=1) and first excited state (n=2) and $E(X_{ns},D_{1s})$ the emission energy due to the ground (n=1) and first excited state (n=2) excitons bound to a ground state neutral donor (D_{1s}). Eq.(2) can apply to the excitons bound to a groud state neutral acceptor (X_{1s},A_{1s}). The emission energy of $E(X_{2s},A_{1s})$ and $E(X_{2s},D_{1s})$ due to the first excited state of I_1 and I_2 lines can be estimated from eq.(2) at 2.708 and 2.715 eV, respectively and these agree with the emission energies of A and B lines, respectively. Therefore, A and B lines are due to the radiative recombination of bound excitons in the first excited state.

(4) Attempt of intentional doping of Zn

Doping of Zn was attempted to obtain the sample with p-type conductivity.

Zn was added to the charge for the melt growth, aiming the substitution of Zn for Ga site and so, the same amount of Ga in the charge is replaced with that of Zn. Fig.12 shows band-edge PL spectra at 4.2 K for the sample grown from the charge with 100 ppm Zn. It is known that I_1 line and its excited state are only seen. This is the possible evidence that Zn is replaced by Ga and p-type conductivity.

The authors would like to thank to Profs. Y.Furukawa and Y.Noda at Tohoku University, and Mr E.Niwa and Dr. N.Nakamura at The Res. Inst. for Electric and Magnetic Materials for helping the experiments and discussing the results and encouragements.

REFERENCES

1. K.Mochizuki and K.Masumoto, J. Crystal Growth 98 (1989) 855.
2. V.M.Cound, P.H.Davies, K.F.Hulme and D.Robertson, J. Phys. C3 (1970) L83.
3. H.M.Kasper, Spec. Publ. Natl. Bur. Stand. (U.S.) 364 (1972) 671.
4. Y.Noda, T.Kurasawa, N.Sugai, Y.Furukawa and K.Masumoto, J. Crystal Growth 99 (1990) 757.
5. T.Arizumi and T.Nishinaga, Japan J. Appl. Phys. 4 (1965) 165.
6. B.Tell and H.M.Kasper, Phys. Rev. B4 (1971) 4455.
7. P.W.Yu, W.J.Anderson and Y.S.Park, Solid State Commun. 13 (1973) 1883.
8. P.W.Yu and Y.S.Park, J. Appl. Phys. 45 (1974) 823.
9. J.P.Aicardi and G.Aguero, phys. stat. sol. (a) 95 (1986) 679.
10. H.Roppischer, J.Jacobs and B.V.Novikov, phys. stat. sol. (a) 27 (1975) 123.
11. D.D.Sell and P.Lawaetz, Phys. Rev. Lett. 26 (1971) 311.
12. A.Kasuya, Y.Nishina and T.Goto, J. Phys. Soc. Japan 51 (1982) 922.

SOLUTION GROWTH OF BULK $CuGaS_2$ CRYSTALS

Hideto Miyake and Koichi Sugiyama

Faculty of Engineering, Mie University, Tsu,
Mie 514, Japan

Growth of $CuGaS_2$ chalcopyrite crystals at temperatures below 1000 °C from In solutions has been studied. Bulk single crystals of $CuGa_xIn_{1-x}S_2$ ($1-x\sim0.05$) have been grown at 930 °C by the traveling heater method (THM) using zones of In solution containing S-excess solute.

1. Introduction

Bulk single crystals of chalcopyrite compounds are required for both device application and detailed characterization of the compounds/1/. Recently, bulk crystals of $CuInS_2$/2/ and $CuGaSe_2$/1/ were obtained by the THM growth with In solvent. For $CuGaS_2$, detailed optical and electrical properties have been investigated using crystals grown by iodine transport and melt growth methods/3/, but reports on bulk single crystal growth are rather few. Solution growth technique using In as a solvent/4,5/ is promising for obtaining large $CuGaS_2$ crystals, as in the case of $CuGaSe_2$/1/. We investigated the phase diagram of $CuGaS_2$-In pseudobinary system and revealed that there exists a miscibility gap in the liquid phase; i.e., the In solutions saturated with stoichiometric $CuGaS_2$ solutes at temperatures below 1020 °C are separated into two liquid phases (S-excess and S-deficient)/6/. On the basis of the result, we obtained relatively large single crystals of $CuGa_xIn_{1-x}S_2$ ($1-x<0.06$) by using the solution Bridgman method (SBM) with S-excess In solutions/7/, and by using the THM at 1050 °C with In solutions containing a stoichiometric $CuGaS_2$ solute/8/. However, for growth of high quality bulk single crystals without strains and defects, it is desired that the THM growth is performed at lower temperatures. S-excess non-stoichiometric $CuGaS_2$ solutes are required for the solution growth of $CuGaS_2$ chalcopyrite crystals at temperatures below 1020 °C/7/. But the range of amounts of the excess sulfur for the $CuGaS_2$ growth has not been determined. In this work, we investigated the range of the excess sulfur for obtaining $CuGaS_2$ chalcopyrite crystals from In solutions below 1000 °C. THM growth of bulk $CuGaS_2$ crystals was carried out at 930 °C using zones of the S-excess In solutions.

2. Compositions of solutes in In solutions for growth of $CuGaS_2$ at temperatures below 1000 °C

For investigation of the growth conditions of $CuGaS_2$ chalcopyrite crystals from In solutions, the SBM growth was employed/7/. The amount of a mixture of elemental Cu, Ga and S for the solute was 6-8 g, and that of In used as a solvent was about 5 g and was taken as Ga:In=1:1.5. The atomic ratios of the solutes are listed in table 1. The purities of all elements were 6N grade. They were inserted in a pointed carbon-coated quartz ampoule with 9.5 mm ID and were vacuum-sealed at 100 mm in length. Preparation of In solution from the mixture, determination of the liquidus temperature and SBM growth were performed in the same way as in refs. 6 and 7. The liquidus temperature for the In solution containing a stoichiometric $CuGaS_2$ solute is about 930 °C, and that for the In solution containing a solute with a composition of Cu:Ga:S=1:1:3 is about 945 °C. The lowest portion of the grown crystal, that solidified initially from the In solution, was used for characterization. The crystal structure was examined by X-ray powder diffraction (XD), and the composition was determined using energy-dispersive X-ray microanalysis (EDX). Existence of two liquid phases was examined in the same way as in ref. 6.

Figure 1(a) shows an XD pattern of the crystals grown from In solution containing a solute with a composition of Cu:Ga:S=1:1:2.4. The crystal was confirmed to be single phase with a chalcopyrite structure. Chalcopyrite crystals were also obtained from In solutions having solute compositions of Cu:Ga:S=1:1:2.7-3.3. For In solutions having solute compositions of Cu:Ga:S=1:1:2.0-2.3, the solutions were separated into two liquid phases at the liquidus temperatures, as described in ref. 7. For In solutions having solute compositions of Cu:Ga:S=1:1:3.5-4.0, growth of dark red crystals was observed at the lowest portion of solidified ingot. Their XD patterns indicate a cubic

Table 1. Structures and compositions of grown crystals and numbers of liquid phases at liquidus temperatures.

solute atomic ratio* Cu:Ga:S	grown crystal crystal structure**	composition (at.%) Cu	Ga	S	In	liquidus temperature (°C)	liquid phase
1: 1:2	Ch	25.7	24.0	49.2	1.0	930	two phases
1: 1:2.4	Ch	24.7	23.5	50.5	1.3		single phase
1: 1:2.7	Ch	25.4	23.7	49.9	1.2	940	
1.1: 1:2.7	Ch	25.5	24.1	49.6	0.3		
1: 1:3	Ch	26.7	22.2	47.8	3.3	945	
1: 1:3.3	Ch	24.9	18.4	50.0	6.7		
1: 1:3.5		23.7	17.5	45.5	13.3		
1: 1:4		25.2	18.6	42.5	13.8		

* Amount of In solvent is taken such as Ga:In=1:1.5.

** Ch:chalcopyrite

structure, as shown in fig. 1(b). The crystals are considered to be $Cu_1(Ga_yIn_{1-y})_5S_7$ from the composition determined by EDX, but the structure was unknown. The experimental results are also summarized in table 1.

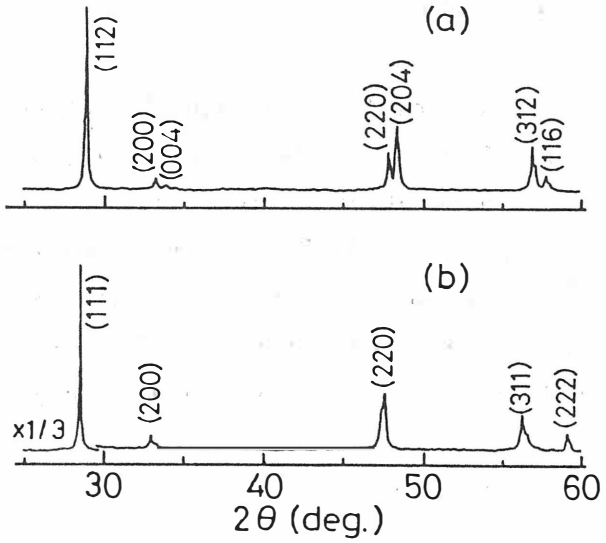

Fig. 1. XD patterns of crystals grown by SBM. The compositions of solutes: (a)Cu:Ga:S=1:1:2.4, (b)Cu:Ga:S=1:1:3.5.

3. Single crystal growth by THM

The THM growth of $CuGaS_2$ was carried out at zone temperatures of about 930 °C. On the basis of the above experimental results, we chose the In solutions with a solute composition of Cu:Ga:S=1:1:2.53, which correspond to a single phase and from which chalcopyrite crystals can be grown. For the THM, a pointed carbon-coated quartz ampoule (10 mm ID and 80 mm in length) was used. After indium ingots of 2 g and sulfur powders of 0.2 g were charged at the bottom of the ampoule as initial zone material, and a $CuGaS_2$ polycrystal ingot of 10-15 g was inserted as a feed material, the ampoule was vacuum-sealed. The ampoule was then inserted in a vertical THM furnace/8/, whose temperature profile had a maximum at 960 °C. The THM growth was performed by lowering of the ampoule at a speed of 8 mm/day.

The obtained bulk single crystals, whose dimensions are 10 mm in diameter and 25-35 mm in length, are solid solutions $CuGa_xIn_{1-x}S_2$ with a chalcopyrite structure. The mole fraction 1-x of $CuInS_2$ was almost constant with values of 0.05±0.01 along the growth direction. Figure 2 shows wafers cut perpendicularly to the growth axis from one of the single crystals with a thickness of 0.5 mm. The color of the crystals is reddish orange.

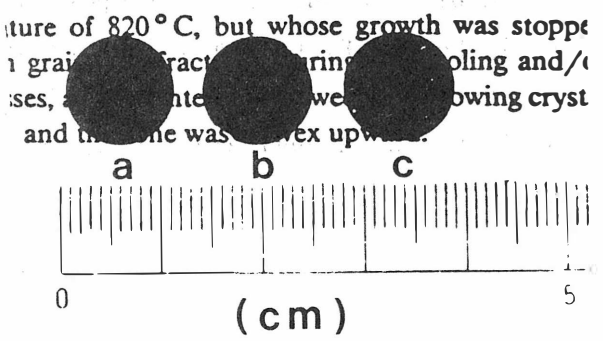

Fig. 2. Wafers cut from THM grown crystal. a:10 mm, b:20 mm, c:25 mm from the tip.

The electrical properties of the crystals were measured at room temperature by four-probe and van der Pauw methods. Ohmic contacts were made with evaporated Ni dots. For the as-grown crystals, the resistivities were over 10^6 Ωcm, but the Hall coefficients could not be obtained because of the poor ohmic contacts. After annealing in an atmosphere of 1 atm S at 850 °C for 24 h, the resistivities decreased to ~0.7 Ωcm, and hole concentrations and mobilities were ~1×10^{18} cm^{-3} and ~9 cm^2/V sec, respectively.

4. Conclusion

The solution growth of $CuGaS_2$ from S-excess In solution at temperatures below 1000 °C has been investigated. It has been established that crystals grown from In solutions containing solutes with Cu:Ga:S=1:1:2.4-3.3, corresponding to a single liquid phase, have a chalcopyrite structure. On the basis of the results, bulk single crystals of $CuGa_xIn_{1-x}S_2$ ($1-x \sim 0.05$), whose dimensions are 10 mm in diameter and 25-35 mm in length, have been grown at 930 °C by the THM using In solutions containing a solute with Cu:Ga:S=1:1:2.53.

Acknowledgment

This presentation has been partially supported by Iketani Science and Technology Foundation.

REFERENCES

1.K.Sugiyama, H.Kato and H.Miyake, J.Crystal Growth 98(1989)610.
2.H.J.Hsu, M.H.Yang, R.S.Tang, T.M.Hsu and H.L.Wang, J.Crystal Growth 70(1984) 427.
3.J.L.Shay and J.H.Wernick, Ternary Chalcopyrite Semiconductors,(Pergamon Press, Oxford, 1975).
4.N.Yamamoto and T.Miyauchi, Japan.J.Appl.Phys. 11(1972)1383.
5.H.J.Höbler, G.Kühn and A.Tempel, Kristall und Technik 53(1980)K45.
6.H.Miyake and K.Sugiyama, Japan.J.Appl.Phys. 29(1990)L998.
7.H.Miyake and K.Sugiyama, Japan.J.Appl.Phys. 29(1990)L1001.
8.H.Miyake and K.Sugiyama, to be published in Japan.J.Appl.Phys. 29 No.10(1990).

STOICHIOMETRIC CONTROL FOR $CuInSe_2$ BULK SINGLE CRYSTALS

S.Nomura, M.Sugiyama and T.Takizawa,
Department of Physics & Applied Physics, College of Humanities & Sciences, Nihon University, Tokyo 156, Japan.

Compositional variation around the stoichiometry of the melt-grown $CuInSe_2$ was investigated. Location-dependence of composition in bulk crystals was studied by the EPMA method. The crystallizing mechanism is proposed on the basis of these experimental results.

1.Introduction

In general, it is difficult to make some systematic discussion on thin film properties which have some complex problems such as grain boundary conditions. Also, in the case of $CuInSe_2$, more systematic interpretation for the fundamental properties should be made first on bulk crystals /1/.

In this paper, compositional shift from the stoichiometry for $CuInSe_2$ is systematically classified into nine types in terms of the differences in (Cu/In) and (Cation/Anion) molar ratios. Some types of single crystals which have the compositions near the stoichiometry were synthesized from highly refined elements by the melting method. Vapor pressure of selenium was controlled during the crystallization. The location-dependence of composition in bulk crystals was measured by the EPMA method. Then, the relationship between the conductivity types and the mean valence is discussed. A new idea for the chemical equilibrium reaction in the melt of Cu-In-Se system is presented.

2. Classification of the compositional shift around the stoichiometry

On considering the stoichiometric control for $CuInSe_2$, (Cu/In) and (Cation/Anion) (or (Anion/Cation)) molar ratios are frequently used as parameters /2/ in order to explain the properties. However, systematic treatment of these parameters has not been completed. Table 1 lists respective

three types of the (Cu/In) and the (Cation/Anion) (abbreviated as (Cn/An) hereafter) molar ratios classified according to whether these parameters are more than, equal to or less than unity. Every combination of the respective three types of (Cu/In) and (Cn/An) ratios listed in Table 1 corresponds to nine types of the compositional shift as shown in Table 2, where the (Cu/In) and (Cn/An) ratios vary with the compositional shift parameters δ and ε, respectively. These types of the compositional shifts can be expressed onto the mean valence variation as a function of δ with ε varing from 0 to 10% as shown in Fig.1.

In adamantines, conductivity types are determined by the mean valence. The mean valence is more than "4" in n-type, and less than "4" in p-type, respectively. Moreover, values of the mean valence largely deviated from "4" indicate bad crystallinity having many defects such as vacancies or interstitials. Materials design with wide variation in carrier concentration of both types in conduction would be made in the γ c-type (i.e. $CuIn_{1+\delta}Se_{2+\delta+\varepsilon}$) materials by adjusting shift parameters δ and ε without some bad influences on crystallinity.

In this paper, we treat the α-type materials (i.e. α a-, α b- and α c-types) as the first step to the destination, i.e. the γ c-type.

Table 1 Respective three types of (Cu/In) and (Cation/Anion)

	=1	>1	<1
Cation/Anion	α	β	γ
Cu/In	a	b	c

Table 2 Nine compositional types around the stoichiometry of $CuInSe_2$.

Type	Composition
α a	$CuInSe_2$
α b	$Cu_{1+\delta}InSe_{2+\delta}$
α c	$CuIn_{1+\delta}Se_{2+\delta}$
β a	$(CuIn)_{1+\varepsilon/2}Se_2$
β b	$(Cu_{1+\delta}In)_{1+\varepsilon/2}Se_2$
β c	$(CuIn_{1+\delta})_{1+\varepsilon/2}Se_2$
γ a	$CuInSe_{2+\varepsilon}$
γ b	$Cu_{1+\delta}InSe_{2+\delta+\varepsilon}$
γ c	$CuIn_{1+\delta}Se_{2+\delta+\varepsilon}$

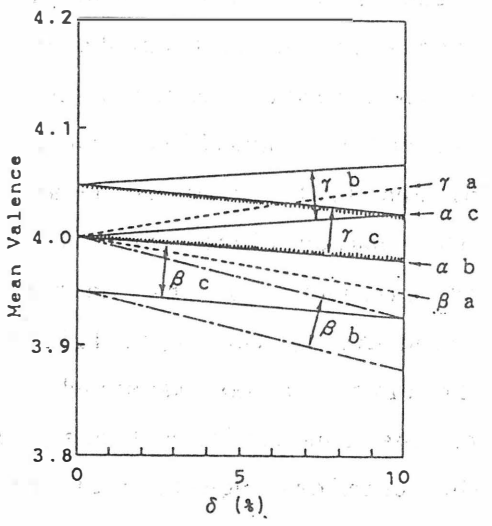

Fig.1 Compositional types expressed onto the mean valence variation as a function of δ with ε varing from 0 to 10 %.

3. Experimental Procedures

Single crystals of various types in composition were synthesized from copper, indium and selenium elements of 99.9999% purity by the melting method under the control of the vapor pressure of selenium.

Location-dependence of the composition in bulk crystals was studied using the electron probe microanalyzer (EPMA), JEOL JEM-2000EX.

4.Results and Discussions

4.1 Location-dependence of the composition in a bulk of the α a-type.

Location-dependence of the composition was analyzed on a single crystal chip of 7x3x1 mm^3 cut from an α a-type sample. This monolithic chip consists of a part of n-type conduction and a part of rather low resistive p-type one. The conduction types were confirmed by the heat probe measurement. Composition was analyzed in 12x3 matrix points in the bulk. As shown in Fig.2, the three lines in the matrix represent the upper, the middle and the lower parts against gravity in the crystallization. The maximum temperature applied in the crystal growth was higher in the n-type region than in the p-type one. Figure 2 shows the location-dependence of the (Cu/In), the (Cn/An) and the mean valence V_m in the bulk. From the n-type region to p-type one, the composition varies from In-rich (or Cu-deficient) to Cu-rich (or In-deficient) and anion-rich to cation-rich. As mentioned in Section 2, this n-type to p-type transition can be simply understood by the mean valence variation from more than "4" to less than "4". The influence of gravity was remarkable especially in the lower temperature part.

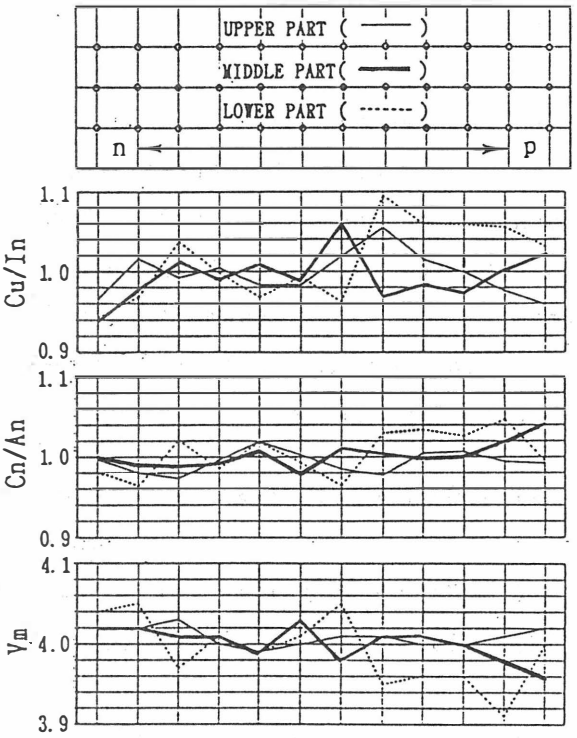

Fig.2 Location-dependence of the fundamental parameters in a bulk of α a-type.

4.2 Effect of selenium vapor pressure on the α b- and the α c-types.

Figures 3(a) and (b) are so-called radar charts showing the relative relation in three parameters, the (Cu/In), (Cn/An) ratios and the mean valence V_m, in the In-deficient α b- and Cu-deficient α c- types, respectively. In these figures, for example, the $\alpha b_{150}10$ represents α b-type sample of δ =10% applied with the vapor pressure of selenium of 150 torr. In

both cases, the initial charge of elements was retained most in the materials of δ=10% applied with the selenium vapor pressure of 150 torr. Moreover, there are close resemblances between $\alpha b_0 10$ and $\alpha b_{150} 05$, and also between $\alpha c_0 10$ and $\alpha c_{150} 05$, which suggests that the solubilities of Cu and In into Cu-In-Se melt are increased by supplying the vapor pressure of selenium.

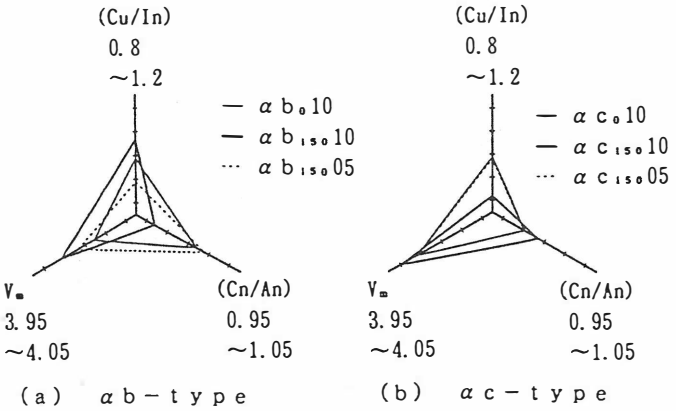

Fig.3 Effect of the vapor pressure of selenium on fundamental parameters for (a) α b- and (b) α c-types.

4.3 Chemical equilibrium reaction in Cu-In-Se system

In our crystal preparation, two binary compounds In_2Se_3 and Cu_3Se_2 were found to be chemically vapor-deposited on the lower temperature part inner a quartz ampoule, indicating volatile decomposition of these binary compounds from the melt. We assume the following series of the chemical equilibrium reactions for the melt of Cu-In-Se system in the case of including some extra amount of selenium:

(A) $12CuInSe_2(l) + Se_2(g)$; the vapor pressure of selenium (P_{Se}) decreases, or the temperature of the melt (T_m) decreases,

(B) $12CuInSe_2(l) + 2Se(l)$; P_{Se} increases, or T_m increases,

(C) $4Cu_3Se_2(g) + 6In_2Se_3(g)$; P_{Se} decreases, and T_m further increases,

where the chemical equilibrium moves toward each state according to the condition for the vapor pressure of selenium and the temperature of the melt.

5. Conclusion

The n-type to p-type transition in the electrical conduction near the stoichiometry of $CuInSe_2$ can be interpreted as the change in the mean valence. In the melt growth of $CuInSe_2$, control of the vapor pressure of selenium is inevitable not only for preventing the volatile decomposition of selenium but also for keeping the (Cu/In) ratio of initial charge.

REFERENCES

1. R.D.Tomlinson, Solar Cells 16 (1986) 17.
2. For example: S.K.Deb, Thin Solid Films, 163 (1988) 75.

GROWTH OF $CuGaS_2$ BY TRAVELLING HEATER METHOD

N. Yamamoto, Y. Kimura and H. Horinaka
College of Engineering, University of
Osaka Prefecture, Mozu, Sakai, Osaka 591, JAPAN

Travelling heater method (THM) is applied to grow bulk $CuGaS_2$ crystal using In as solvent. Yellow colored polycrystal, which includes single crystal grains of 3x5x5 mm^3, are grown. Luminescence and accidental isotropic wavelength are measured.

Growth of bulk single crystal of $CuGaS_2$ is important not only as a substrate crystal of epitaxial growth for light emitting device /1/, but also as a narrow band pass and/or elimination filter tunable for 647nm line of Kr^+ laser /2/. Growth by direct solidification has found to be unfavourable due to the peritectic reaction at melting point of stoichiometric composition /3/. Iodine vapour transport method, which has been usually applied for growing a small single crystal for optical measurements, is also inadequate, because controlled growth of the size and shape of single crystal has not yet been achieved.

As an alternative, solution growth method using In as solvent was first applied by one of the authors to $CuGaS_2$ and $CuGa_{1-x}In_xS_2$ /4/ and also to $CuAlS_2$ and $CuAl_{1-x}Ga_xS_2$ /5/. Other possible solvents, succeedingly reported, are Sn /6,7/, Pb /7/, $CdCl_2$ and CdI_2 /8/, and Te /9/. Small size of $CuGaS_2$ single crystals have been obtained using these solvents. However, there exists a critical minimum temperature, T_{CMT}, for each solvent, below which some second phases

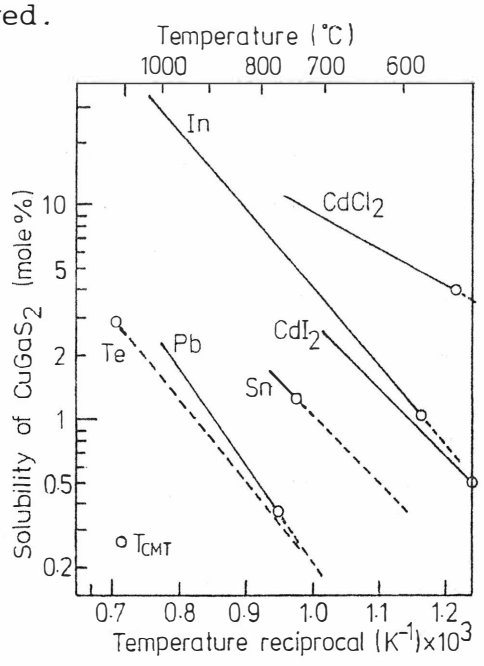

Fig.1 Solbility of $CuGaS_2$ and T_{CMT} for some solvents

are precipitated, typically as binary compounds. Solubility of $CuGaS_2$ and approximate T_{CMT} of these solvents are summarized (Fig. 1). Among these, superior excellency of In solvent, *i.e.*, high solubility at relatively low temperature and wide applicable temperature range, can be clearly recognized.

Hsu *et al.* /10/ was the first to grow a large size of single crystal of $CuInS_2$ by travelling heater method (THM) using the excellent In solvent. Succeedingly, a good bulk single crystal of $CuGaSe_2$ has been grown by the same method using In as solvent by Sugiyama *et al.* /11/. Thus, travelling heater method using In as solvent (THM-In) is about to be established as the optimum growth method to obtain a large size of single crystal of chalcopyrite compounds, such as $CuInS_2$, $CuGaSe_2$, $CuGaS_2$, $CuAlS_2$ and $CuAlSe_2$. Very recent report by Miyake and Sugiyama has won a success to grow single crystal of $CuGaS_2$ by solution Bridgman method (SGM) /12/ as a preliminary work for THM growth /13/. This paper deals with a trial stage of THM growth of $CuGaS_2$. Since THM should take rather a long time for each run, typically 20 days, a description of the result of failure should be useful as much as that of success.

Polycrystalline feed crystal of $CuGaS_2$ for THM growth was prepared by sintering a stoichiometric mixture of Cu_2S and Ga_2S_3 at 950°C for 2 days. Fused silica ampoule of 8 mm ID with a conical termination was used as a crucible. Indium metal solvent (about 1.9 g) was first melted and located at the ampoule terminal, on which then, the feed crystal of $CuGaS_2$ (about 3.1 g) was sealed under evacuation. The silica ampoule was then inserted into another silica tube of 12 mm ID, which may protect the inclusions from oxydation when the inner silica amoule happend to crack during the growth.

Growth experiment of THM was carried out using a specially constructed three zone virtical furnace (Fig. 2) with a typical temperature profile as shown. A muximum temperature was set as 850°C and average temperature gradient of 44°C/cm is realized down to 600°C. The silica ampoule, its terminal

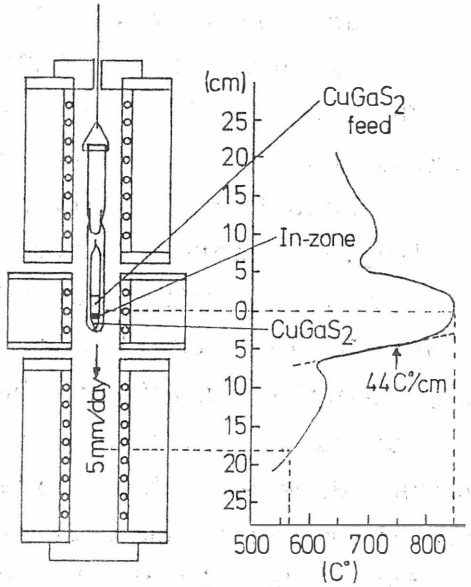

Fig.2 THM furnace and its temperature profile

was first located at the maximum temperature zone, was then moved downward at the rate of 5 mm/day. This made the travelling zone about 5 mm thick indium solvent to move upward at the same rate, and $CuGaS_2$ crystal about 30 mm in length may be grown within 20 days.

In the first run (THM-1), accidental power cut off occurred during growth and this caused a rapid temperature quenching. There observed about 20 mm long yellow colored $CuGaS_2$ crystal on the bottom, on which In solution zone and the residual $CuGaS_2$ feed crystals were covered. This showed a favorable growth process of THM. In the second run, again, an accidental power cut off occurred just after the starting stage of THM (after heat up to maximum temperature). A rapid temperature quenching caused a cracking of inner silica tube. The cracked silica tube, however, was reheated and a full THM process was performed. The result appeared THM growth both first in the inner tube and secondly, in the outer tube, where the spilt materials from the cracking part of the inner tube existed. The crystal grown in the inner tube (THM-2Y) was yellowish colored crystal and crystal grown in the outer tube (THM-2R) was reddish colored one.

After these accidental experiments due to the power cut off, the third run could be carried out without any trouble during the growth period. Polycrystal including some 3x5x5 mm^3 yellow colored single crystal grains (THM-3) were grown.

Grown crystals were took out without any mechanical damage by dissolving the silica ampoule in the HF bath. The lattice constants were measured by X ray powder method, and this revealed somewhat larger lattice constants of the THM grown crystals than the feed crystal. In inclusion of x=0.03 -0.09 in $CuGa_{1-x}In_xS_2$ alloy was suggested in the THM crystals as mentioned by Miyake *et al.* /12/.

Photoluminescence spectra at 77K were measured on single crystal grains cut from the polycrystals of each growth run (Fig. 3). Crystals of THM-1 and THM-3 showed a single sharp green peak at 2.38eV. However, yellowish crystal of THM-2Y

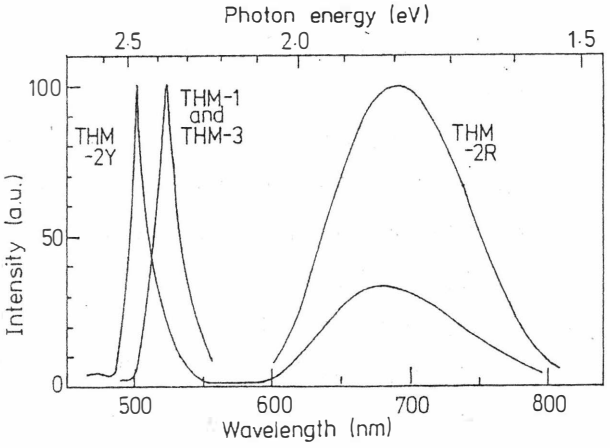

Fig.3 Photoluminescence spectra of THM grown $CuGaS_2$ at 77K

showed a strong and sharp peak at 2.47eV and a week broad band peaked at 1.8eV, whereas reddish crystal of THM-2R showed only a broad red peak at 1.8eV. Because the sharp green peak is the band edge luminescence including the exciton luminescence, the red shift of this peak can be used to evaluate the content of indium in $CuGa_{1-x}In_xS_2$ alloy. Indium content, about 3% (THM-2Y) and 10% (THM-1 and THM-3), agrees with those from the lattice constants.

Since $CuGaS_2$ has a large optical activity and an accidental isotropic wavelength in their birefringence dispersion curve, one can construct a line eliminating filter at the isotropic wavelength /2/. The isotropic wavelength was measured by fringes technique on some polished THM grown single crystal grains. The measured isotropic wavelength is 655 nm at room temperature which is very close to the 647 nm line of Kr^+ ion laser. Hence, the THM grown $CuGaS_2$ crystal is very suitable for the filter of Kr^+ laser line.

REFERENCES

1. S. W. Wagner, J. L. Shay, B. Tell and H. M. Kasper, Appl. Phys. Lett. 22 (1973) 351.
2. H. Horinaka, T. Okudo and N. Yamamoto, Jpn. J. Appl. Phys. 28 (1989) 1328.
3. H. M. Kasper, in: NBS Special Publication No. 364, Solid State Chemistry, Proceedings of the 5th Materials Research Symposium, (July, 1972), p. 671.
4. N. Yamamoto and T. Miyauchi, Jpn. J. Appl. Phys. 11 (1972) 1383.
5. N. Yamamoto, H. Kubo and T. Miyauchi, Jpn. J. Appl. Phys. 14 (1975) 299.
6. R. H. Plovnik, Mat. Res. Bull. 10 (1975) 555.
7. H. J. Höbler, G. Kühn and A. Tempel, J. Cryst. Growth 53 (1981) 451.
8. H. J. Höbler, G. Kühn, A. Tempel and H. Neumann, Jpn. J. Appl. Phys. 20 (1981) 307.
9. K. Hirakawa, H. Nakamura and M. Aoki, Jpn. J. Appl. Phys. 24 (1985) 265.
10. H. J. Hsu, M. H. Yang, R. S. Tang, T. M. Tsu and H. L. Hwang, J. Cryst. Growth 70 (1984) 427.
11. K. Sugiyama, H. Kato and H. Miyake, J. Cryst. Growth 98 (1989) 610.
12. H. Miyake and K. Sugiyama, Jpn. J. Appl. Phys. 29 (1990) L1001.
13. H. Miyake and K. Sugiyama, Jpn. J. Appl. Phys. to be published.

ANOMALOUS TEMPERATURE DEPENDENCE OF THE ELECTRICAL RESISTIVITY OF $CuGa(S_{1-x}Se_x)_2$ SYSTEM

S.Endo, H.Matsushita, H.Nakanishi and T.Irie
Science University of Tokyo, Tokyo, Japan
S.Nomura
Nihon University, Tokyo, Japan

The $CuGa(S_{1-x}Se_x)_2$ system have peculiar optical and electrical properties. On some of the samples of CuGaSSe, drastic changes in the electrical resistivity and the optical transmission were observed in the temperature range from 90 to 160℃.

The $CuGa(S_{1-x}Se_x)_2$ system is a mixed crystal system between $CuGaS_2$ and $CuGaSe_2$ and belong to the ternary chalcopyrite type semiconductors. The optical properties of this system have been reported by several authors /1-5/. However, the electrical and thermodynamical properties have been studied little. In this work, the crystallographic, optical and electrical properties of the $CuGa(S_{1-x}Se_x)_2$ system are investigated.

The samples of this system were prepared by the normal freezing method. It was confirmed that all of the samples showed a chalcopyrite structure. The compositions of the samples were determined by electron probe microanalysis (EPMA). It was found that all of the samples have the band gap of direct transition and show p-type conduction. The phase diagram of this system indicates a perfect solubility throughout the system /5/. The compositional dependence of the lattice constants and the optical band gap of this system obeyed Vargard's law /2,3,5/. This system showed an orange photoluminescence for $x \leq 0.5$ with an excitation by Ar^+-laser (2.54eV). The peak energy of the emission spectrum decreases

linearly with an increase of composition x /3,5/.

It was found that this system have some peculiar properties as follows:

1) Temperature coefficient of the optical band gap, $|dE_g/dT|$, in the region between room temperature and about 125℃ is largest for the composition x=0.5 and is 7.2×10^{-4}eV·K^{-1}.

2) The Hall mobility has a maximum of about 40cm²·V^{-1}·s^{-1} at x=0.5, in contrast to the general tendency expected from the alloy scattering theory as shown in Fig.1.

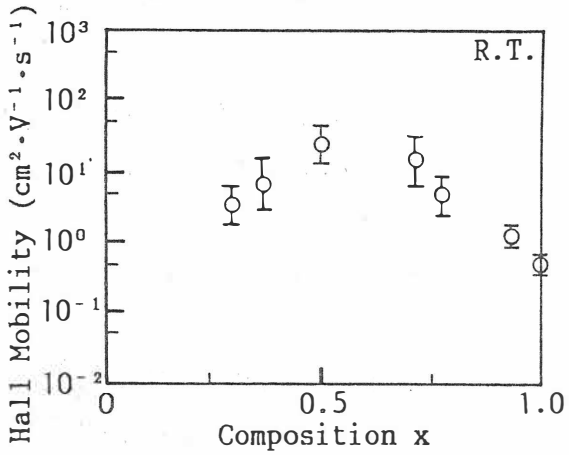

Fig.1. Hall mobility as a function of composition x.

On some of the samples of CuGaSSe, it was found that the electrical resistivity decreases more than a factor of 10^6 in the temperature range from 90 to 160℃ as shown in Fig.2. This drastic change in the electrical resistivity does not due to the intrinsic conduction as the slope of the curve leads to an activation energy much higher than the energy gap.

The optical transmission at the wave length of 700 nm was also measured on this sample as a function of temperature. It should be noted that the transmission also decreases with an increase of temperature in the similar manner to that of the change in the electrical resistivity as shown in Fig.3.

Figure 4 shows the powder X-ray diffraction patterns at the temperatures below and above the phase transition temperature, indicating that some structure change occurs at this temperature. The transition phenomena above mentioned in the electrical, optical and crystallographic properties were found to be reversible.

We have also measured differential scanning calorimetry (DSC) of the sample near the transition temperature, and the result is shown in Fig.5. It is noted that a broad endothermic reaction

occurs at the temperature range from 90 to 140℃.

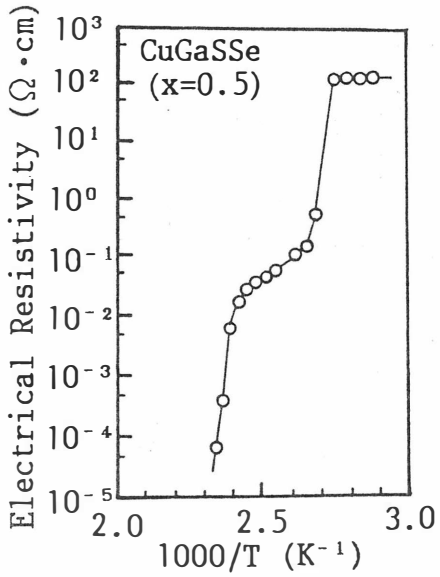

Fig.2.Electrical resistivity of CuGaSSe as a function of temerature.

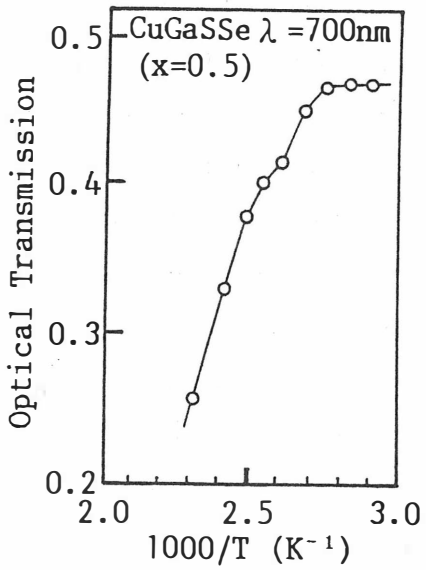

Fig.3.Optical transmission at 700 nm of CuGaSSe as a function of temperature.

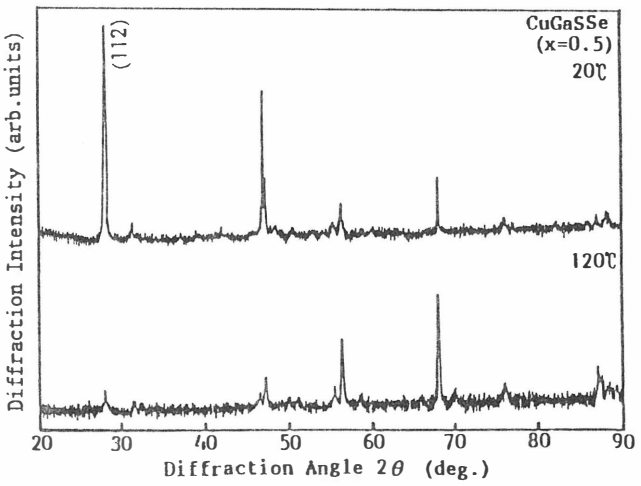

Fig.4.Powder X-ray diffraction patterns of CuGaSSe at 20 and 120℃.

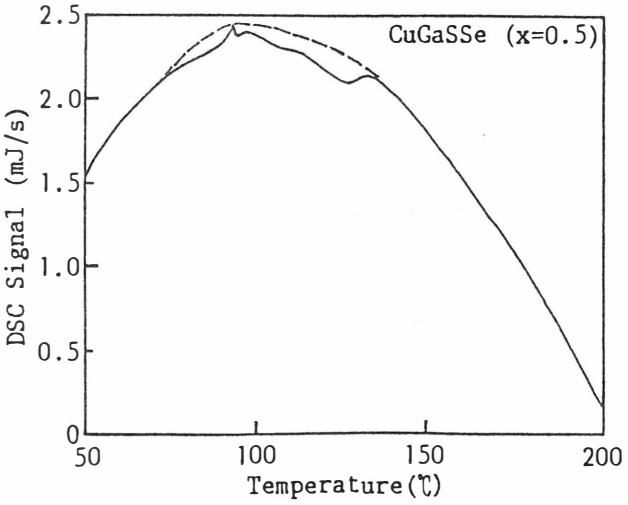

Fig.5.DSC signal curve of CuGaSSe as a function of temperature.

In order to examine whether the transition phenomena, we have found in CuGaSSe is related with the order-to-disorder transition, a structural calculation by the computer simulation method has been made.

Figure 6(a) shows the pattern calculated assuming the usual chalcopyrite structure. Figure 6(b) shows the pattern calculated

assuming the sphalerite structure in which two kinds of cation, i.e., Cu and Ga, are in disorder. In this case, the decreasing of the (112) line can not be explained. Figure 6(c) shows the pattern calculated assuming chalcopyrite structure in which two kinds of anions, i.e., S and Se, is in order. In this model, The decreasing of the (112) line can not also be explained. From these calculations, it is considered that the phase transition we have found on CuGaSSe is not a simple order-to-disorder transition. In order to better understand the origin of the phase transition more detailed information concerning the quaternary phase diagrams Cu,Ga,S,Se are needed.

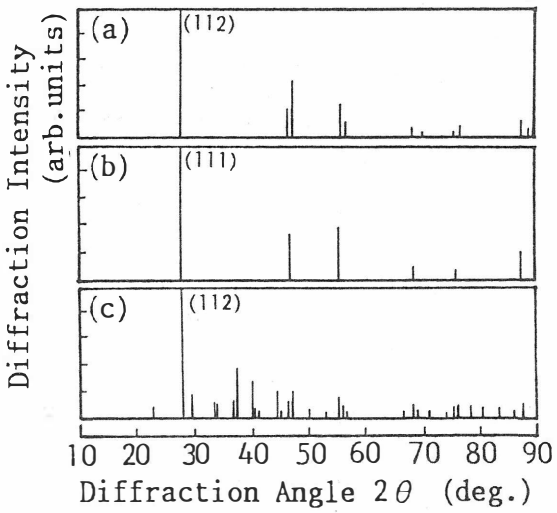

Fig.6.A comparison of X-ray powder diffraction patterns of CuGaSSe with those calculated ones by computer simulation method.

REFERENCES

1.M.Quintero, K.Yoodee and J.C.Woolley: Can.J.Phys. 64(1986)45.
2.M.Robbins and V.G.Lambrecht: Mater.Res.Bull. 8(1973)703.
3.S.Tanaka, S.Kawani, H.Kobayashi and H.Sasakura: J.Phys.Chem. Solids 38(1977)680.
4.N.Yamamoto, H.Horinaka, K.Okada and T.Miyauchi: Jpn.J.Appl.Phys. 16(1977)1817.
5.H.Matsushita, S.Endo, H.Nakanishi, S.Nomura and T.Irie: Jpn.J.Appl.Phys. 29(1990)484.

PHOTOLUMINESCENCE AND RAMAN SPECTRA OF $CuInSe_2$ SINGLE CRYSTALS

H.NAKANISHI, T.MAEDA, S.ANDO, S.ENDO and T.IRIE
Science University of Tokyo, Noda 278 (Japan)
H.TANINO and T.YAO*
Electrotechnical Laboratory, Tsukuba 305 (Japan)

Peak energies of the emission band of Cd- and Zn-doped $CuInSe_2$ single crystals were found to decrease with an increase of doping concentration. New phonon modes at 212, 228, and 260cm^{-1} were observed in the Raman spectrum of pure $CuInSe_2$.

The chalcopyrite-type ternary semiconductor $CuInSe_2$ is a technologically interesting material, because of the potential application to the optoelectronic devices and solar cells. The electrical and optical properties of $CuInSe_2$ have been reported in many literatures and it has been found that $CuInSe_2$ can be made both n- and p-type by suitable choice of the growth conditions, the subsequent thermal treatment, or Cd-implantation./1,2,3/ However, the photoluminescence of $CuInSe_2$ in connection with carrier concentration and absorption edge has not yet been studied. In this paper, the experimental result on the photoluminescence of p-type (with excess Se) and n-type (doped with Cd, Zn, or excess In) $CuInSe_2$ single crystals grown by normal freezing in connection with the doping concentration are presented. We also report on the results of the Raman scattering experiments.

The single crystals were grown by melting the elements in an evacuated quartz tube followed by directional freezing. The purity of the starting materials was 99.9999%. When the crystal is grown from a melt with the composition Cu:In:Se=1:1:2.005 -2.1 and with impurity (Cd or Zn) doping by X at atomic ratio Cu:In:Se:X=1:1:2.005:0.02 0.08, it shows p- and n-type conduction, respectively.

*present address: Hiroshima University, Higashihiroshima 724 (Japan)

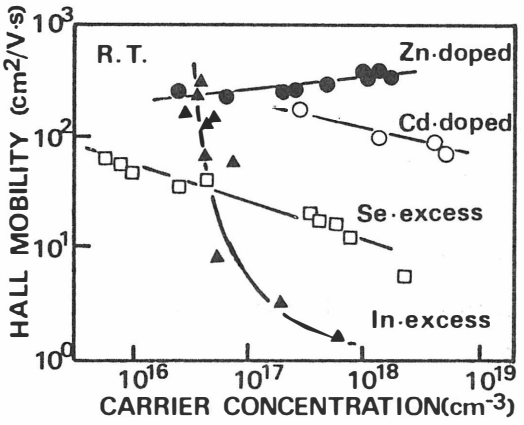

Fig.1 Hall mobility - carrier concentration dependences.

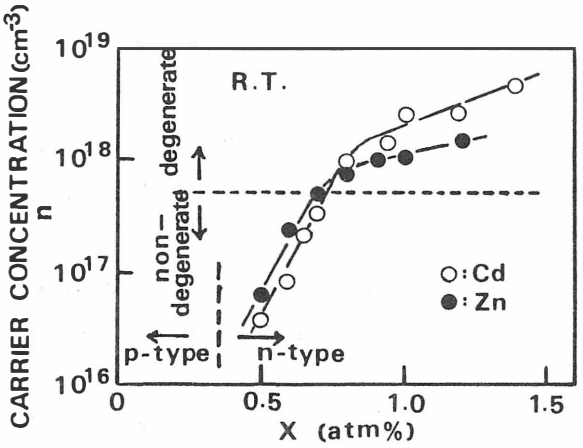

Fig.2.Carrier concentration as a function of doping X(Cd,Zn).

We have made a comparison of the carrier concentration dependence of Hall mobility among several $CuInSe_2$ samples doping with various impurities. The result is shown in Fig.1. It was found that the effect of doping on the lowering of mobility is large in order of In, Se, Cd and Zn. The electrical resistivity and the Hall coefficient of the Cd- or Zn-doped $CuInSe_2$ were measured in the temperature range from 77K to 300K. The temperature dependence of the Hall mobility indicated that the carriers are scattered by the ionized impurities at low temperatures. It was found that the donor levels are located at 0.01 eV (Cd) and 0.02 eV (Zn) below the conduction band edge, and that n-type $CuInSe_2$ samples with the carrier concentration than $5\times10^{17}cm^{-3}$ are degenerate. The carrier concentration n as a function of X for n-type $CuInSe_2$ (Cd,Zn) is shown in Fig.2. In the non-degenerate region, it can be seen that *log* n increases linearly from X=0.5 atm% to 0.7 atm%.

The optical absorption spectra of p- and n-type $CuInSe_2$ with various carrier concentrations were measured. It was found that the absorption edges of the n-type samples lie in the lower energy region in the spectrum than those of the p-type samples and depend on the carrier concentration. The tendency is consistent with the effect of doping on the lowering of mobility mentioned above.

The photoluminescence spectra of p- and n-type samples were measured with an Ar^+ laser (488nm) excitation. Figure 3 shows the typical photoluminescence spectra of p- and n-type samples. The p-type samples showed three emission bands peaked at about 1.03 eV, 1.01 eV and 0.98 eV. These values are in good agreement with the published values assigned as free-to-bound

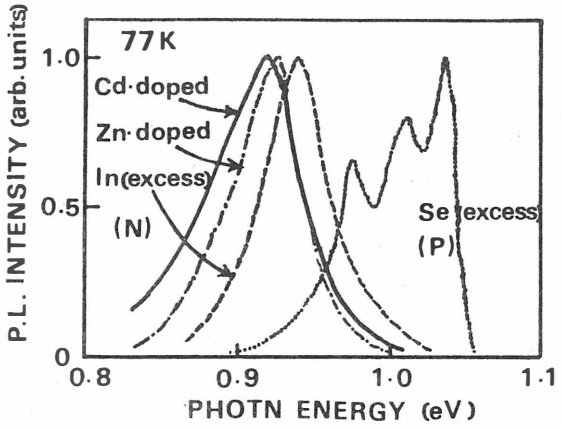

Fig.3.The typical PL spectra of p- and n-$CuInSe_2$ samples.

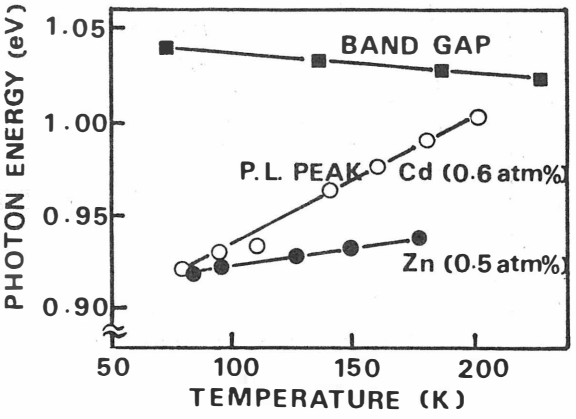

Fig.4.Temperature dependence of peak energy of PL.

or donor-to-acceptor transitions attributed to Se vacancies (donor) and Cu vacancies (acceptor)./2,4,5/ The n-type samples doped with In, Zn and Cd showed emission bands peaked at about 0.94 eV, 0.92 eV and 0.91 eV, respectively. Figure 4 shows the peak energy of the photoluminescence for Cd- and Zn-doped samples as a function of temperature. For comparison, the band gap energies obtained by the absorption measurements/6,7/ are also plotted. The temperature coefficients of the peak energies are 6.7×10^{-4} eV/K and 1.9×10^{-4} eV/K for Cd- and Zn-doped samples, respectively. We have also measured the photoluminescence for various excitation intensities and found that the peak energy increases with increasing excitation intensity for both Cd- and Zn-doped samples. These results indicate that the emission in Cd- and Zn-doped samples is probably due to donor-acceptor pair recombinations, i.e. transitions from donor level by Cd or Zn impurities to acceptor level by probably In vacancy or Cu-In antisite defects./8/ Figure 5 shows the peak energy as a function of doping concentration for Cd- and Zn-doped samples. It was found that the peak energies decrease with an increase of the doping concentration between 0.6 and 1.2 atm%. Taking the band gap energy equal to 1.04 eV at 77K and using the donor ionization energies determined from the Hall measurements, an acceptor ionization energy can be determined as 0.10 eV. This value is in good agreement with the published value of acceptor level due to In vacancy or Cu-In antisite defects.

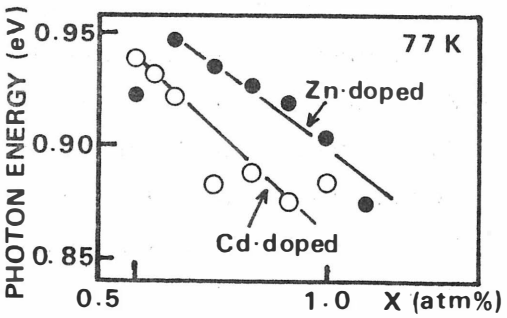

Fig.5.Doping concentration dependence of peak energy.

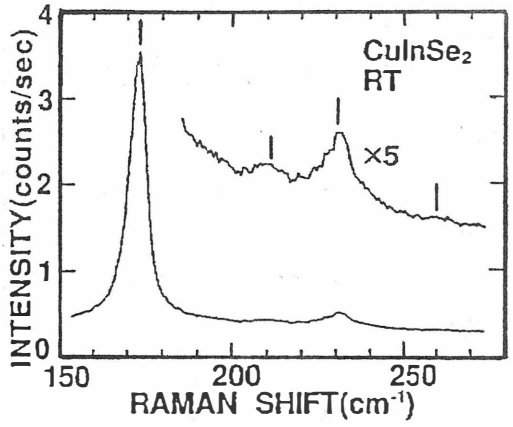

Fig.6.Raman spectra of $CuInSe_2$ for (112)face at RT.

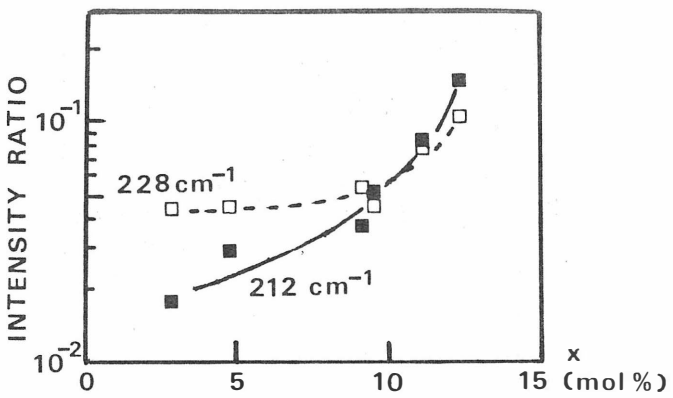

Fig.7.Intensity ratio of new Raman modes to A_1 mode as a function of x in $(1-x)CuInSe_2-xIn_2Se_3$.

The Raman scattering experiments were performed at room temperature in a back-scattering configuration. The excitation light source was the Ar or Kr ion laser line at 2.41 eV and 1.92 eV. The A_1 mode which involves motion of Se atom is not observed at $186cm^{-1}$/9,10/,but at $173cm^{-1}$(Fig.6). In addition, we have found new modes at $212cm^{-1}$, $228cm^{-1}$, and $260cm^{-1}$. All of them are assigned to B_2+E,respectively, by polarized scattering experiment.

Furthermore, we have studied the Raman spectra of the single crystals in the $(1-x)CuInSe_2-xIn_2Se_3$ alloy system. As In_2Se_3 content increases, the Raman intensity ratios of the $212cm^{-1}$ and $228cm^{-1}$ modes to the A_1 mode increase as shown in Fig.7. The modification of the structure and the electronic state of alloys may affect the resonance Raman scattering efficiency of each mode.

REFERENCES

1.P.Migliorato,J.L.Shay,H.M.Kasper and S.Wagner:J.Appl.Phys.46 (1975)1777.

2.P.W.Yu:J.Appl.Phys,47(1976)677.

3.S.Endo,T.Irie and H.Nakanishi:Solar Cells 16(1986)1.

4.C.Rincón,J.González and G.S.Pérez:J.Appl.Phys,54(1983)6634.

5.F.A.Elfotouh,D.J.Dunlavy,L.L.Kazmerski,D.Albin,K.J.Bachman and R.Menner:J.vac.sci.Technol.A6(1988)1515.

6.R.E.Hollingsworth and J.R.Sites:IEEE,(1985)1409.

7.H.Nakanishi,S.Endo,T.Irie and B.H.Chang:Ternary and Multinary Compounds,eds,S.K.Deb and A.Zunger(MRS,1987),p.99.

8.S.M.Wasim:Solar Cells,16(1986)289.

9.J.N.Gan,J.Tauc,V.G.Lambrecht,Jr. and M.Robbins:Phys.Rev.B13 (1976)3610.

10.H.Neumann:Sollar Cells,16(1986)399.

BEHAVIOR OF AMPHOTERIC IMPURITIES OF Zn AND Cd IN $CuGaS_2$ CRYSTALS

Akihiro OOE*, Nozomu TSUBOI, Hitoshi KINTO,
Seishi IIDA and Hiroshi FURUSAKI
Nagaoka University of Technology
Kamitomioka, Nagaoka 940-21, Japan

Photoluminescence studies of Zn- and Cd-doped $CuGaS_2$ crystals grown by the iodine transport method present clear evidence that both atoms make several isolated donor and acceptor levels in p-type $CuGaS_2$. The level origins are discussed.

INTRODUCTION

Group-II elements Zn and Cd impurities in $CuGaS_2$ are possibly amphoteric, being donors on the Cu sites and acceptors on Ga sits. Our recent photoluminescence study revealed that Zn atoms make isolated shallow donor and acceptor levels in $CuGaS_2$ at relative low doping levels[1]. The origin assignments of these levels were done by a careful consideration for possible combinations of substitutional Zn_{Cu} and Zn_{Ga}, vacancies which could arise from a difference in numbers of Zn_{Cu} and Zn_{Ga}, and pair complexes formed from substitutional Zn atoms and vacancies.

The purpose of this paper is to reconsider the assignments described in the previous paper by studying photoluminescence (PL) of Zn-doped crystals made under different preparation conditions and to examine the situation of Cd-doped crystals for comparison.

SAMPLES and MEASUREMENTS

Zn or Cd doped single crystals used in this study were grown by the iodine transport method in a manner reported in reference 1. Zn-doped crystals used in this study were prepared from sources satisfying $Cu_{1-x}Zn_xGaS_2$ (x=0.0005) and $CuGa_{1-x}Zn_xS_2$ (x=0.0005) relations, since preferential doping of Zn impurities on Cu site or Ga sites was intended in contrast to the previous study. Cd-doped crystals were prepared from sources satisfying $(CuGa)_{1-x/2}Cd_xS_2$ (x=0.005, 0.01, 0.05), $Cu_{1-x}Cd_xGaS_2$ (x=0.05) and $CuGa_{1-x}Cd_xS_2$ (x=0.05) relations.

The amounts of Zn in $(CuGa)_{1-x/2}Zn_xS_2$ crystals were reported to correspond roughly to those added in sources by EPMA studies[1]. The amounts of Zn included in the present crystals are thought also to correspond to those added in sources[2] as in the case of $(CuGa)_{1-x/2}Zn_xS_2$ crystals. The amounts of Cd in the crystals detected by EPMA studies were, however, smaller than those added in sources by about one to two order(s) of magnitude. The crystal composition x appearing in

*Present address: The Univ. of Electro-Communications, Chofugaoka Chofu 182, Japan

this paper always corresponds to the source composition and does not mean actual one. However, in the case of Zn-doped crystals, the composition x is believed to be close to the real one, as described above.

The resistivity values of $CuGa_{1-x}Zn_xS_2$ (X=0.0005) crystals were reduced down to 10^2~10^3 Ωcm, while those of all other doped crystals were in the same range of 10^5~10^7 Ωcm as in undoped crystals. Room temperature thermal-probe measurements indicated p-type conductivity for all crystals regardless of dopants.

All steady-state PL spectra as well as time-resolved (TR) spectra were measured using the same apparatus and techniques as in the previous report[1].

RESULT and DISCUSSION

The emission line at 2.504 eV seen all Zn and Cd doped crystals as well as undoped crystals under excitation by a 476.5 nm line of an Ar^+ laser is thought to be due to free exciton decay. This fact indicates that any change of band gap energy did not occur in these doped crystals.

PL spectra of Zn- and Cd-doped $CuGaS_2$ crystals are shown in Fig. 1(a) and (b), respectively. The PL spectrum of $CuGa_{1-x}Zn_xS_2$ (x=0.0005) in Fig. 1(a) shows a peak at 2.393 eV. The lower energy shoulders are thought to be due to phonon replicas. The PL spectrum of $Cu_{1-x}Zn_xGaS_2$ (x=0.0005) in Fig. 1(a) show a peak at 2.387 eV and the spectral width of this emission is broader compared to that observed for the $CuGa_{1-x}Zn_xS_2$ (x=0.0005) crystal. A considerable difference in spectral widths of these emissions seems to imply that the spectrum of $Cu_{1-x}Zn_xGaS_2$ (x=0.0005) crystal is affected by another emission at lower energy side in spite of small difference in peak energies. The PL spectrum of $(CuGa)_{1-x/2}Zn_xS_2$ (x=0.0005) which was reported previously[1] is shown again in Fig. 1(a) for comparison. The highest energy peak of this spectrum seems to coincide with the spectral peak of the emission seen for the $CuGa_{1-x}Zn_xS_2$ (x=0.0005) crystal.

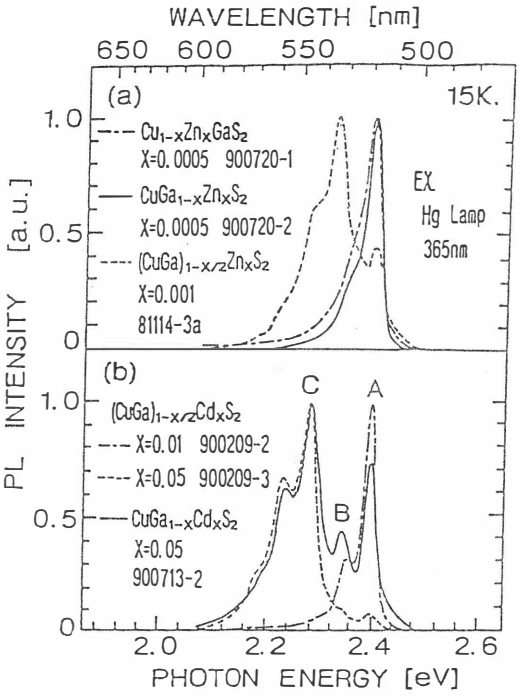

Fig. 1 Low temperature photoluminescence spectra of $CuGaS_2$ crystals doped with Zn(a) and Cd(b) in various ways.

PL spectra of Cd-doped crystals are shown in Fig. 1(b). The spectrum of $(CuGa)_{1-x/2}Cd_xS_2$ is relatively simple, showing a main peak at 2.39 eV (denoted by A), with a low energy peak and shoulders probably due to phonon replicas of the main emission. The spectrum of $CuGa_{1-x}Cd_xS_2$ crystal shows four peaks; The highest energy peak correspond to the A peak in the $(CuGa)_{1-x/2}Cd_xS_2$ crystal, and the next two peaks (labeled B and C in Fig. 1(b)) are due to different emissions being proper in this sample. The lowest energy peak is considered to be a phonon replica of the C peak. The spectrum of $(CuGa)_{1-x/2}Cd_xS_2$ crystal is believed to be

composed of these emissions (i.e. A, B and C). For $Cu_{1-x}Cd_xGaS_2$ (x=0.05) crystals, no emission was observed.

TR spectra during decay were measured for these Zn- and Cd-doped crystals. The result for $CuGa_{1-x}Cd_xS_2$ (x=0.05) is shown in Fig. 2. These spectra show shifts with time after excitation, characteristic to donor-acceptor pair transitions. Analyses of these spectra similarly as the previous report[1] gave the ionization energies of relevant shallower (E_1) and deeper (E_2) levels and the reaction constants (W_0) as summarized in Table I. The values of $E_1=64\pm^{22}_{14}$ meV, $E_2=124\pm^{3}_{3}$ meV and $W_0=2\times10^7$ s^{-1} were obtained from TR spectra of the $CuGa_{1-x}Zn_xS_2$ (x=0.0005) crystal, while those for $Cu_{1-x}Zn_xGaS_2$ (x=0.0005) could not be obtained due to broadenning of the TR spectra with time, probably related to the existence of another lower energy emission mentioned before.

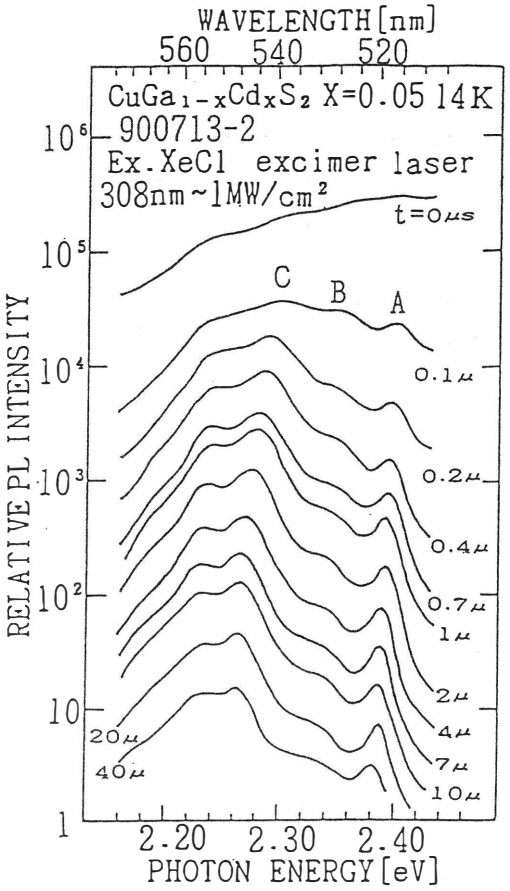

Fig. 2 Time resolved photoluminescence spectra of $CuGa_{1-x}Cd_xS_2$ (x=0.05) after pulse excitation by an XeCl excimer laser.

Table I Donor and acceptor levels relevant to the pair emissions A and C in $CuGa_{1-x}Cd_xS_2$ (x=0.05) crystal. Values of ionization energies (E_1 and E_2) and reaction constants with their accuracy were evaluated by analysing the time resolved spectra of Fig. 2 during each decay.

Emission	A	C
E_1 (meV)	$38\pm^{11}_{8}$	$89\pm^{10}_{18}$
E_2 (meV)	126±2	227±2
W_0 ($\times10^7 s^{-1}$)	$9\pm^{1}_{3}$	$4\pm^{0}_{1}$

Although there is an interesting difference between the doping efficiency of Zn and Cd in $CuGaS_2$ crystals, the small fraction incorporation of Cd does not induce V_{Cu} or V_{Ga} as far as the charge neutrality condition holds. This allows an introduction of similar assumptions for Cd doped crystals, as in $(CuGa)_{1-x/2}Zn_xS_2$ crystals[1]. For the case of $(CuGa)_{1-x/2}Cd_xS_2$ crystals, following three cases are considered possible. Case 1-1 (equal participation of Cd on Cu and Ga sites): donors; Cd_{Cu}. acceptors; Cd_{Ga}. Case 1-2 (larger participation of Cd on Cu sites): donors; Cd_{Cu}, Cd_{Ga}-V_S and V_S. acceptors; Cd_{Ga}, Cd_{Cu}-V_{Ga} and V_{Ga}. Case 1-3 (larger participation of Cd on Ga sites): donors; Cd_{Cu}, Cd_{Ga}-V_S and V_S. acceptors; Cd_{Ga} and V_{Cu}. Since only one shallower level of ~38 meV and one deeper level of ~120 meV were observed in $(CuGa)_{1-x/2}Zn_xS_2$ (x=0.005, 0.01) crystals, the defect formation in the crystals is thought to correspond to case 1-1. This is not unreasonable at the low Cd concentration described above.

In the case of x=0.05 in $(CuGa)_{1-x/2}Cd_xS_2$ where x is larger than the previous

case, the defect formation is considered to correspond either to case 1-2 or to case 1-3, since observed two donor and two acceptor levels can not be explained with case 1-1.

For $CuGa_{1-x}Cd_xS_2$ crystals, possible situations are following two cases. Case 2-1: Cd atoms occupy only on Ga sites. Sulfer vacancies (V_S) are induced from the neutrality condition. Case 2-2: Cd atoms occupy not only on Ga sites but also on Cu sites. Gallium and sulfer vacancies (V_{Ga} and V_S) are induced. Case 2-1: donors; V_S. acceptors; Cd_{Ga}. Case 2-2: donors; Cd_{Cu}, V_S, Cd_{Ga}-V_S. acceptors: Cd_{Ga}, V_{Ga}, Cd_{Cu}-V_{Ga}. The existence of three emissions (A, B and C) in $CuGa_{1-x}Cd_xS_2$ ($x=0.05$) crystals excludes case 2-1. Since the ionization energies of the two shallower levels relevant to A and C emissions is smaller than the calculated hydrogenic acceptor binding energy (110 meV)[1], it is not unreasonable to ascribe these levels to donors rather than to acceptors. If we adapt the previous assignments[1] that the level of ~155 meV or ~204 meV is due to V_{Ga}, the origin of the level of ~227 meV is considered to be not due to V_{Ga} but to Cd_{Cu}-V_{Ga} in case 2-2. Taking into account this possible assignments that two different acceptors are due to Cd_{Ga} and Cd_{Cu}-V_{Ga}, the defect formation in $CuGa_{1-x}Cd_xS_2$ ($x=0.05$) may correspond to case 1-2. It becomes necessary to select either Cd_{Cu}-V_S or V_S as the origin of the donor of ~89 meV in case 1-2. It is not unreasonable to consider that the B emission in Fig. 1(b) is caused by the pair transitions between the donors of E_D ~89 meV and acceptors of E_A ~126meV.

The reported E_1 and E_2 values[1] for the highest energy emission of $(CuGa)_{1-x/2}Zn_xS_2$ ($x=0.001$) in Fig. 1(a) are ~70 meV and ~120 meV, respectively. These values are close to the values of E_1=64 meV and E_2=124 meV obtained for $CuGa_{1-x}Zn_xS_2$ ($x=0.0005$) crystal in this study. However, the reported reaction constant (~6×10^7 s^{-1}) for the emission in $(CuGa)_{1-x/2}Zn_xS_2$ ($x=0.001$) differs slightly from the value of 2×10^7 s^{-1} obtained here. If we conceive the difference, the situation for $CuGa_{1-x}Zn_xS_2$ ($x=0.0005$) would be similar to the case 2-1 for the Cd doped crystal. On the other hand, if we ignore this difference, the situation would be similar to the case 2-2 for the Cd doped crystal, and the most simple assignments are to ascribe the observed E_1 and E_2 levels to Zn_{Cu} donors and Zn_{Ga} acceptors, similar to the case of $(CuGa)_{1-x/2}Zn_xS_2$ ($x=0.001$). The reduced resistivity observed for the $CuGa_{1-x}Zn_xS_2$ ($x=0.0005$) crystal imply the existence of shallow acceptors. This result is consistent with the observation[2] of reduced resistivity associated with annealing in a Zn plus S atmosphere.

We thank H. Ishikawa and M. Igarashi for their help in the experiments. TR spectra were taken at the laser laboratory of the university. This work was partly supported by a Grant-in-Aid for Scientific Research, No. 01604001.

REFERENCES

1. A. Ooe and S. Iida: Jpn. J. Appl. Phys. 29(1990) 1484.
2. A. Ooe, S. Iida, M. Yagi, H. Kawaguchi and T. Inagaki: Proc. 7th Int. Couf. Ternry and Multinary Compounds, Snowmass, Colorad, 1986, (Materials Res. Soc. Pittsburg, 1987) p471.

OPTICAL CHARACTERIZATION OF Fe ATOMS IN $CuMS_2$ (M=Al, Ga AND In) CRYSTALS

Katsuaki Sato
Faculty of Technology, Tokyo University of Agriculture and Technology, Koganei, Tokyo 184, Japan

Transition atom impurities are known to introduce optical absorption bands and photoluminescence lines in the below-gap spectra of semiconductors, resulting in coloration of crystals. This paper focuses on the optical properties introduced by Fe impurities in Cu-III-S_2 semiconductors.

Introduction

We have been working with optical characterization of transition atom impurities in chalcopyrite semiconductors containing Cu as a constituent element/1-13/. Through these works we elucidated that transition atoms introduce characteristic absorption bands in the below-gap energy region and pointed out that some of them are responsible for coloration of crystals.

Some of the sub-gap optical spectra have been interpreted in terms of ligand field transition between multiplets in the $3d^n$ system. Some have been understood as so-called charge transfer transitions between the ligand orbitals and the 3d orbitals of transition atoms. This type of transition is often referred to as a photoionization transition by the researchers in the semiconductor field and is considered to be directly related to the relative energy position of the transition atom to the host band edge. In addition to these "on-site" energy states, incorporation of the transition atom often introduces some defects or vacancy aggregates. Formation of these defect occurs partly due to the difference in the atomic radius from that of the host atom and partly due to the requirement to hold the charge neutrality condition.

The present paper focuses on the optical properties of Fe atoms in chalcopyrite crystals and discusses on the electronic and crystallographic aspects of the Fe impurity.

Results and Discussion

(1) Origin of Coloration of $CuGaS_2$ and $CuAlS_2$ Grown by Chemical Transport

Wide-gap chalcopyrite-type crystals of $CuAlS_2$ and $CuGaS_2$ grown by the chemical vapor transport (CVT) technique are usually colored in blue and green, respectively. These colors are caused by the strong absorption band located between 0.6 and 2.5 eV, which is greatly reduced by annealing the crystals in the vacuum. Through the EPR measurements von Bardeleben et al. ascribed the origin of the absorption band to the trace Fe or Ni impurities/14/. We showed that Fe ions doped in these crystals result in a strong charge-transfer type transition below the absorption edge of the host crystals/1/. The molecular orbital calculation by Kambara et al./15/ in the 17 atom-cluster surrounding the Fe impurity located empty d levels in the band gap supporting our assumptions. However, the origin of the coloration seems not so simple. Even those crystals made from the purest sources are colored. In contrast to CVT-crystals, those grown from the melt or the solution are often colored in dark brown.

In Fig. 1 absorption spectra of undoped and Fe-doped crystals grown by CVT are plotted./12/ We performed the chemical analysis of Fe impurities in undoped and Fe-doped single crystals of $CuGaS_2$, by which it was found that even the undoped crystals contained Fe-impurities to the concentration of the order of 100 ppm. It was also elucidated that the analyzed concentration of iron in the grown crystal was approximately the same with the nominal Fe concentration of the starting material as listed in Table 1.

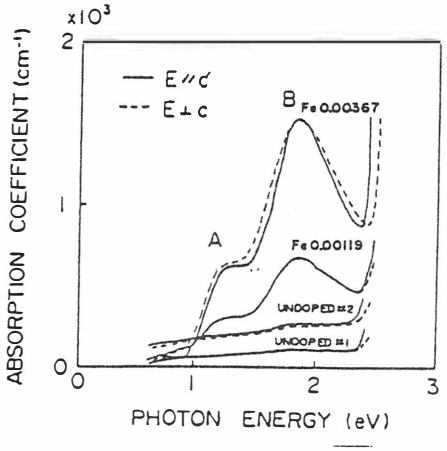

Fig. 1 Polarized absorption spectra in single crystals of undoped and Fe-doped $CuGaS_2$.

Table 1 Results of the quantitative Chemical analysis of Fe in undoped and Fe-doped $CuGaS_2$.

Sample name	Fe concentration X	
	nominal	analyzed
Fe 0.01	0.01	0.0102
Fe 0.003	0.003	0.00367
Fe 0.0001	0.0001	0.00119
Undoped #1	0	0.00011
Undoped #2	0	0.00034

Using the analyzed concentration the absorption cross section per Fe atom was estimated. As seen in Fig. 2 the estimated absorption cross section in the undoped samples was about twice that of Fe-doped samples. It is, therefore, clear that absorbing centers other than Fe are involved.

We, then, measured absorption spectra of $CuGaS_2$ doped with 1 mol% Ni impurities. The result is plotted in Fig. 3, from which it is found that Ni also introduces strong absorption below the band gap similar to that observed in Fe-doped crystals, although details of the structure seem to be different.

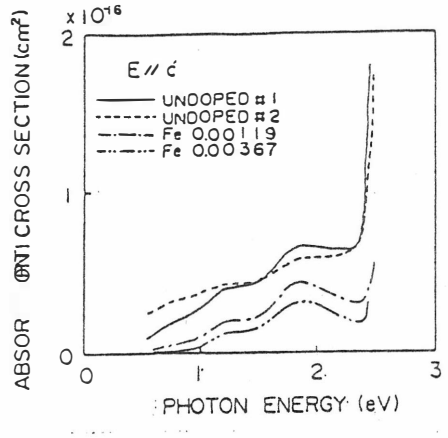

Fig. 2 Absorption cross sections per one Fe atom in undoped and Fe-doped $CuGaS_2$ deduced from the spectra shown in Fig.1.

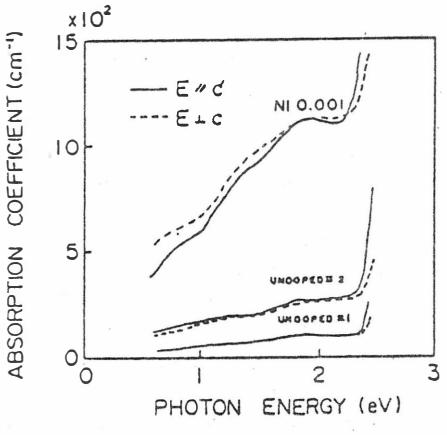

Fig. 3 Polarized absorption spectra in undoped and Ni-doped $CuGaS_2$.

More than 15 years ago we discovered sharp infrared photoluminescence(PL) lines at 0.613 eV in $CuGaS_2$ and at 0.73 eV in $CuAlS_2$./2/ PL spectra of undoped crystals measured at 20 K are shown in Figs. 4(a) and (b).

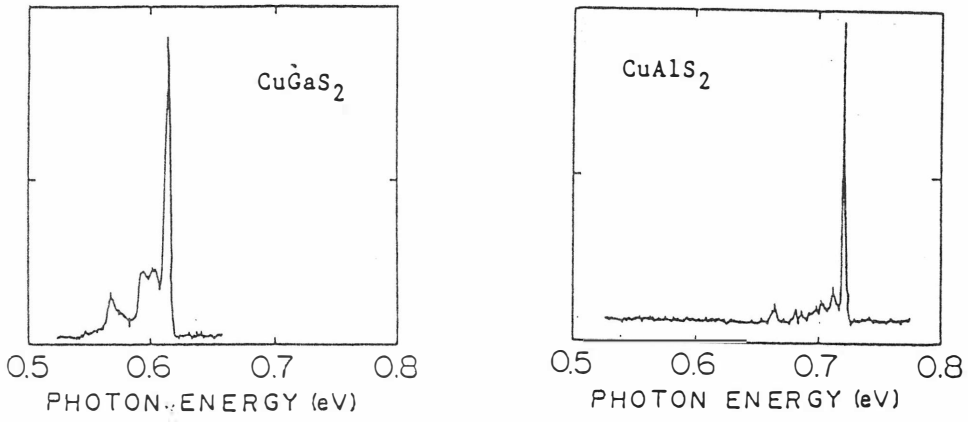

(a)$CuGaS_2$ (b)$CuAlS_2$

Fig. 4 Infrared photoluminescence spectra of undoped $CuGaS_2$ and $CuAlS_2$ crystals measured at 20 K with the excitation by the 514.5 nm line of Ar^+ ion laser.

With the help of the Zeeman spectrum shown in Fig. 5 and the spin Hamiltonian determined by EPR/16/ the PL line in $CuGaS_2$ was assigned to the ligand field transition between the excited multiplets $^4T_1$ and the ground multiplets $^6A_1$ of Fe^{3+} in the tetrahedral coordination/2/. The anomalously low energy position of the transition was explained by the theoretical approaches taking into account the configuration interaction between the $3d^5$ multiplet states and the charge-transferred states./17/

We, recently, measured the PL-excitation spectra of the Fe-related luminescence, which are shown in Figs. 6(a) and 6(b) by solid curves. For comparison absorption spectra of Fe-doped crystals are plotted by dotted curves in both figures. It is clearly observed that the threshold energy of the excitation band agrees with that of the iron-induced absorption band However, of the two absorption peaks introduced by iron, only the low-energy peak is found to be able to excite the Fe-related infrared luminescence. The high-energy peak which makes crystals dark in the visible region seems not to be directly related to the Fe^{3+} center.

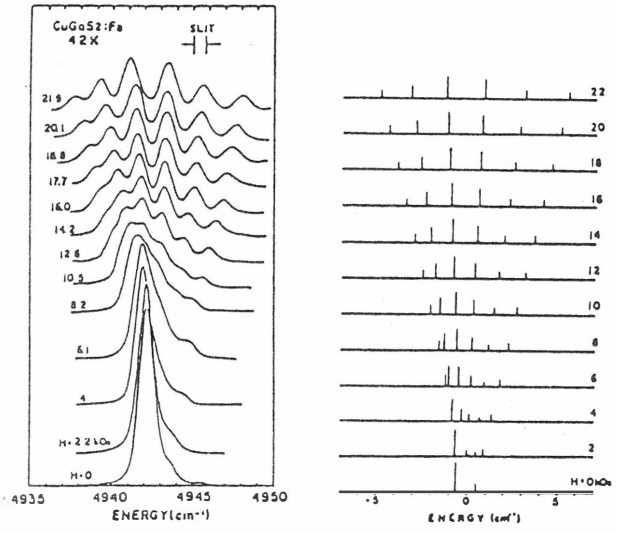

(a) (b)

Fig. 5 Zeeman spectra of the infrared PL line in $CuGaS_2$.
(a)Observation and (b)calculation assuming $^4T_1 \rightarrow {}^6A_1$ in Fe^{3+}.

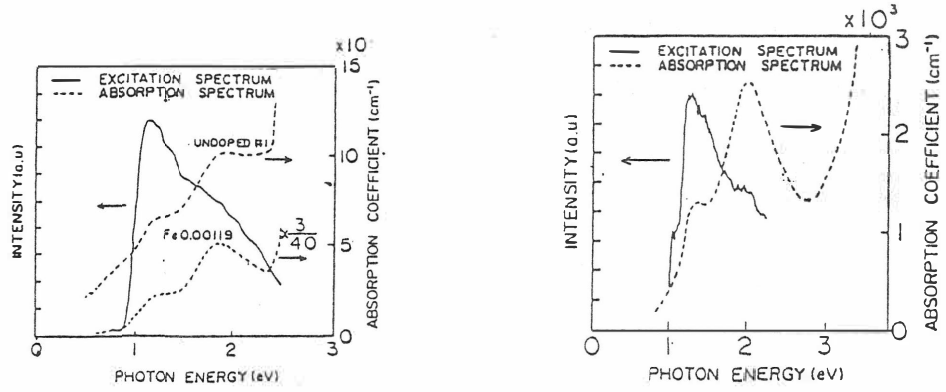

(a) $CuGaS_2$ (b) $CuAlS_2$

Fig.6 Excitation spectra of the Fe^{3+}-related infrared photoluminescence in (a) $CuGaS_2$ and (b) $CuAlS_2$ at 20 K.

It is concluded that the absorption band in the visible region in CVT-grown crystals is not directly associated with the Fe^{3+} center but related to some other centers likely to be assigned to a defect. The defect may be introduced either by doping of the transition elements or by thermal treatments.

(2) Relation between the below-gap absorption spectra and infrared photoluminescence in undoped $CuGaS_2$ grown by the chemical transport

We measured both below-gap absorption spectra and infrared photoluminescence spectra on three samples supplied by Nagaoka Technical University. These crystals were grown by the chemical transport technique with different growth conditions. As shown in Fig. 7 these three samples show different features of absorption spectra although starting materials with the same purity were employed. Of the three curves, the solid one has rather different feature from the other; the sample was the darkest of the three samples measured. This crystal was prepared by quenching from the high temperature during the chemical transport.

The Fe^{3+} photoluminescence spectra at 20 K are shown in Fig. 8. The Fe-related emission loses intensity as the below-gap absorption increases. No infrared luminescence line was observed in the quenched sample in which strong below-gap absorption was observed.

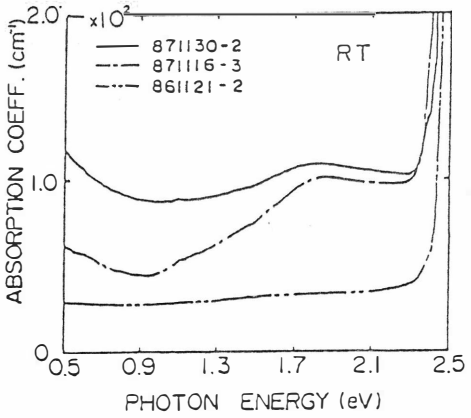

Fig. 7 Absorption spectra in three $CuGaS_2$ crystals prepared with different growth conditions.

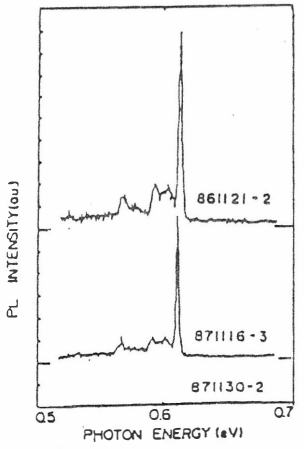

Fig. 8 Infrared photoluminescence in the same $CuGaS_2$ single crystals as shown in Fig. 7.

This results apparently denies a direct relationship between the Fe^{3+} center and the below-gap absorption band. However, it should also be noted that re-absorption of the emitted light may occur in dark sample. Another interpretation is that valency of Fe changed from trivalent to divalent. Therefore, we would like to leave the conclusion to the future works including EPR characterizations.

(3) Assignment and Characterization of Fe-related Infrared Luminescent Centers in $CuGaS_2$ and $CuAlS_2$/13/

In chalcopyrite-type compounds, iron ions are usually assumed to substitute the group III atom site, since there exists a compound $CuFeS_2$. However, it is not self-evident whether transition atoms substitute the group-I or group-III sites when they are doped in very low concentration. In order to elucidate this point we grew solid-solution crystals with different composition of two group III elements, ie. $CuAl_xGa_{1-x}S_2$ with x varied between 0 and 1.0. We employed the Fe^{3+}-related infrared photoluminescence as a probe to estimate the local atomic arrangements around the impurity atom.

Fig. 9(a) shows infrared PL spectra in undoped single crystals of $CuAl_{1-x}Ga_xS_2$. Essentially the same trend was observed in the Fe-doped samples. As shown in the figure, crystals with the extreme compositions, i.e. x=0 ($CuAlS_2$) and x=1 ($CuGaS_2$), show a sharp PL line with linewidth less than 1 meV. On the other hand, those with intermediate compositions show no sharp PL line but a broad PL band consisting of several equally-spaced fine structures.

In $CuAl_{1-x}Ga_xS_2$:Fe all of the four next neighbor (nn) sites of Fe are occupied by sulfur atoms, and the twelve nnn sites are occupied by Cu and group III elements. There are two cases in the occupancy of Ga or Al atoms in the n.n.n. sites depending on whether the Fe ion substitutes the group III atom site (Case I) or the Cu site (Case II). In Case I eight of the twelve nnn sites are reserved for Cu atoms, so that only the remaining four are occupied by the group III atoms (either Ga or Al). Therefore, there are five kinds of atomic arrangements depending on the occupation number of Al and Ga in the four sites, thus giving five zero-phonon lines, provided that one zero line corresponds to each atomic arrangement. On the other hand, in Case II the nnn sites have eight seats for group III elements and four for Cu, resulting in nine zero-phonon lines associated with nine possible local atomic arrangements.

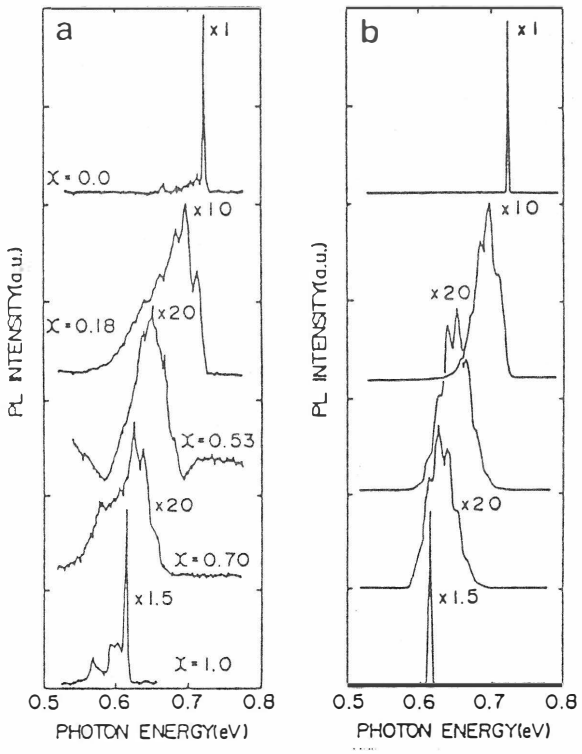

Fig.9 Infrared photoluminescence spectra in $CuAl_{1-x}Ga_xS_2$.
(a)Experiment an, (b)calculation.

From the PL spectra shown in Fig. 9(a), one finds that the fine structures are approximately equally-spaced with a separation of about 13 meV. The value agrees quite well with the one calculated by dividing the energy separation between the PL energies of $CuAlS_2$:Fe and $CuGaS_2$:Fe by eight spacings, i.e. (0.72-0.613)/8=0.0134. This suggests that the Case II holds in our system.

Assuming that one zero-phonon line corresponds to each atomic arrangement, we can simulate the spectrum by using nine equally spaced Gaussian lines with relative intensity given by the probability P_n. We adjusted the line positions so as to give the best fit to the observed spectrum. In Fig. 9(b) the simulated results are demonstrated. Most of the observed structures are reproduced by the simulation, although agreement is not satisfactory for the low energy part of the spectrum. The disagreement may be due to our neglect of phonon side bands which exist in the low energy side of the zero-phonon line as observed in the case of x=0 or x=1.

We conclude that the Fe^{3+} ion substitutes the Cu-site, contrary to the commonly accepted concept that the Fe^{3+} may substitute the Ga^{3+} or Al^{3+} site to attain the charge neutrality.

(4) Photoluminescence Decay Characteristics of the Fe^{3+}-Related Infrared Luminescent Center

From the above-mentioned studies we found that the Fe^{3+}-related infrared luminescence has a narrow line-width and an efficient excitation band in higher energy. So it can be a candidate of a three-level solid-state laser material. For this purpose it is necessary to know the recombination life-time of the photoluminescence.

We measured a time-resolved spectrum of the Fe-related photoluminescence using a pulsed Xe-flash lamp and a boxcar integrator. The decay curves of the photoluminescence lines are plotted in Fig. 10.

The decay time of the PL was found to be 1 ms and 0.7 ms for $CuGaS_2$ and $CuAlS_2$, respectively. Thus it is concluded that the recombination life-times observed were sufficiently long to construct a solid state laser.

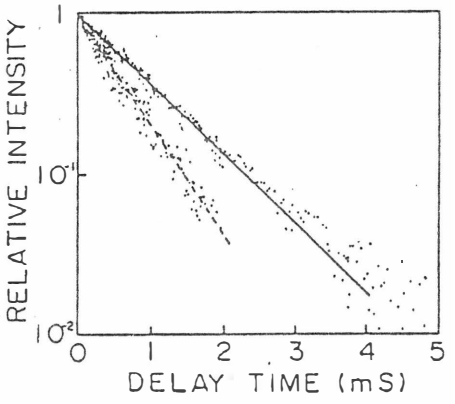

Fig. 10 Photoluminescence decay curve of the Fe-related emission in (a)$CuGaS_2$ and (b)$CuAlS_2$.

(5)What occurs when the iron concentration is increased.

When the Fe concentration exceeds 1 wt% one finds an increase in the absorption below 0.6 eV towards low energies. This tendency is clearly seen in the absorption and photoconductivity spectra of $CuInS_2$:Fe shown in Fig. 11./10/ The rise in the absorption coefficient towards low energies is thought to be a foot of an absorption band existing in the middle-infrared region. Due to an experimental difficulty we have not obtained a complete spectral shape yet. However, it can be assigned to the ligand field transition in $3d^6$ manifold localized at the Fe^{2+} center since Fe doped in $CuGaS_2$ at the concentration of 6mol% shows an intense absorption in the 0.3-0.6 eV region as shown in Fig. 12./9/

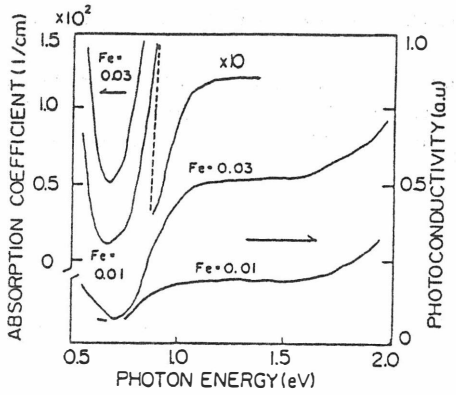

Fig. 11 Absorption spectra in $CuInS_2$ doped with Fe.

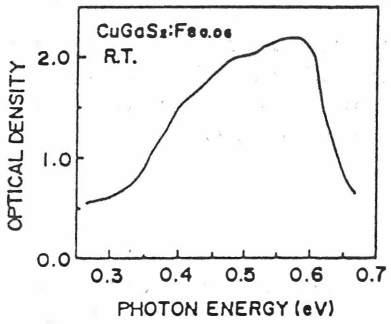

Fig. 12 Absorption spectrum of $CuGaS_2$ doped with 6 mol% Fe

Further increase in Fe concentration makes the crystal black to red-black. When the iron concentration exceeds 12-14 mol%(nominal value) sample becomes shiny with golden luster./7/ Simultaneously, the absolute value and the activation energy of electric conductivity show a jump at the concentration./6/ These experimental results were interpreted as due to the formation of Fe-related band in the crystal. However, EPR observation at Strasbourg indicated the formation of pairs, triads or such clusters, indicating that some kind of percolation path problems in the random network are involved./18/ Trace of Fe^{2+} was also observed. It is, therefore, important to re-examine the accurate composition and uniformity of Fe concentration.

Formation of d-band is obvious in $CuFeS_2$, which is the concentrated limit of $CuGa_{1-x}Fe_xS_2$. The reduced sublattice magnetization could be accounted for only by the band formation. This conjecture was also confirmed by the band calculation./19/

It has also been demonstrated by the Mössbauer measurement/20/ that Néel temperature increases with Fe concentration and the temperature dependence curves of the spontaneous magnetization for wide range of Fe concentration scales to one curve, indicating the formation of d-band occurs from the very dilute region of the Fe concentration.

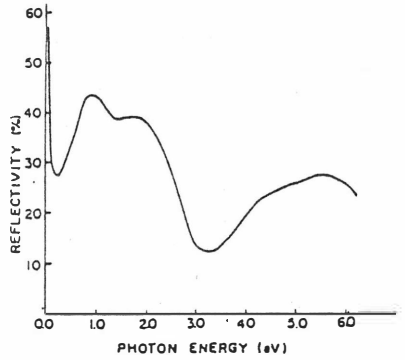

Fig. 13 Reflectivity spectrum of $CuFeS_2$ from 0.02 to 6 eV.

(6) Optical Properties of $CuFeS_2$

A reflectivity spectrum from 0.02 eV up to 6 eV measured on the polished surface of a $CuFeS_2$ single crystal grown by Bridgman technique is shown in Fig. 13./21/ The absorption spectrum of $CuFeS_2$ calculated from the reflectivity spectrum is shown in Fig. 14. Strong absorption bands denoted as A and B are seen between 0.6 and 3.5eV ,which was assigned to the band-to-band transition from valence band to the Fe-originated conduction band. Existence of the strong absorption in the

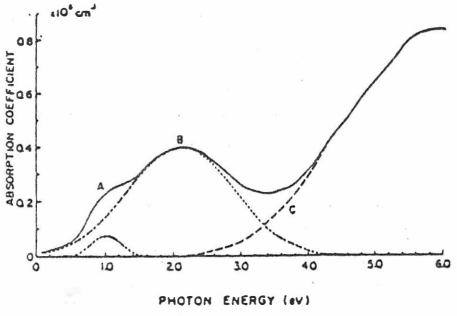

Fig. 14 Calculated absorption spectrum of $CuFeS_2$.

near-infrared to visible region accounts for the golden luster of this crystal.

We have also measured photoelectron spectra in $CuFeS_2$ using synchrotron radiation to elucidate the electronic states of the valence band. By resonant photoemission the structure just below the Fermi level has been assigned to the Fe 3d state hybridized with the S 3p state./22/

Conclusion

Electronic structures associated with the iron atoms in the chalcopyrite crystal were investigated. In the low concentration, the iron was found to substitute the Cu site as Fe^{3+} resulting in a sharp infrared photoluminescence. Higher concentration causes the crystal opaque. This is interpreted as due to the charge transfer type transition. Further doping leads to a formation of the d-band or the percolation network. In $CuFeS_2$ the golden luster is attributed to a strong absorption associated with the d-band.

Acknowledgment

This work has been partly supported by the Grant-in-Aid for Scientific Research on Priority Areas from the Ministry of Education, Science and Culture of Japan.

References

1. T.Teranishi, K.Sato and K.Kondo, J. Phys. Soc. Jpn. **36**, 1618 (1974).
2. K.Sato and T.Teranishi, J. Phys. Soc. Jpn. **37**, 415 (1974).
3. K.Suzuki, T.Kambara, K.I.Gondaira, K.Sato, K.Kondo and T.Teranishi, J. Phys. Soc. Jpn. **39**, 1310 (1975).
4. T.Teranishi and K.Sato, J. Phys. (Paris) **36** C3-149 (1975).
5. K.Sato, T.Kawakami, T.Teranishi, T.Kambara and K.I.Gondaira, J.Phys. Soc. Jpn. **41**, 937 (1976).
6. T.Teranishi, K.Sato and Y.Saito, Inst. Phys. Conf. Ser. **35** 59 (1977).
7. K.Sato and T.Teranishi, Jpn. J. Appl. Phys. **19** suppl.19-3, 101 (1980).
8. K.Sato, S.Okamoto, M.Morita, A.Morita, T.Kambara and H.Takenoshita, Prog. Crystal Growth and Charact. **10**, 311(1984).
9. K.Sato, H.Tsunoda and T.Teranishi, Ternary & Multinary Compounds, eds. S.Deb and A.Zunger, (Mat. Res. Soc., Pittsburg), p459 (1987).
10. K.Sato, M.Isawa, N.Takahashi and H.Tsunoda, Jpn. J. Appl. Phys. **27**, 979(1988).
11. K.Sato, K.Ishii, K.Tanaka, S.Matsuda and S.Mizukawa, Electroluminescence, eds. S.Shionoya and H.Kobayashi, (Springer, Berlin), p390 (1989).
12. K.Tanaka, K.Ishii, S.Matsuda, Y.Hasegawa and K.Sato, Jpn. J. Appl. Phys., 28, 12 (1989).
13. K.Sato, K.Tanaka, K.Ishii and S.Matsuda, J. Crystal Growth, **99** 772 (1990).
14. H.J.von Bardeleben, A.Goltzene, B.Meyer and C.Schwab, Phys. Stat. Solidi (a) **48** K145 (1974).
15. T.Kambara, J. Phys. Soc. Jpn. **36**, 1625 (1974).
16. J.Scneider, A.Rauber and G.Brandt, J. Phys. Chem. Solids **34** 443 (1973).
17. T.Kambara, K.Suzuki and K.I.Gondaira, J. Phys. Soc. Jpn. **39**, 764 (1975).
18. C.Schwab, private communication.
19. T.Hamajima, T.Kambara and K.I.Gondaira, Phys. Rev. **24** 3349 (1981).
20. M.DiGiuseppe, J.Stegaer, A.Wold and E.Kostiner, Inorg. Chem. **13** 1828 (1974).
21. T.Oguchi, K.Sato and T.Teranishi, J. Phys. Soc. Jpn. **48** 123 (1980).
22. M.Fujisawa, M.Taniguchi, S.Shin, H.Daimon, H.Sakamoto, K.Sato and S.Suga, Proc. 18th Int. Conf. Phys. Semiconductors, 1137 (1986).

OPTICAL PROPERTIES OF Mn-DOPED CRYSTALS OF $CuAlS_2$ AND $CuAlSe_2$

K. Sato, K. Ishii, K. Ohe, K. Watanabe and Y. Kudo
Faculty of Technology, Tokyo University of Agriculture and Technology, Koganei, Tokyo 184, Japan

Optical properties of Mn ions in $CuAlS_2$ and $CuAlSe_2$ were investigated. Mn becomes divalent in $CuAlS_2$ to be a red luminescence center. Time-resolved photoluminescence studies revealed an energy transfer between the host and the center. Red photoluminescence due to Mn^{2+} was observed in dilute $CuAlSe_2$:Mn. Mn^{3+} is suggested in heavily doped samples .

Introduction

Band gaps in ternary chalcopyrite semiconductors take a wide range of values from the infrared to the ultraviolet. Of these compounds $CuAlS_2$ is the only one stable material that has a band gap in the ultraviolet region: This makes this material a possible host for visible luminescence centers. We already reported spectra of the photoluminescence(PL)/1/ and the electroluminescence(EL)/2/ in manganese-doped single crystals of $CuAlS_2$. Measurements of excitation spectra and subsequent theoretical analyses allowed us to assign the luminescence to the ligand-field transition in the $3d^5$-manifolds of Mn^{2+} similar to the case of Mn^{2+} luminescence in zinc sulfide/1/. However, the mechanism of recombination has not fully been understood.

In the present work we studied the optical properties such as absorption and PL spectra in single crystals of $CuAlS_2$ doped with various concentration of Mn ions. Optical studies on undoped crystals were also carried out for the sake of comparison. We also carried out similar experiments in undoped and Mn-doped crystals of $CuAlSe_2$ with an energy gap at 2.7 eV.

Experimental

Single crystals were grown by the chemical vapor transport technique using iodine as a transporting agent. Starting materials were polycrystalline powder of Cu_2S or Cu_2Se, Al, and S or Se. These were sealed in vacuo with appropriate amount of iodine into a fused silica ampoule with its inner wall coated by pyrolytic carbon. Manganese doping were performed by mixing appropriate amount of MnS powder to starting materials. In the following we denote the concentration of Mn by the ratio of MnS to the total amount of starting materials in weight percent.

Undoped crystals of $CuAlS_2$ were colored in deep blue due to the presence of an intense absorption in the red-to-green wavelengths. Manganese doping, however, bleached the color, increasing transparency of the material. On the other hand, undoped crystals of $CuAlSe_2$ were transparent with a yellow color. Manganese doping in high concentration changed the color into dark reddish orange.

Optical absorption spectra were measured with a Hitachi U-3100 type spectrophotometer. CW-PL spectra were measured with the 488 nm line of an Ar^+ ion laser. The photodetector used was either a photomultiplier or a cooled Ge photodiode. For time-resolved PL measurement we employed a pulsed N_2 laser and a Boxcar Averager. Details of the time-resolved measurements will be published elsewhere/3/. Reflection phase shift-difference(PSD) spectroscopy has been known to provide an exact position

of the absorption edge in optically anisotropic materials like chalcopyrites/4/. We measured the PSD spectra by means of polarization modulation technique with a help of a piezobirefringent modulator.

Results and Discussion

(1) $CuAlS_2$:Mn

Figure 1 shows absorption spectra of undoped and manganese-doped single crystals of $CuAlS_2$. The undoped crystal (curve (1)) has a cosiderably large absorption coefficient in the below-gap energy region, showing characteristic absorption bands with peaks at 1.3 and 1.9 eV as well as a shoulder structure around 3 eV. As plotted by curve (2) only the slight doping of manganese leads to a dramatic reduction of the below-gap absorption. When the manganese concentration is increased the absorption edge shifts towards low energies. As shown by the curve (4) the absorption edge of the 1 wt% Mn-doped sample appears at 3.1 eV. The shift amounts to as large as 0.3 eV.

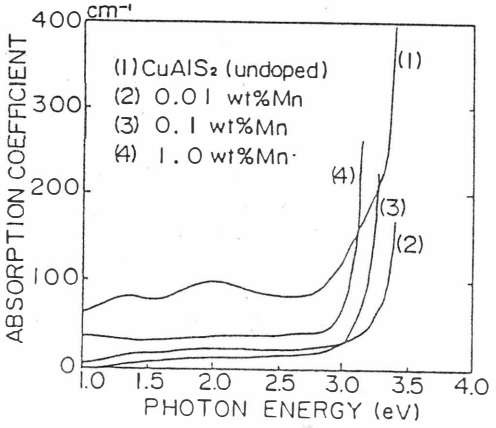

Fig.1 Absorption spectra of undoped and Mn-doped $CuAlS_2$ at RT.

Reflection PSD spectra in undoped and Mn-doped crystals at room temperature were measured to find whether the absorption edge shift is caused by the reduction of the energy gap or by the foot of an intense absorption band just below the edge. The peaks in the PSD spectrum in chalcopyrites have been associated with band edge excitons. The results are plotted in Fig. 2. We find only a small difference in the peak positions between undoped and Mn-doped samples. The shift was as small as 0.04 eV, which could not account for the observed absorption edge shift of 0.3 eV. We, therefore, conclude that the edge shift is caused by an extra absorption band just below the gap.

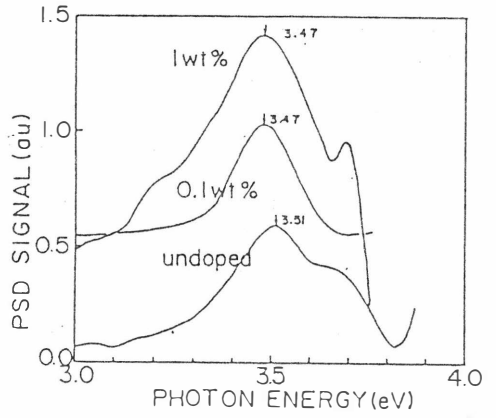

Fig.2 Phase shift difference spectra in undoped and Mn-doped $CuAlS_2$.

As reported in our previous papers, a CW-PL spectrum of $CuAlS_2$:Mn shows a luminescence band with a peak at 1.96 eV. The spectral shape and the peak position show no substantial changes by changing the excitation wavelength. A time-resolved PL measurement in a 5 mol%(=1.7 wt%) Mn-doped crystal revealed that the spectral shape did not show a substantial change throughout the time interval of the measurement/2/. The decay time of the red band was determined as 120 us. In that study, however, we observed only for the wavelength region longer than 500 nm. In the present study we extended the wavelength region to cover all over the below-gap energies.

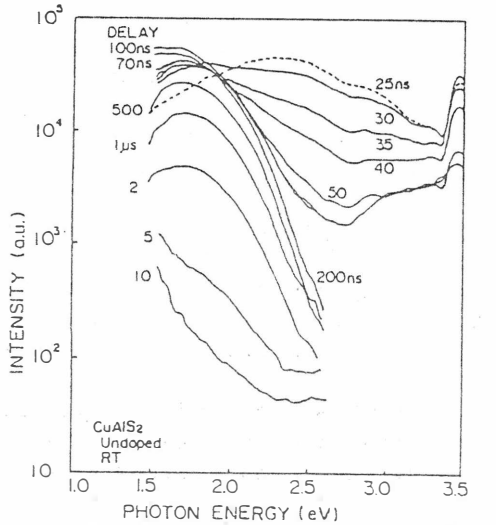

Fig.3 Time-resolved PL spectra in undoped $CuAlS_2$ at RT.

In Fig. 3 time-resolved PL spectra in an undoped

$CuAlS_2$ measured at room temperature are illustrated. Luminescence intensity(vertical axis) is plotted in a logarithmic scale. Spectra are corrected for the spectral responce of the measuring system. At the least measurable delay time of 25 ns after excitation the PL spectrum has a broad maximum around 2.2 eV. The higher energy part of the peak rapidly lose intensity in less than 50 ns and intense part of the luminescence band moves towards low energies. Finally a peak at 1.7 eV remains and decays by 10 us.

In Fig. 4 time resolved spectra in 0.1 wt% Mn-doped crystal are presented. At 25 ns after excitation there appear two peaks at 1.7 and 2.9 eV. The lower peak decays with a lifetime of 500 ns, while the higher peak decays by 50 ns. The relative intensity of Mn-originated emission with a peak at 1.96 eV is very weak at the initial stage of relaxation and becomes prominent only at a delay time as late as 1 us. With the use of Xe lamp excitation we determined the decay time of the 1.96 eV peak as 1.4 ms.

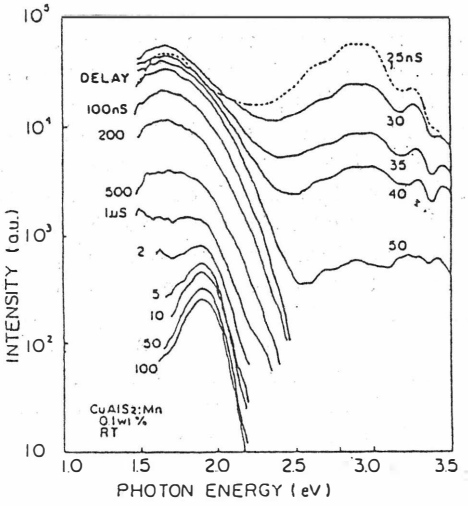

Fig.4 Time-resolved PL spectra in 0.1 wt% Mn-doped $CuAlS_2$.

The sample showing the most bright luminescence was one doped with 1 wt% manganese. As illustrated in Fig. 5 time-resolved spectra of the 1 wt% Mn-doped sample show a prominent peak at 3 eV with a decay time of 50 ns. The Mn-originated 1.96 eV-band is clearly observed from the delay time of as early as 30 ns. The lifetime of 1.96 eV-peak in 1 wt% Mn-doped sample is reduced to approximately one tenth of that in dilute sample.

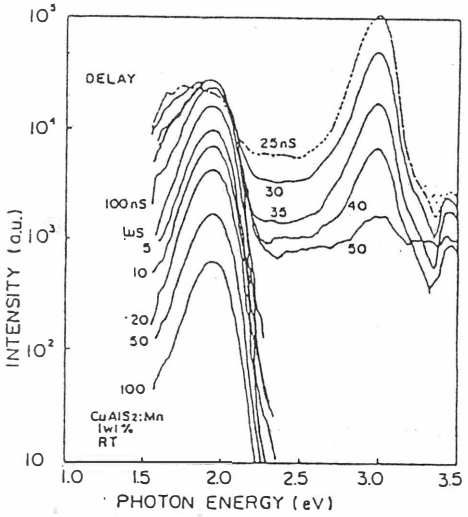

Fig.5 Time-resolved PL spectra in 1 wt% Mn-doped $CuAlS_2$.

It seems that an efficient energy transfer occurs from the host lattice to the luminescent manganese center, just like the case of ZnS:Mn/5/. In this connection, existence of the purple (3 eV) emission should be noticed.What is the origin of the purple line? As stated above, the 1 wt% Mn-doped sample shows an apparent absorption edge around 3 eV, which is caused by an additional absorption band below the edge of the host crystal. We suspect this absorption is responsible for the purple emission.

Our experimental finding that doping of Mn reduces the below-gap absorption may be accounted for by a change of the valency of the impurity Fe from 3+ to 2+. By our infrared PL studies we have elucidated that the Fe in a very low concentration is trivalent/6/ and occupies the Cu-site/7/. Fe^{3+} at Cu-site would be reduced to Fe^{2+} when Mn^{2+} ion occupies the Ga site. Change of Fe-valency may account for the dramatic reduction of below-gap absorption. For higher Mn concentration, however, the dopant ion would substitute both Cu and Al sites. The extra absorption band and the purple emission may be associated with $[Mn]_{Cu}$ (i.e. the Mn^{2+} occupying the Cu-site) or the donor-acceptor pair consisting of $[Mn]_{Cu}$ and $[Mn]_{Al}$.

(2) $CuAlSe_2$:Mn

Mn ions show more complicated behaviors in $CuAlSe_2$ crystals. Figure 6 illustrates PL spectra of undoped(#0), 0.05 wt% Mn-doped(#1 and #2) and 5 wt% Mn-doped(#3) $CuAlSe_2$ single crystals measured at low temperatures with the 488 line of Ar^+ ion laser. Even the undoped crystal shows a red photoluminescence band with a peak around 1.5 eV. There is a striking similarity in the PL line shapes between undoped and 5 wt% Mn-doped crystals. Slightly Mn-doped sample emits a red PL with a peak around 1.8 eV at low temperatures, as shown by curves #1 and #2 in Fig. 6. We tentatively assign the PL band to Mn^{2+}. Spectra are completely different when excited by different excitation wavelength.

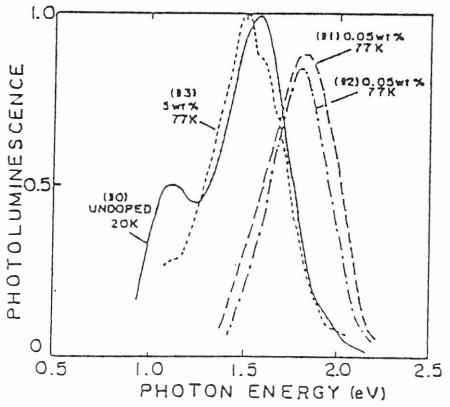

Fig.6 Low temperature PL spectra in undoped and Mn-doped $CuAlSe_2$.

Absorption spectra measured at 20 K are shown in Fig. 7 for two samples with different Mn-concentration; 0.05 wt% and 5 wt%. No structures are found in the spectrum of the 0.05 wt% Mn-doped sample, while several structures with a distinctive polarization dependence were observed in the 5 wt% Mn-doped crystal. The overall feature of the spectrum in the 5 wt% sample is quite similar to the absorption spectrum of the Cr^{2+} ion doped in ZnS/8/, although the information of the lowest band is missing due to the limitted energy region of the present measurement. Since the electronic configuration of Cr^{2+} is the same as Mn^{3+} we may conclude that heavily doped Mn ions in $CuAlSe_2$ become Mn^{3+} substituting the Al-site in contrast with the case of Mn in $CuAlS_2$.

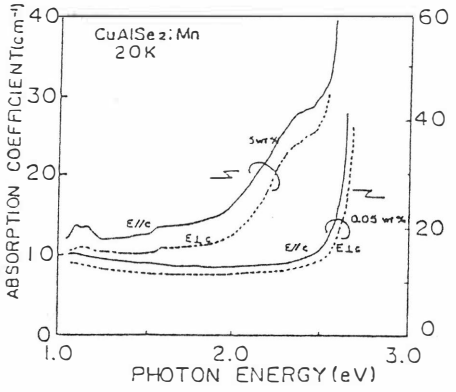

Fig.7 Polarized absorption spectra in 0.05 wt% and 5 wt% Mn-doped crystals of $CuAlSe_2$.

Acknowledgement

Authors are very grateful to Prof. H. Kobayashi for invaluable discussions. We note with gratituteds that this work has partially been supported by a Grant-in-Aid for Priority Areas from the Ministry of Education, Science and Culture of Japan.

References

1. K.Sato, S.Okamoto, M.Morita, A.Morita, T.Kambara, K.I.Gondaira and H.Takenoshita, Prog. Cryst. Growth and Charact. **10**, 311 (1984).
2. K.Sato, K.Ishii, K.Tanaka, S.Matsuda and S.Mizukawa, Electroluminescence, eds. by H.Kobayashi and S.Shionoya, (Springer, Berlin 1989) p390.
3. K.Sato, K.Ishii, K.Watanabe and K.Ohe, submitted to Jpn. J. Appl. Phys.
4. K.Yamamoto, H.Horinaka, K.Okada and T.Miyauchi, Jpn. J. Appl. Phys. **16**, 1817 (1977).
5. S.Tanaka and H.Kobayashi, J. Appl. Phys. **47**, 5393 (1976).
6. K.Sato and T.Teranishi, J. Phys. Soc. Jpn. **37** 415 (1975).
7. K.Sato, K.Tanaka, K.Ishii, and S.Matsuda, J. Cryst. Growth **99**, 772 (1990).
8. J.T.Vallin, G.A.Slack, S.Roberts and A.E.Hughes, Phys. Rev. **B2**, 4313 (1970).

ELECTROREFLECTANCE AND PHOTOLUMINESCENCE IN $CuAl_xGa_{1-x}S_2$

S. Shirakata, K. Saiki and S. Isomura
Faculty of Engineering, Ehime University,
Matsuyama, Ehime 790, Japan

Electroreflectance (ER) and photoluminescence (PL) have been studied on $CuAl_xGa_{1-x}S_2(0 \leq x \leq 0.3)$ alloys grown by iodine-transport method. Their crystal quality has been examined by the broadening in ER spectra in connection with PL properties.

1. INTRODUCTION

The $CuAl_xGa_{1-x}S_2$ alloy is a promising material for the application of light-emitting devices operating in the green-blue region /1/. Recently, heteroepitaxial growth of this alloy has been investigated for such optical device applications /2/. However, only a few basic properties of this bulk alloys have been studied by phase-shift difference (PSD) /3/, photoluminescence (PL) /1/, cathodoluminescence (CL) /4/, absorption and reflectance /5/ methods.

On the other hand, it is well known that an electroreflectance (ER) method is a powerful tool for the characterization of crystal quality as well as for the determination of the critical point energy /6,7/. No ER study has been reported for $CuAl_xGa_{1-x}S_2$ alloys except for $CuGaS_2$ /8,9/ and $CuAlS_2$ /8/.

In this work, both ER and PL measurements have been done on the $CuAl_xGa_{1-x}S_2$ $(0 \leq x \leq 0.3)$ alloys grown by the iodine-transport method for the purpose of characterizing crystal qualities. Transition energies and broadness of the ER spectra are examined. ER results are discussed in terms of PL spectra.

2. EXPERIMENTAL

The $CuAl_xGa_{1-x}S_2$ alloys were grown by the iodine-transport method. Stoichiometric amount of constituent elements were transported with iodine of 18 mg/cm^3. The source and growth temperatrues are 900 and 700°C, respectively.

For ER measurements, an electrolyte ER method was used with 0.1N NH_4Cl aqueous solution at room temperature. The ER measurements were performed on the (112) face of as grown crystals. In order to compare the ER spectra with PL ones, heat treatment in sulphur atmosphere was not done though crystals were highly resistive. The measurement system and condition are the same as those in our previous report /9/.

PL was excited by 457.9 nm line of an Ar-ion laser. The emissions were dispersed by the same monochromator as the ER measurements and detected by Hamamatsu R-636 photomultiplier. PL measurements were carried out at both room temperature and liquid N_2 temperature.

3. RESULTS AND DISCUSSION

Figure 1 shows the polarized ER spectra for $CuAl_xGa_{1-x}S_2$ crystals. Solid and dashed curves show the ER spectra taken under the light with E polarized parallel (||) and perpendicular ($\perp$) to the c-axis, respectively. Labels "A" and "B,C" show the E_0 and $E_0+\Delta_{CF}$ transitions, respectively. Transition energies and broadening parameters have been obtained by the three-point method /6/. The broadness of ER spectra is characterized by the broadening parameter (Γ). Experimentally obtained ER spectra are affected by broadening due to crystal imperfections other than the intrinsic life-time broadening effect. Therefore, the magnitude of Γ can be sometimes considered to be a measure of the quality of the crystal under consideration. It can be seen in Fig. 1 that the ER peaks are sharp in the range of x up to 0.13.

Further increase in x causes rapid broadening of ER peaks. This result shows that the crystal quality degrades with increasing x. Figure 2 shows the Γ value of the A-transition plotted as a function of x. The data points are rather scattering. But, we can classify them into two groups, (i) small Γ value (18–30 meV) indicated by the solid curve, and (ii) large Γ value (40–70 meV) indicated by the dashed curve. The ER spectra shown in Fig. 1 are those taken with samples shown by the solid curve in Fig. 2. In $CuGaS_2$, it has been shown that the transitions with small Γ value (near 26 meV, kT value at 300 K) are due to exciton transitions, while those with large ones (typically larger than 40 meV) are due to band-to-band transitions /9/. Based on this result, it is considered that narrow ER spectra with small Γ value (18–30 meV) are due to the exciton transition, and broad ones with large Γ value (40–70 meV) are due to band-to-band transitions.

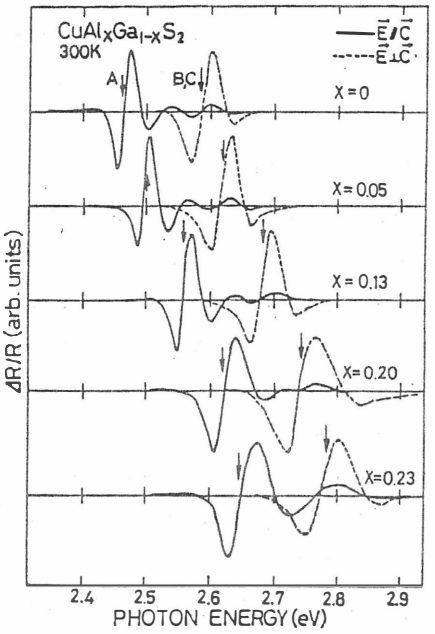

Fig.1. ER spectra in $CuAl_xGa_{1-x}S_2$.

In order to correlate the ER results with PL, PL spectra at 77 K have been measured for the two types of crystals having the same alloy composition; (a) crystals with small ER Γ value, and (b) crystals with large one. Figures 3 and 4 show ER and PL spectra taken for $CuAl_{0.13}Ga_{0.87}S_2$, respectively. It can be seen that the crystal exhibiting sharp ER spectrum (small Γ value of 23 meV) show strong exciton emission at 2.60 eV, while the PL spectrum of the crystal exhibiting broad ER (large Γ of 63 meV) is dominated by the broad red PL band at 1.9 eV.

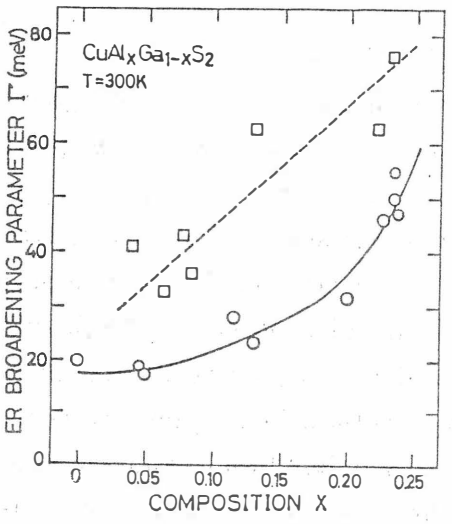

Fig.2. ER broadening parameter plotted as a function of x.

Room temperature PL spectra in the near-bandgap region have been examined, and the spectra are shown

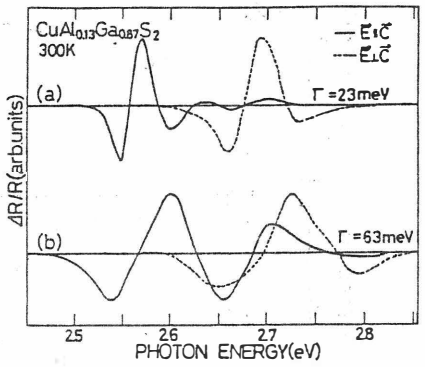

Fig.3. ER spectra of $CuAl_{0.13}Ga_{1.87}S_2$ with small (upper curve) and large (lower curve) ER broadening parameter.

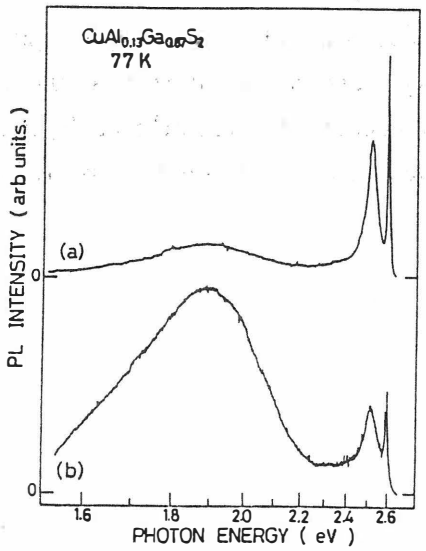

Fig.4. PL spectra at 77 K taken with the same samples in Fig. 3.

in Fig. 5. As composition x increases, the following results have been obtained: (i) increase in the full-width at half-maximum (FWHM) value of PL peaks as shown in Fig.6(a), (ii) remarkable tailing of low-energy side of PL peak, (iii) increase in the energy shift of the PL peak from the energy of the A-transition determined by ER measurement as can be seen in Fig.6(b). These results indicate that the near-band edge PL at room temperature is affected by defect levels as x increases, corresponding to the increase in intensity of the broad red PL band around 1.8 eV at 77 K. Previously reported CL results have shown the increase in the red band with increasing x /4/. These PL results indicate that the crystal quality degrades with increasing the Al composition x, and the results are consistent with the magnitude of the broadening parameter in ER spectra mentioned above.

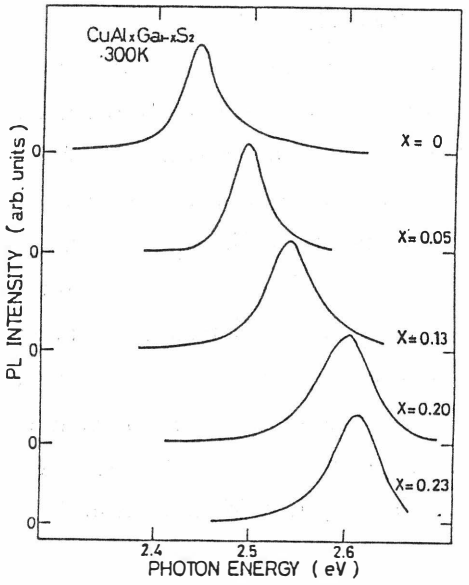

Fig.5. Near-band edge PL at room temperature in $CuAl_xGa_{1-x}S_2$.

The crystals with x >0.3 exhibit no ER spectra, and their PL spectra at 77 K are dominated by red emission band. Even in the range of x <0.3, some crystals with poor PL properties did not show any detectable ER signals. Therefore, we believe that no ER signal is mainly due to the poor quality of the crystals with x >0.3.

4. SUMMARY

ER and PL measurements have been done for $CuAl_xGa_{1-x}S_2$ with the composition range $0 \leq x \leq 0.3$. Based on the broadening parameter in the ER spectra, crystal quality has been examined. We showed that the mutual comparison of ER and PL spectra in this $CuAl_xGa_{1-x}S_2$

alloy is useful for the characterization of crystal quality. The results show that increase in Al composition causes the remarkable degradation of the crystal quality of the iodine-transported crystals.

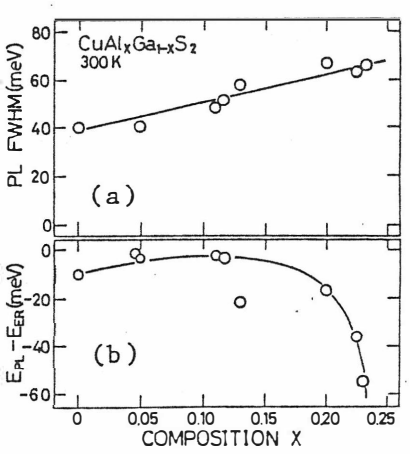

Fig.6. (a) FWHM of near-band edge PL, and (b) energy shift of PL peak from A-transition, plotted as a function of x.

REFERENCES

1. N.Yamamoto, in Proc. 4th Int. Conf. Ternary and Multinary Compounds, Tokyo, 1880, Jpn. J. Appl. Phys. 19(1980) Suppl. 19-3, p. 95.
2. K.Hara, T.Shinozawa, J.Yoshino and H.Kukimoto, J. Cryst. Growth 93(1988)771.
3. N.Yamamoto and T.Miyauchi, in Proc. 2nd Int. Conf. Ternary Semiconducting Compounds, Strasbourg, 1975, J. de Physique 36(1975) Suppl. C3, p.155.
4. N.Tsuboi, S.Kobayashi, K.Kimura and F.Kaneko, Oyo Butsuri 56(1987)1209.
5. N.Tsuboi, S.Kobayashi, F.Kaneko and T.Maruyama, Jpn. J. Appl. Phys. 27(1988)972.
6. D.E.Aspnes, Surf. Sci. 37(1973)418.
7. S.Shirakata, M.Kondo, T.Nishino and Y.Hamakawa, Jpn. J. Appl. Phys. 25(1986)435.
8. J.L.Shay, B.Tell, H.M.Kasper and L.M.Schiavone, Phys. Rev. B5(1972)5003.
9. S.Shirakata, K.Murakami and S.Isomura, Jpn. J. Appl. Phys. 28(1989)1728.

PHOTOLUMINESCENCE IN Yb-DOPED I-III-VI_2 COMPOUNDS

S. Shirakata, K. Ishii and S. Isomura
Faculty of Engineering, Ehime University,
Matsuyama, Ehime 790, Japan

Near-infrared photoluminescence (PL) has been measured in $CuGaS_2$, $CuGaSe_2$, $AgGaS_2$ and $AgGaSe_2$ crystals doped with Yb. Sharp PL lines are discussed in terms of the transitions between the spin-orbit levels of Yb^{3+}.

1. INTRODUCTION

Recently, much attention has been paid to the rare-earth related luminescence in semiconductor. Rare-earth impurities such as Er, Yb and Nd show sharp luminescence lines in near- infrared region /1–4/. They are expected as new luminescence centers for the application of laser diodes and LED operating in near-infrared region /5,6/. It is striking that the laser emission due to Er^{3+} has been realized in the Er-doped InGaAsP DH laser /7/.

However, few has been reported for the emission due to 4f rare-earth ion in the chalcopyrite crystal, although Er and Yb impurities have been studied for ternary and quaternary chalcogenides; $CdIn_2S_4$, $ZnIn_2S_4$ and $CdInGaS_4$ /8,9/.

The purpose of this work is to investigate the infrared emission due to the trivalent rare-earth ion, Yb^{3+}, in the I-III-VI_2 compounds. In this work, the Yb impurity has been doped in $CuGaS_2$, $CuGaSe_2$, $AgGaS_2$ and $AgGaSe_2$ crystals. Low-temperature photoluminescence (PL) measurements have been carried out, and sharp PL lines observed in the 1μm region are discussed in terms of the spin-orbit levels of Yb^{3+}.

2. EXPERIMENTAL

The Yb impurity was doped during crystal growth. $CuGaS_2$ was grown by the iodine-transport method in a closed quartz ampoule. The other compounds were grown by cooling (10°C/hour) the melts. In both case, Yb metal element was charged with an amount of 2 mole % with respect to Ga, together with other constuent elements.

PL was excited by the 514.5 or 488.0nm lines of an Ar-ion laser, while the samples were immersed in LN_2. The emissions were dispersed by a monochromator with 50 cm focal-length, and phase-sensitively detected by a Ge-photodiode cooled down to 77 K. No corrections for system response were performed.

3. RESULTS AND DISCUSSION

Figure 1 shows the PL spectrum of $AgGaSe_2$:Yb at 77 K. We can see PL peaks in two different

wavelength regions, (i) near bandedge region, and (ii) the region around 1μm. Near bandgap, emissions due to an exciton (1.813 eV) and a shallow impurity/defect (1.7 eV) can be seen /10/. Around 1.24 eV, sharp PL lines are observed, which are characteristic of Yb-doped semiconductors. The energy and the line shape of the PL spectrum are very similar to those in Yb-doped InP /1,6/.

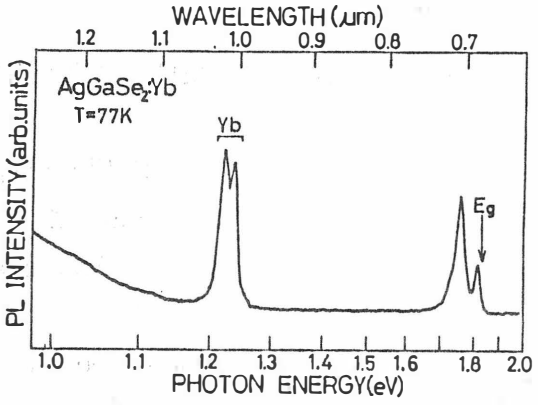

Fig.1. PL spectrum in $AgGaSe_2$:Yb at 77K.

Similar sharp PL lines have been observed for $AgGaS_2$:Yb and $CuGaS_2$:Yb in the 1μm region except for $CuGaSe_2$:Yb. The detailed PL spectra in the energy region between 1.1 and 1.3 eV are shown for these compounds in Fig. 2. The energy positions of these lines are summarized in Table I. The PL spectrum for $AgGaS_2$:Yb is dominated by strong line at 1.249 eV. In its lower energy side, as many as fifteen weak lines spread down to 1.11 eV. On the other hand, only a few lines (1.22–

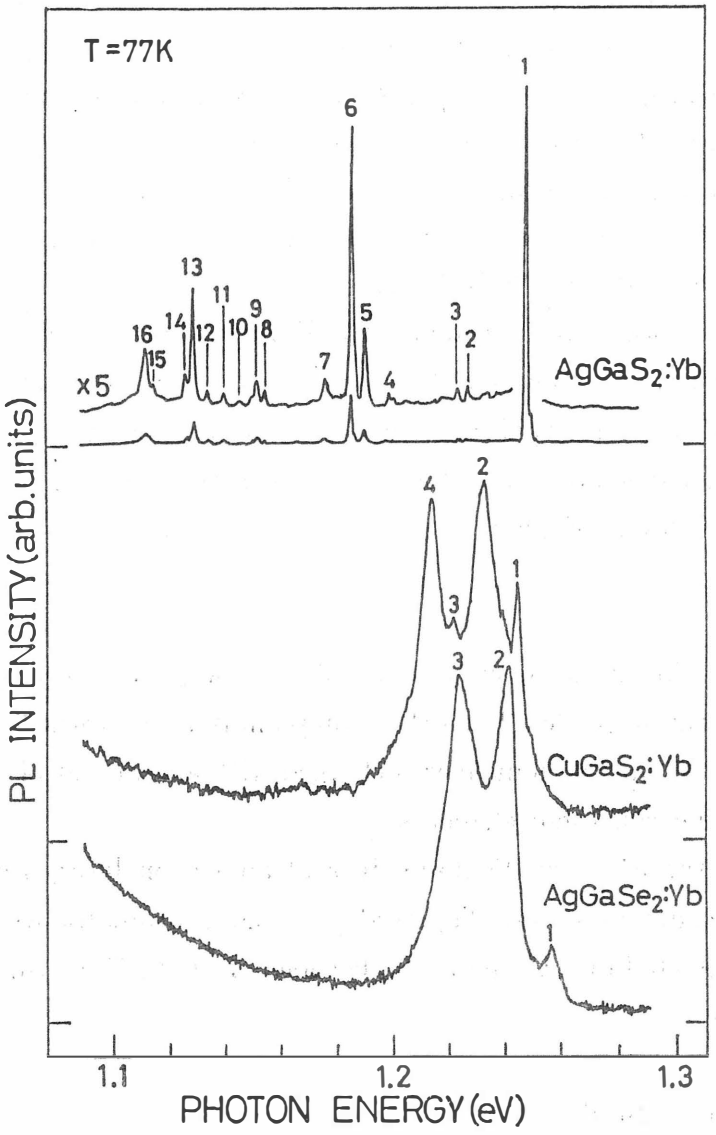

Fig.2. Near-infrared PL spectra in Yb-doped $AgGaS_2$,$CuGaS_2$ and $AgGaSe_2$.

1.25 eV) which are closely spaced have been found in $AgGaSe_2$ and $CuGaS_2$. From energies and sharpness of the PL lines, they are considered to be due to the transitions between the spin-orbit levels ($^2F_{\frac{5}{2}}$-$^2F_{\frac{7}{2}}$) of Yb^{3+} ($4f^{13}$).

Figure 3 shows the energy level scheme of Yb^{3+} ($4f^{13}$). For the free ion, the strong spin-orbit interaction splits the multiplet ^2F into $^2F_{\frac{5}{2}}$ (excited state) and $^2F_{\frac{7}{2}}$ (ground state). In the chalcopyrite lattice, the excited state splits into three levels (Γ_6,Γ_6 and Γ_7), and the ground state into four levels (Γ_7,Γ_6,Γ_7 and Γ_6) due to the crystal field at the Yb^{3+} site. The splitting of the Γ_8 level (zinc blende) into Γ_6 and Γ_7 levels (chalcopyrite) is due to reduction of the site symmetry in the presence of tetragonal distortion of chalcopyrite lattice.

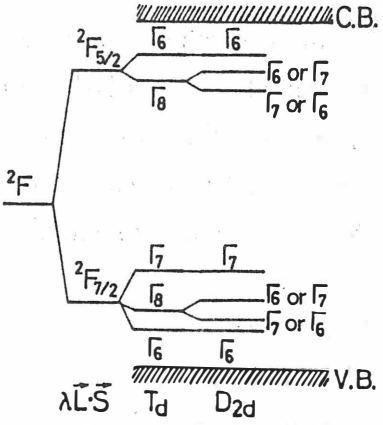

Fig.3. Level scheme of Yb^{3+} in chalcopyrite lattice.

In Yb doped InP, it has been confirmed that Yb^{3+} occupies the group III atom, In, site /11/. Analogously, in I-Ga-VI_2 crystals, Yb^{3+} is considered to substitute the Ga site. The Yb atom is tetrahedrally coordinated by four ligands, S or Se in this case, and the tetrahedron is compressed due to the tetragonal distortion ($c/a<2$). Therefore, Yb^{3+} suffers the compressive axial crystal field. The differences in the tetragonal distortion and the ligands may affect the crystal field. Such crystal field is considered to be reflected in fine structures in PL spectra.

The large difference in the PL spectra between $AgGaS_2$:Yb and $CuGaS_2$:Yb may reflect the difference in the tetragonal crystal field. Both crystals have the same sulphur ligand, but the tetragonal distortion of $AgGaS_2$ ($c/a=1.789$) is much larger than that of $CuGaS_2$ ($c/a=1.948$). The $AgGaSe_2$ crystal has also large tetragonal distortion ($c/a=1.793$). But the PL lines locate in much narrower energy region than that in $AgGaS_2$:Yb. The reason may be the difference of the ligands; S and Se. In chalcopyrite lattice, there is a possibility that the Yb ion substitutes the

Table I. PL line in Yb doped $AgGaS_2$, $CuGaS_2$ and $AgGaSe_2$ taken at 77K.

$AgGaS_2$		$CuGaS_2$		$CuGaSe_2$	
Line	Energy(eV)	line	Energy(eV)	line	Energy(eV)
1	1.249	1	1.245	1	1.257
2	1.227	2	1.233	2	1.242
3	1.224	3	1.222	3	1.224
4	1.200	4	1.215		
5	1.191				
6	1.185				
7	1.175				
8	1.154				
9	1.151				
10	1.145				
11	1.139				
12	1.133				
13	1.128				
14	1.126				
15	1.117				
16	1.111				

group I atom site, where the local environment around Yb ion is different from that at the Ga site. In Yb doped InP and II-VI compounds, the emissions due to Yb^{3+}-defect complex have been reported /11–13/. Therefore, much care should be taken on the assignment of the Yb-related PL lines. In $AgGaS_2$:Yb which shows a large number of PL lines, several centers such as Yb at Ag site and Yb-defect complex should be taken into account.

4. SUMMARY

Photoluminescence related to Yb impurity has been studied for $CuGaS_2$, $CuGaSe_2$, $AgGaS_2$ and $AgGaSe_2$. Sharp PL lines have been observed in the 1μm wavelength region. They are considered to be the transitions between the spin-orbit levels of Yb^{3+}. The difference in the fine structure in the PL spectra among these compounds may reflect the crystal field around Yb impurity.

REFERENCES

1. H.Ennen, U.Kaufmann, G. Pomrenke, J.Schneider, J.Windscheif and A.Axmann, J. Crystal Growth, 64 (1983) 165.
2. H.Ennen, G.Pomrenke and A.Axmann, J.Appl.Phys. 57 (1985) 2182.
3. K.Uwai, H.Nakagome and K.Takahei, Appl. Phys. Lett. 50 (1987) 977.
4. H.D.Muller, H.Ennen, J.Schneider and A.Axmann, J.Appl. Phys. 59 (1986) 2210.
5. F.Auzel, A.M.Jean-Louis and Y.Toudic, J.Appl.Phys. 66 (1989) 3952.
6. W.H.Haydl, H.D.Muller, H.Ennen, W.Korber and K.W.Benz, Appl. Phys. Lett. 46 (1985) 870.
7. W.T.Tsang and R.A.Logan, Appl. Phys. Lett. 49 (1986) 1686.
8. M.R.Brown and W.A.Shand, J.Phys. C, 4 (1971) 83.
9. M.R.Brown, M.D.Martin and W.A.Shand, J. Phys.C, 3 (1970) 1329.
10. B.Tell and H.M.Kasper, Phys. Rev. B4 (1971) 4455.
11. G.Aszodi, J.Weber, C.Uihlein, L.Pu-lin, H.Ennen, U.Kaufmann, J.Schneider and J.Windscheif, Phys. Rev. B 31 (1985) 7767.
12. D.M.Williams and B.W.Wessels, Appl. Phys. Lett. 56 (1990) 566.
13. M.R.Brown, A.F.J.Cox, W.A.Shand and J.M.Williams, J. Phys. C, 4 (1971) 2550.

EPR STUDIES OF ELECTRON-IRRADIATED $CdIn_2S_4$ SINGLE CRYSTALS

T. TAKIZAWA, E. CHRISTOFFEL,* A. GOLTZENE,* and C. SCHWAB*

Department of Physics, College of Humanities and Sciences, Nihon University, 3-25-40 Sakurajosui, Setagaya-ku, Tokyo 156.
**Groupe "Recherches Physiques et Matériaux", Centre de Recherches Nucléaires, IN2P3-CNRS, Université Louis Pasteur, BP20, 67037 Strasbourg Cedex, France.*

To investigate defect levels in the single crystal of $CdIn_2S_4$, EPR experiments have been performed on both as-grown and electron-irradiated samples over the 4.2-100 K temperature range with and without illumination of the band-gap light. Two EPR signals are observed in as grown samples, and two new ones emerge out after the irradiation.

§ 1. Introduction

The electron paramagnetic resonance (EPR) is a well known method especially useful to investigate the properties of magnetic centers in crystals, e.g., F-centers, electrons trapped in imperfections or impurities, intentionally doped paramagnetic ions and even carriers. In $CdIn_2S_4$ as is common to other ternary compound semiconductors, many structural defects are known to exist to give strong influence on their electric properties. Normally, such defects give no EPR signal when the sample is highly compensated as in $CdIn_2S_4$, but the excitation by light or other external stimulation will often produce EPR signals useful for the study of the mechanisms of defects.

The purpose of the present paper is to study the defect levels in both as-grown and electron irradiated single crystals of $CdIn_2S_4$ by the EPR method under illumination of light and discuss the origins of these defects.

§ 2. Experimental procedure

Single crystals of $CdIn_2S_4$ were grown from stoichiometric compositions of each element by the normal freezing method. In the growing process, a 0.25% excess sulfur was added to make crystals highly resistive (5×10^6 Ω.cm in the dark at room temperature). Samples were cut into blocks of about $2\times1\times7$ mm^3, the long edge being oriented along the [110] direction.

EPR experiments were performed using the X-band Arpeggio system equipped with a TE_{102} cavity under the microwave power from 0.01 to 100 mW, and the field modulation of 100 kHz with an amplitude between 1.25 and 25 G under a sweep-rate between 1 and 20 G/s. An Oxford helium-gas-flow-type cryostat was used for the temperature variation.

Illumination was made with monochromatic light using a 250 W halogen lamp. Samples were irradiated with 1.8 MeV electrons of a beam current of 8 μA/cm^2 at room temperature. EPR

measurements were carried out for samples irradiated at doses of 0.1, 0.5, 2.0 and 7.5 $\times 10^{17}$ cm^{-2}.

§ 3. Results and Discussion

3-1. EPR signals for as-grown samples

Before illumination, two EPR signals (one at g=4.3 and the other at g=2.03) were observed in the dark as shown in Fig.1(a). The former is considered to arise from an Fe contamination, and the latter narrow line is due to unknown impurities. In the following, we neglect these and focus our attention to signals affected only by illumination and/or electron irradiation.

During illumination with the band-gap light ($\lambda \approx 530$nm), two strong symmetric and isotropic singlets emerged out at g=2.02 (S1) and g=1.66 (S2) as shown in Fig. 1(b). By using the least square fitting method, the line shape of S1 was shown to be gaussian and that of S2 lorentzian. Both singlets were completely saturated after five minutes of illumination under the condition above, and began to similarly decrease with time after the light off as shown in Fig.2; the lifetime is estimated as two hours for both singlets.

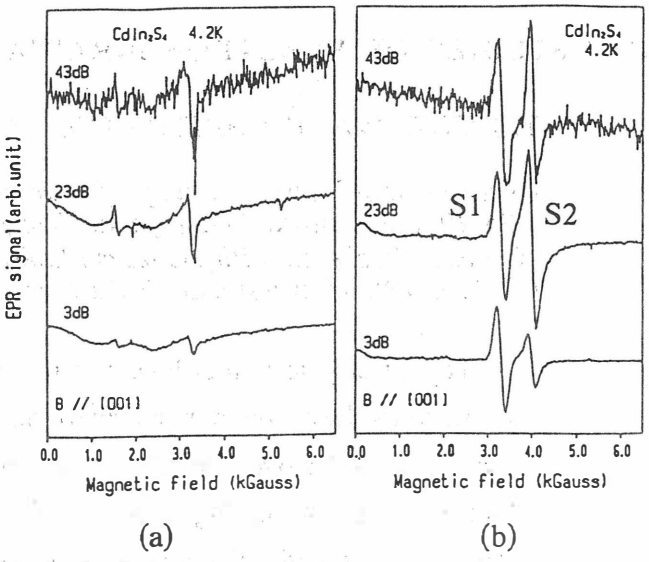

Fig. 1 EPR signals of an as-grown $CdIn_2S_4$ (a) in the dark and (b) under illumination of the 530nm light.

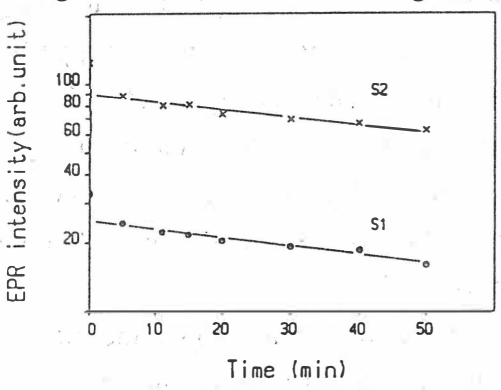

Fig. 2 Relaxation of EPR signals after light off.

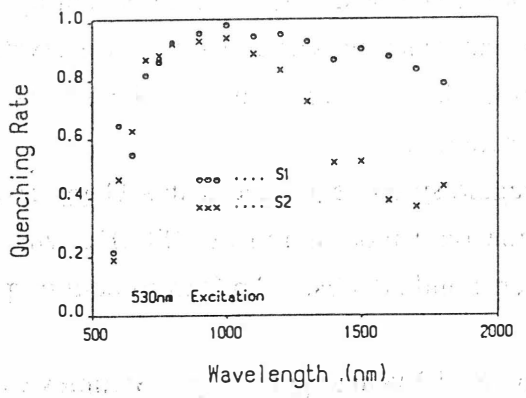

Fig. 3 The rate of quenching for each EPR signal vs. the wavelength.

The S1 and S2 signals are quenchable by light of an energy below the band gap. Figure 3 shows the rate of quenching for both singlets as a function of the wavelength. The rate is the highest at the wavelength of about 1μm, and is higher for S1 than for S2 in the longer wavelength side. At the wavelength near the band edge, it was observed that the EPR signal first increased with time and then decreased again, indicating that both excitation and quenching occured simultaneously.

Figure 4 shows the temperature variations of S1 and S2 recorded under illumination with 530nm light in the temperature range from 4 to 100 K. The EPR intensity of S1 times temperature remains constant up

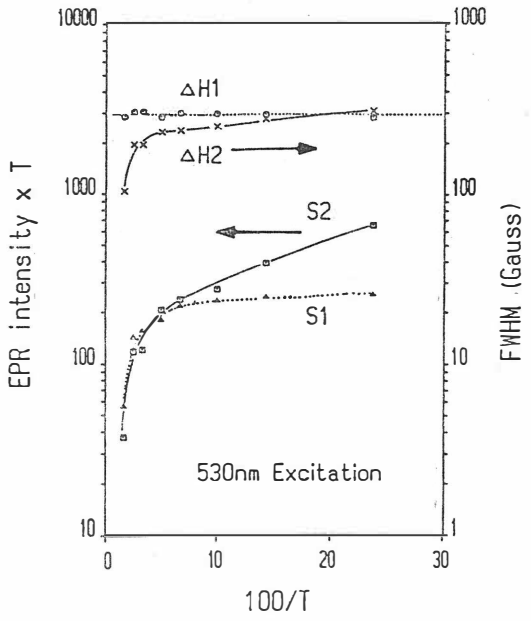

Fig. 4 The EPR intensity and FWHM for S1 and S2 signals vs. inverse temperature.

to about 20 K showing that it obeys the Curie's law ; on the contrary, S2 deviates from the Curie's law over the whole temperature range. In contrast to the line width FWHM for S1 ($\Delta H1$) which is kept constant, that for S2 ($\Delta H2$) decreases with increasing temperature, hinting at a motional narrowing /1/ of S2.

The lorentzian shape, the negative g-shift and the decrement of both intensity and linewidth with temperature strongly suggest that S2 should be ascribed to electrons in trapping centers; the electrons can interact with each other and also can move by hopping among the centers. On the other hand, the line shape of S1 is gaussian with positive g-shift and its intensity and $\Delta H1$ do not change as temperature is increased, so that the origin of S1 is considered to be holes trapped in the acceptors.

The trapped holes are rather independent each other and may not do hopping between centers. The unresolved hfs (hyper fine structure) splittings and/or inhomogeneous magnetic fields at the centers may give rise to the gaussian shape of S1. From the abrupt decrease of the EPR signals above 20 K for both singlets (see Fig.4), activation energies of the trapped electrons and holes are estimated as 35 meV, which is comparable to the value obtained by TSC measurements /2/.

3-2. EPR signals after electron irradiation

Figure 5 shows EPR spectra measured in the dark before and after electron (e^-) irradiation of different doses. At the lowest dose of $1\times10^{16}\,cm^{-2}$, a new singlet S3 was induced together with a trace of S2. Both intensities increase with doses of up to about $1\times10^{17}\,cm^{-2}$. Above this value, S3 disappears and a new sharp singlet SF2 (g=1.66) emerges out at nearly the same g-value as S2. The intensity of SF2 was not saturated up to the microwave power of 100 mW in contrast to SF1 which was saturated even at 0.01 mW.

The intensity, FWHM and g-value of SF2 as a function of temperature are shown in Fig. 6. FWHM decreases rapidly with the increase of temperature,

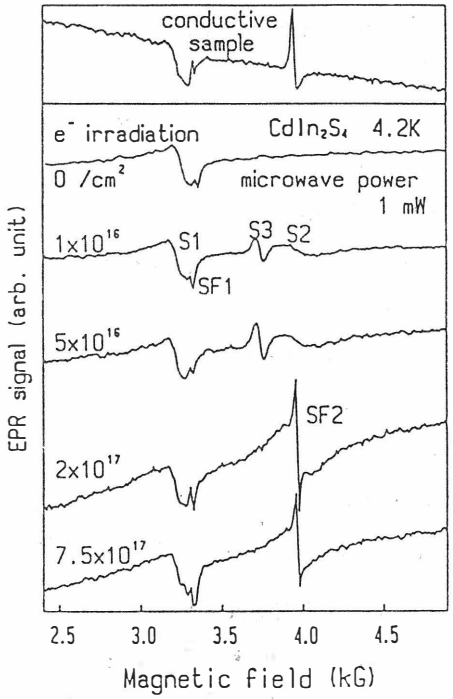

Fig. 5 EPR signals in the dark for different doses of electron irradiation.

indicating a strong motional narrowing below 20 K.

By the e^- irradiation, S vacancies (V_S) are expected to be introduced in $CdIn_2S_4$, which is also suggested by the smell of sulfur just after the irradiation. The initial compensation between carriers may be destroyed by these extra vacancies. Electrons released from these are captured again by the electron trapping centers, and thus S2 appears even in the dark. As the dose of irradiation increases, the number of V_S also increases, and finally, electrons in V_S may move freely in some region in a crystal /3/, giving rise to the EPR line of SF2. A deficiency of sulfur can be realized by growing a sample without an excess sulfur. As shown in the top of Fig.5, such a sample gives a signal similar to SF2, supporting the above presumption.

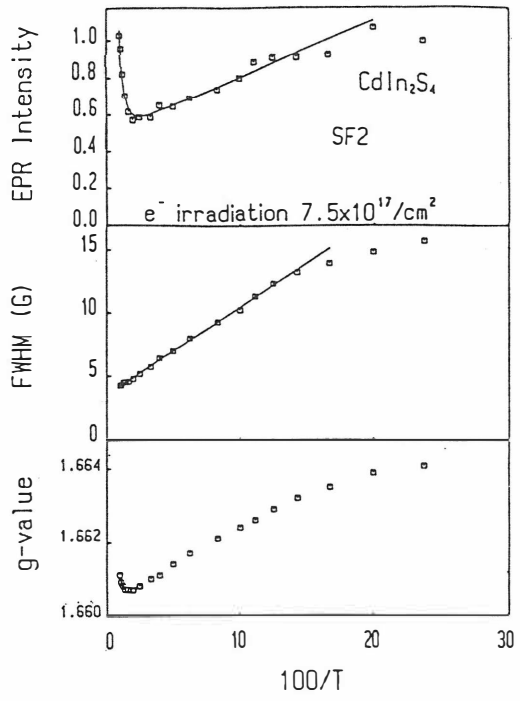

Fig. 6 The EPR intensity, FWHM and g-value of SF2 singlet vs. inverse temperature.

At temperatures above 40 K, the intensity of SF2 again increased with temperature as shown in Fig. 6. Since the number of conduction electrons obeys the so-called exponential law, the Curie's or Pauli's law will no more hold above a certain temperature. Since the EPR signal is proportional to the number of the paramagnetic electrons, its intensity changes according to the exponential law. By fitting the exponential law to the observed spectra, the activation energy is estimated as about 40 meV in good agreement with the value from Fig. 4. Above about 100 K, samples are too conductive for EPR to be detected.

Illumination by 530 nm light again raises the intensity of S1, S2 and S3, which are independent of the fluence value as shown in Fig. 1. A new singlet S3 appears only in the spectra of electron-irradiated samples both in the dark and after illumination. S3 has the gaussian shape and obeys the Curie's law. The g-value of S3 is exactly the same as that of donors in CdS. The origin of S3 may be ascribed to donors in CdS-like regions created by the e^- irradiation.

§ 4. Conclusion

Several types of defect levels in $CdIn_2S_4$ are revealed by the EPR method. Among those, the lines named as S1 and S2 are intrinsic ones related to the trapping centers. S3 is due to the defects generated only by the e^- irradiation, presumably arising from donors in CdS-like regions. SF2 is due to conduction electrons released from the sulfur vacancies introduced by the e^- irradiation.

REFERENCES

1. K.MORIGAKI, S.TOYOTOMI and Y.TOYOTOMI, *J. Phys. Soc. Jpn.* **31**, 511 (1971).
2. T.TAKIZAWA and K.KANBARA, *J. Phys. Soc. Jpn.* **55**, 3503 (1986).
3. K.MORIGAKI and S.MAEKAWA, *J. Phys. Soc. Jpn.* **32**, 462 (1972).

OPTICAL PROPERTIES OF LAYERED SEMICONDUCTOR $CdInGaS_4$ AND RELATED PHENOMENA

Taizo Irie, Saburo Endo and Hisayuki Nakanishi
Department of Electrical Engineering, Faculty of Engineering, Science University of Tokyo
1-3 Kagurazaka, Shinjuku-ku, Tokyo 162, Japan

Optical properties such as optical absorption, photoconductivity, photoluminescence and Raman scattering of the layered semiconductor $CdInGaS_4$ are reviewed. Experimental results and analyses of the green emission in $CdInGaS_4$ are presented.

The quaternary compound $CdInGaS_4$ shows an intense red photoluminescence even at room temperature /1/ and photoconductive in the visible region of the spectrum. Furthermore, it has a layer structure with easy cleavage along the layers. Therefore, this compound is considered to be a promising material for many optoelectronic devices. In this paper, the optical properties of $CdInGaS_4$ reported by several authors are reviewed.

In the course of our investigation about $CdInGaS_4$, we have found that this material shows an intense green photoluminescence as well as the red emission at low temperatures, in some portion of the crystals /2/. In this paper, our investigation about finding materials which show the same intense green emission as observed in a portion of the $CdInGaS_4$ crystal is also reviewed. It will be shown that such a material can be obtained from a laminated structure composed of CdS and $CdInGaS_4$.

It is reported that $CdInGaS_4$ has a rhombohedral structure with a = 12.53 Å, α = 17°43′ and belongs to the space group C_{3v}^5(R3m) /3/. The lattice structure in the hexagonal representation is reported to give a=3.86 Å and c=37.0 Å, i.e. an elongated structure along the direction of c-axis /4/. We have prepared $CdInGaS_4$ single crystals by normal freezing and by Bridgman method as well as by chemical vapour deposition (CVD) using iodine as a transport agent. The lattice constants for the crystals grown by normal freezing were determined from X-ray powder diffraction and X-ray photograph by oscillating crystal method

to be a=3.85 Å and c=36.97 Å /5/. The atomic arrangement in the unit cell of $CdInGaS_4$ was determined by a computer simulation assuming a structure derived by analogy with that of $ZnIn_2S_4$ /5/. Takizawa observed a lattice fringe image of our sample by transmission electron microscope and found that the spacing between successive fringes was about 13 Å. Electron microscopy and electron diffraction study of $CdInGaS_4$ has been made by Manolikas and Anagnostopoulos and a superstructure was found on well-annealed samples /6/.

The optical absorption spectra of $CdInGaS_4$ have been measured by several authors /7-13/. We have measured the optical absorption spectra as functions of temperature and hydrostatic pressure on the crystals prepared by normal freezing /8,9/. Recently, we have measured the absorption coefficient in the range from 10 cm^{-1} to 10^5 cm^{-1} near edge region using various samples having thickness from 0.2 μm to 200 μm. We have also measured the temperature-modulated absorption spectra, in order to make distinction between direct and indirect trnsitions. The result is shown in Fig.1. It can be seen that the experimental data near the absorption edge can be fitted with the curve for indirect transition and yield the energy gap of 2.52 eV, in good agreement with our previous data /8/. For the higher photon energies, the data can be fitted with the curve for direct transition as shown in the figure and give the direct gap of 3.08 eV at 300 K. The value of $d\alpha/dT$ obtained by the temperature-modulated measurement increases with increasing photon energy in the indirect transition region, reaching a maximum at the photon energy for the direct gap, then decreases rapidly as predicted by the theory for temperature modulation spectroscopy /14/. We ascertained that the spectra shown in Fig.1 is essentially identical between the crystals prepared by melting methods and those by CVD. Table 1 lists the band gap parameters of $CdInGaS_4$ at 300 K determined from the absorption measurements and reported so far in the literatures. An exponential absorption in the spectral region below

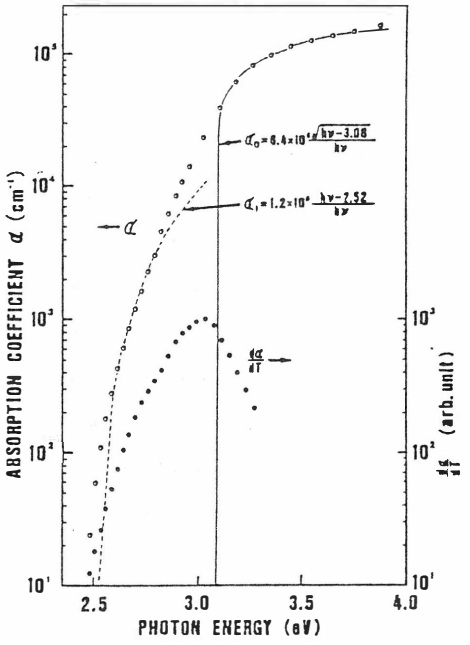

Fig.1. Absorption and thermo-absorption spectra of $CdInGaS_4$.

the fundamental absorption edge of $CdInGaS_4$ was found and analyzed by Toyoda et al. /15,16/. The refractive indeces of $CdInGaS_4$ for the ordinary and extraordinary rays were measured by Allakhverdiev et al./17/.

Table 1. Energy band parameters of $CdInGaS_4$.

Eg (eV)		$\frac{dEg}{dT}$ (eV/K)	$\frac{dEg}{dP}$ (eV/bar)	Reference
direct	indirect			
3.08	2.52	8.0×10^{-4}	6.4×10^{-6}	8,9, this work
2.57		7.3×10^{-4}		11
2.92		5.3×10^{-4}		12
	2.67	6.7×10^{-4}		13

The photoconductivity spectra of $CdInGaS_4$ have been studied by many authors and reviewed by Tarricone et al. /18,19/. It was found that the conductivity increase is about 10^8 and 10^5 in magnitude at 110 K and 300 K, respectively, under an illumination power of about 1 mW/cm^2. Our thermal quenching experiment showed that the level of the sensitizing center is located at about 0.23 eV above the valence band, in good agreement with the result by Tarricone et al. /18/.

As has been stated already, $CdInGaS_4$ shows an intense red photoluminescence even at room temperature. The red emission shows a broad band in the spectrum peaking at about 2.0 eV of the photon energy. We found that the peak energy shifts with the change of the excitation energy, indicating that the red broad band is consisted of several bands. This fact was confirmed by the time-resolved spectroscopy performed by a N_2 pulsed laser or a Coumarin 460 dye laser pumped by a N_2 pulsed laser/20/.The spectrum showed that the red band was composed of three bands peaked at 2.08 eV, 1.96 eV and 1.76 eV at 77 K. The transitions are considered to be band-to-bound for all three bands. On the other hand, Colocci et al./21/ measured the time-resolved spectra of $CdInGaS_4$ prepared by CVD and indicated that the red emission is due to a geminate recombination of e-h pairs. The red emission can be excited by the energy lower than the gap energy indicating that some trapping centers are concerned. Then we have measured the thermoluminescence. By varing the heating rate of the grow curve, the trap depth was determined to be 0.065 eV. Existence of such electron traps in $CdInGaS_4$ have been pointed out by Abdullaev et al. /22/ by voltage-current characteristics. They reported that the trap depth is 0.1 ~ 0.2 eV.

The lattice vibrational properties of $CdInGaS_4$ have been studied by the measurements of infrared reflectivity and infrared absorption by several authors /23,24/. The Raman scattering spectra have been measured in the first place by Abbasov et al. /25,26/ on the samples prepared by Bridgman method at 80 K and 300 K. They observed 13 Raman bands out of 24 predicted Raman-active modes assuming C_{3v} sym-

metry and suggested that $CdInGaS_4$ has the space group D_{3d}^1 rather than C_{3v}^5 . However, Kambas /27/ measured the infrared reflectivity and the Raman spectra and showed that all the infrared modes coincides almost exactly with corresponding Raman bands, indicating that the crystal has the space group C_{3v}^5 . Razzetti et al. /28,29,30/ measured the Raman spectra of the $CdIn_{2x}Ga_{2(1-x)}S_x$ system. We have measured the Raman Scattering of $CdInGaS_4$ single crystal of 5 mm x 5 mm x 1.5 mm dimensions prepared by normal freezing for all kinds of scattering geometries. Comparing the (zz) polarization with (xx) and (yy) ones and with (yz), (zy), (xz) and (zx) ones, we could distinguish between A_1 and E modes assuming C_{3v} symmetry. In all, we have observed 16 modes as shown in Table 2. In this table, observed modes by other authors in infrared spectra are also listed.

Table 2. Vibrational frequencies (cm^{-1}) of $CdInGaS_4$.

Raman (cm^{-1})	Mode	I R (cm^{-1})	Reference
27			
37	E		
85			
		95	27,23
103	A_1		
135		134	27
174	E	164	27
197		202	24,27
		208	24
217		217	24
223		226	23
235		235	24
241		244	24
252	A_1	252	24
		283	23
303	A_1	300	24
		320	24
		328	24
331	E	334	23,24
		344	24
		348	24,27
362	E	366	23,24
		386	24
401	E		

In the course of our investigation about $CdInGaS_4$, we have found that this material shows an intense green photoluminescence at low temperatures in a portion of the crystals prepared by normal freezing /2/. We considered that this green emission was due to polytype such as Cd_3InGaS_6 which might be contained in the crystal of $CdInGaS_4$. Then we sealed raw materials into an evacuated quartz tube by the constitution Cd_3InGaS_6 and heated to about 1100°C and slowly cooled to room temperature. The obtained ingot was a polycrystalline substance, more reddish in color and more difficult to cleave than $CdInGaS_4$. The composition was ascertained by electron probe microanalysis. It was found that this material shows a very intense green emission in any portion of the ingot at low temperatures when excited by Ar^+ laser 488 nm light /31/. The peak energy, spectral shape and the temperature dependence of the intensity of this green emission are same as those of the emission found in the crystals of $CdInGaS_4$. The emission mechanism was determined from the time-resolved spectra and the shift of peak energy with excitation intensity to be donor-to-acceptor recombinations /20/.

However, the green emission of Cd_3InGaS_6 was found to show a peculiar dependence on excitation energy /20/. For excitation at 3.40 eV and 2.85 eV, only a red emission which peaks at about 2.0 eV and very

similar to the red band observed in $CdInGaS_4$ appears. For excitation at 2.54 eV, the shape of the spectrum changes drastically, i.e. the 2.0 eV band disappears and the green emission at 2.38 eV as well as a red emission at about 1.7 eV appear. Such a behavior could be explained when the emission is not from a single substance but from a material composed of two different substances. We considered that $Cd_3I_nGaS_6$ is not a compound but a material composed of $CdInGaS_4$ and CdS because the X-ray diffraction pattern of Cd_3InGaS_6 is consisted of the diffraction lines for $CdInGaS_4$ and CdS as shown in Fig.2. However, relative intensity of the line at the diffraction angle 2θ =26.5° to adjacent two lines on either side is very different from that for CdS. Furthermore, the X-ray diffraction lines from the growth face of Cd_3InGaS_6 are composed of those for $CdInGaS_4$ and α-CdS and are all from the crystal planes perpendicular to the c-axis in the hexagonal structure /5/. These facts indicate that Cd_3InGaS_6 is not a mere mixture of $CdInGaS_4$ with CdS but a laminated material in which $CdInGaS_4$ and CdS are epitaxially grown mutually in the direction of c-axis, though the periodicity of lamination is considerably disordered as can be seen in the diffuse Laue pattern /5/. It is considered that the intensity of the X-ray diffraction line at 2θ=26.5°, which corresponds to (002)CdS, is an indication of the lamination of $CdInGaS_4$ and CdS. We have simulated by computer the diffraction pattern of $CdS/CdInGaS_4$ laminated structure and could nearly reproduce the experimental diffraction pattern /32/.

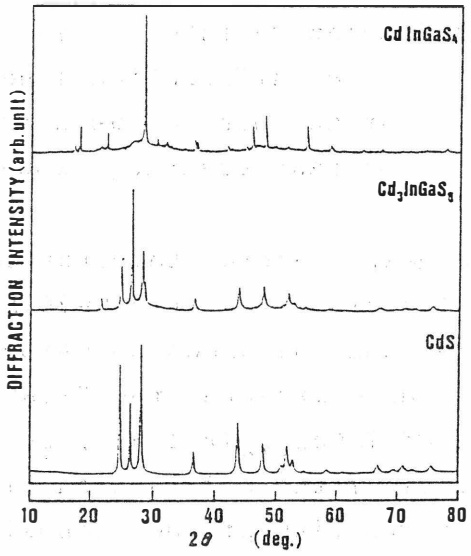

Fig.2. X-ray diffraction patterns of $CdInGaS_4$, Cd_3InGaS_6 and CdS.

In order to examine the effect of lamination on the green emission, mixture of the powders of CdS and $CdInGaS_4$ with 2:1 molar ratio was heat-treated in vaccum for about 1 hour at several temperatures between 600°C and 1200°C and the X-ray powder diffraction and the photoluminescence spectra have been measured. Figure 3 shows the relative intensity of the diffraction line at 2θ=26.5° to the adjacent line at 2θ=24.8° and the green emission intensity as a function of

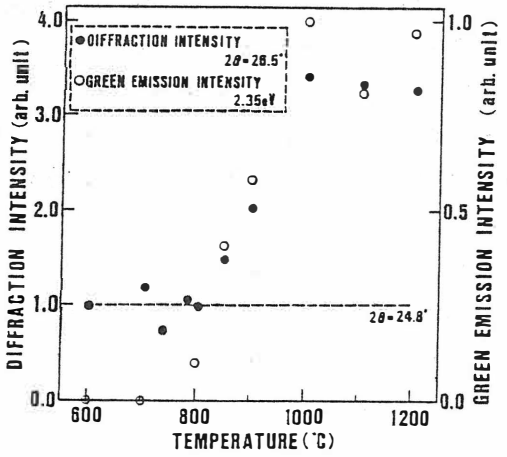

Fig.3. Relative intensities of X-ray diffraction line and green emission as a function of heat-treating temperature.

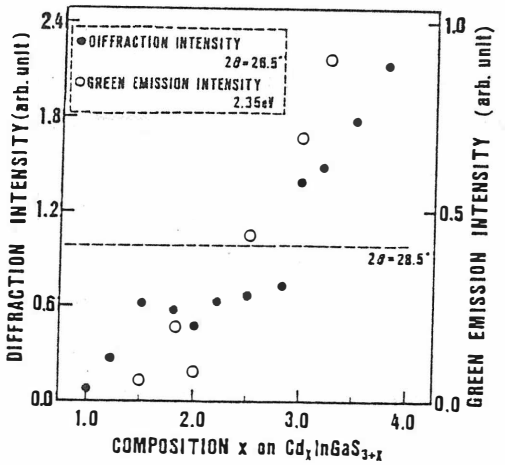

Fig.4. Relative intensities of X-ray diffraction line and green emission as a function of the composition in Cd_xInGaS_{3+x}.

the heat-treating temperature. It can be seen that an increase of the diffraction line at $2\theta = 26.5°$, i.e. the formation of laminated structure, and the green emission are very closely related each other. We have also measured the X-ray diffraction and the photoluminescence of the Cd_xInGaS_{3+x} (x=1 ~ 3) system. Figure 4 shows the relative intensities of the diffraction line at $2\theta = 26.5°$ and the green emission as a function of the composition x.

Thus, results of the X-ray and photoluminescence studies led us to conclude that Cd_3InGaS_6 is a laminated material composed of CdS and $CdInGaS_4$, i.e. a kind of superlattice structure, and that the intense green emission is closely related with such a laminated structure. High intensity of the green emission is interpreted by the laminated structure model as follows: It is known that $CdInGaS_4$ has an energy gap larger than that of CdS and has high density electron traps. The observed green emission is due to D-A pair recombination in CdS. The trapped electrons in $CdInGaS_4$ can act as a source of the recombination in CdS as they can be injected into CdS by the potential gradient formed in the n-n heterojunction and result in an enhancement of the green emission in CdS.

In order to examine our model of laminated structure, we have performed an experiment to intercalate CdS layers into $CdInGaS_4$. It can be expected to form easily the intercalated layers of CdS into CdIn GaS_4 lattice because of the weak Van der Waals binding between the layers. We have heat-treated thin plates of $CdInGaS_4$ single crystals at 400°C in the vapor of CdS heated to 800°C from 10 to 40 hours.

The sample treated 40 hours was found to show very intense green emission. The shape, the peak energy and the dependence on excitation energy of this emission band are same as observed in Cd_3InGaS_6. It was found that the sample treated 40 hours shows an intense line at $2\theta = 26.5°$ in the X-ray diffraction pattern indicating the laminated structure.

In conclusion, $CdInGaS_4$ is a very interesting material in solid state physics as well as optoelectronics and many investigations have been made. However, there are many problems remain to be solved, particularly about the crystal structure, the band structure and the lattice vibrational properties. The intense green emission found in $CdInGaS_4$ was found to be due to a laminate structure composed of CdS and $CdInGaS_4$.

REFERENCES

1. W.A.Shand, Phys.Status Solidi(a)3(1970)K77.
2. T.Irie,H.Miyashita and S.Endo,Nuovo Cimento 2D(1983)2002.
3. F.Lappe,A.Niggli,R.Nitsche and J.G.White,Z.Kristallogr.117(1962)146.
4. V.B.Antonov,N.D.Dzhuraev and R.Kh.Nani,Dokl.Akad.Nauk Azerb.S.S.R. 29(1973)8.
5. S.Endo,S.Ando.H.Matsushita,S.Nomura and T.Irie,J.Cryst.Growth 99 (1990)776.
6. C.Manolikas and A.N.Anagnostopoulos,Phys.Status Solidi(a)80(1983) 503.
7. G.B.Abdullaev,T.G.Kerimova,SH.S.Mamedov,T.R.Mechtiev,R.Kh.Nani and E.Y.Salaev,Phys.Status Solidi(b)73(1976)K69.
8. T.Toyoda,H.Nakanishi,S.Endo and T.Irie,J.Phys.D:Appl.Phys.18(1985) 747.
9. T.Toyoda,H.Nakanishi,S.Endo and T.Irie,Phys.Letters11(1985)283.
10. A.N.Abbasov,R.A.Zamanova,V.V.Panfilov and S.I.Subbotin,Sov.Phys. Semicond.16(1982)731.
11. K.Kambas,A.Anagnostopoulos,B.Floss and J.Spyridelis,Phys.Status Solidi(a)95(1986)K139.
12. N.A.Moldovyan,S.I.Radautsan,V.F.Zhitar,E.D.Arama and D.S.Remenko, Phys.Status Solidi(a)106(1988)K181.
13. L.Tarricone,E.Grilli,M.Guzzi and L.Zanotti,Phys.Status Solidi(a) 92(1985)595.
14. B.Bapz,in: Semiconductors and Semimetals vol.9(Academic Press, New York,London,1972)p.374.
15. T.Toyoda,H.Nakanishi,S.Endo and T.Irie,J.Phys.D:Appl.Phys.19(1986) L21.

16.T.Toyoda,H.Nakanishi,S.Endo and T.Irie,J.Appl.Phys.61(1987)434.
17.K.R.Allakhverdiev,R.I.Guliev,L.A.Kulevskii,A.D.Savelev,E.Yu. Salaev and V.V.Smirnov,Phys.Status Solidi(a)60(1980)309.
18.L.Tarricone,L.Zanotti and J.Filipowicz,J.Phys.D:Appl.Phys.20(1987) 653.
19.A.N.Anagnostopoulos and Karoutis,Phys.Status Solidi(a)79(1983)K29.
20.T.Irie,S.Endo,S.Nomura,K.Igarashi,H.Nakanishi and T.Toyoda,in: Ternary and Multinary Compounds(Material Research Society, Pitsburg,Pennsylvania,1987),p.537.
21.M.Colocci,F.Fermi,R.Querzoli and A.Vinattieri,Phys.Status Solidi (b)133(1986)379.
22.G.B.Abdullaev,V.G.Agaev,N.D.Mamedov,R.Kh.Nani and E.Yu,Salaev, Sov.Phys.Semicond.11(1977)7.
23.G.B.Abdullaev,N.V.Bazhovskaya,N.D.Yuraev,D.B.Kushev,R.Kh.Nani and V.K.Subasheev,Phys.Status Solidi(a)28(1975)K81.
24.K.R.Allakhverdiev,A.N.Abbasov,T.R.Mekhtiev and R.Kh.Nani,Phys. Status Solidi(b)94(1979)K31.
25.A.N.Abbasov,K.R.Allkhverdiev,T.R.Mekhtiev and R.Kh.Nani,Sov.Phys. Solid State 23(1981)370.
26.A.N.Abbasov,K.R.Allakhverdiev and S.S.Babaev,Sov.Phys.Solid State 24(1982)1407.
27.K.Kambas,Phys.Status Solidi(a)76(1983)735.
28.C.Razzetti and P.P.Lottici,in: Ternary and Multinary Compounds (Material Research Society,Pittsburg,Pennsylvania,1987),p.289.
29.C.Razzetti,L.Zanotti,G.Attolini,T.Besagni and M.Curti,in: Ternary and Multinary Compounds(Material Research Society,Pitsburgh, Pennsylvania,1987),p.307.
30.C.Razzetti,P.P.Lottici,L.Tarricone and L.Zanotti,Progress in Crystal Growth and Characterization 10(1985)353.
31.T.Irie,H.Nakanishi,S.Endo,H.Kurogane and T.Toyoda,Jpn.J.Appl.Phys. 24(1985)881.
32.H.Matsushita,S.Nomura,S.Ando,S.Endo and T.Irie,Jpn.J.Appl.Phys. 29(1990)L872.

THE DEPENDENCE OF OPTICAL ABSORPTION IN $CdInGaS_4$ ON TEMPERATURE AND HYDROSTATIC PRESSURE

T.Toyoda[1], H.Nakanishi[2], S.Endo[3] and T.Irie[3]

1.Department of Applied Physics and Chemistry, The University of Electro-Communications, Chofu, Tokyo 182, Japan

2.Department of Electrical Engineering, Faculty of Science and Technology, Science University of Tokyo, Noda, Chiba 278, Japan

3.Department of Electrical Engineering, Faculty of Engineering, Science University of Tokyo, Tokyo 162, Japan

The optical absorption of $CdInGaS_4$ has been measured in the 2.0-3.0 eV photon energy range,at temperatures from 10K to 800K,and over a pressure range up to 40kbar.The interband gap was found to have a temperature coefficient of -8.0×10^{-4}eV/K and a pressure coefficient of $+6.4\times10^{-6}$eV/bar.

The compound $CdInGaS_4$ is a high-resistivity n-type semiconductor, which is of interest as a new photoconducting material sensitive in the visible part of the spectrum /1-3/. It shows an intense red photoluminescence, even at room temperature /4/,and therefore has significant potential for applications in light emitting devices. Recently, a new green emission band of $CdInGaS_4$ has been found at low temperatures /5, 6/. Moreover, it is one of the materials considered for use in optical fiber sensors because it is stable in a high-temperature atmosphere and shows isotropic thermal expansion /7/. Also, it is a good candidate for applications as photovoltaic detector in the ultraviolet spectral region /8/. It belengs to the $Cd(Ga_xIn_{1-x})_2S_4$ system in which end members $CdGa_2S_4$ and $CdIn_2S_4$ have the defect chalcopyrite and cubic spinel structure, respectively. This system has a finite homogeneity range over which rhombohedral crystals grow, and for x=0.5 it crystallizes in the same layered structure as $ZnIn_2S_4$ /9-11/. A recent electron-diffraction measurement shows that the following lattice parameters for $CdInGaS_4$ at room temperature : a=b=6.62 Å and c=24.7 Å /12/. Although several investigations have been carried out recently to study electrical and op-

tical properties, there are a few investigations to clear the nature of type of optical transitions and temperature and hydrostatic pressure dependence of fundamental absorption edge in $CdInGaS_4$. This paper reports a study of the fundamental absorption edge in $CdInGaS_4$ over a wide temperature range from 10K to 800K and over a pressure range up to 40kbar.

$CdInGaS_4$ single crystals were grown by the normal freezing method using high purity (99.999%) starting materials (atomic ratio, Cd:In:Ga:S=1:1:1:4.015) in an evacuated quartz tube ($\sim 10^{-6}$Torr). The X-ray measurements exhibited a six-fold symmetric Laue pattern. $CdInGaS_4$ single crystals were found to cleave easily along the layers and this made it possible to prepare thin high quality specimens sutable for optical investigations. The optical absorption coefficient α was determined from the ratio of transmitted light intensity to incident one using the value of the reflectivity at room temperature.

Fig.1 shows the low level optical absorption spectrum of $CdInGaS_4$ at room temperature using the coordinates $(\alpha\hbar\omega)^{1/2}$ and photon energy $\hbar\omega$ in the case of 32μm sample thickness. The step-like structure can be seen and this was typical of indirect transitions. Similar structure also can be seen in the case of 514μm sample. This structure is very similar to the result by Abdullaev et al./2/ in which the measurements were done at 80K. We can see ten steps. In order to determine the energy gap E_g for the indirect allowed transition, $(\alpha\hbar\omega)^{1/2}$ is plotted as a function of photon energy $\hbar\omega$ in Fig.2. The char-

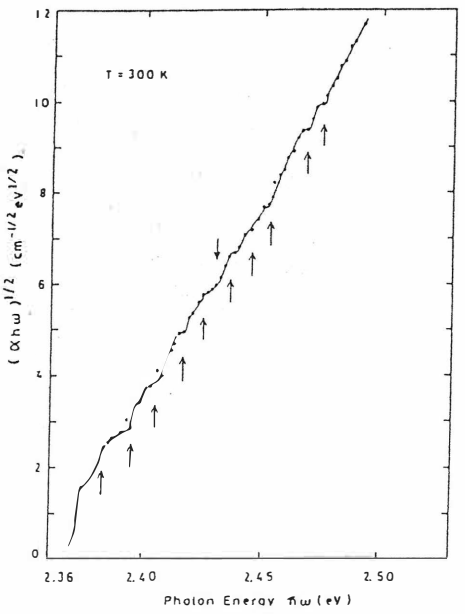

Fig.1.Low-level optical absorption.

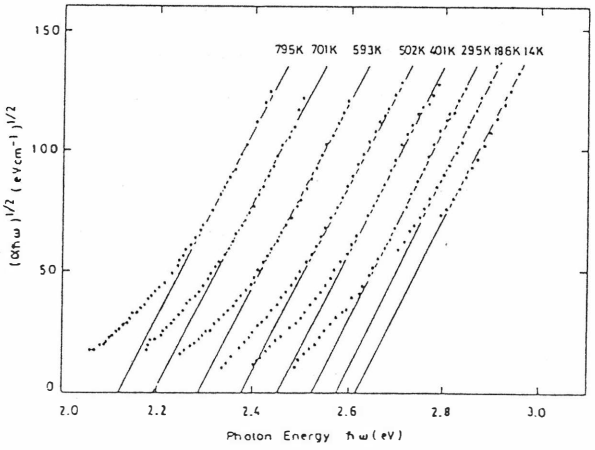

Fig.2.Variation of $(\alpha\hbar\omega)^{1/2}$ on temperature versus $\hbar\omega$.

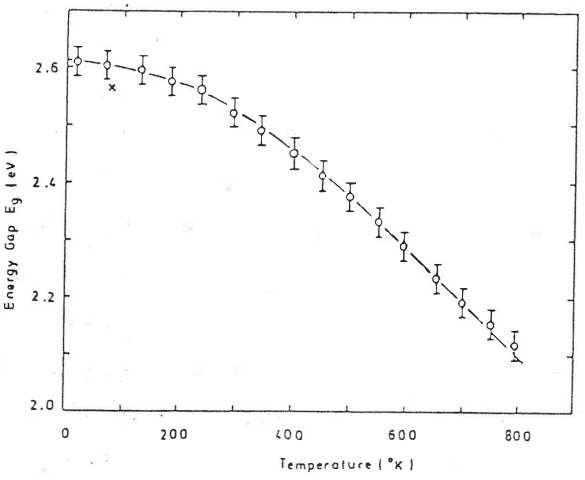

Fig.3.Dependence of the energy gap E_g on temperature.

acter of all slopes in Fig.2 is almost independent of temperature. Extrapolating a linear portion to $(\alpha\hbar\omega)^{1/2}=0$, the indirect allowed energy gap E_g at the respective temperatures can be obtained as shown in Fig.3. The thermal coefficient of energy gap E_g, dE_g/dT, is approximately -8.0×10^{-4} eV/K at high temperature region. The absolute value of dE_g/dT in $CdInGaS_4$ is larger than those for GaP, GaAs and Si. The hydrostatic pressure was applied by the diamond-anvil pressure cell using a mixture of methyl-ethyl alcohol (4:1) as the pressure transmitting medium. $(\alpha\hbar\omega)^{1/2}$ is plotted as a function of photon energy $\hbar\omega$. The character of all slopes in Fig.4 is almost independent of pressure. The indirect allowed energy gap E_g at the respective pressures can be obtained as shown in Fig.5. The pressure coefficient of energy gap E_g, dE_g/dP, is approximately $+6.4 \times 10^{-6}$ eV/bar. The value of dE_g/dP in $CdInGaS_4$ is close to that in $CdIn_2S_4$ /13/ which is a photosensitive semiconductor crystallizing in a cubic spinel structure.

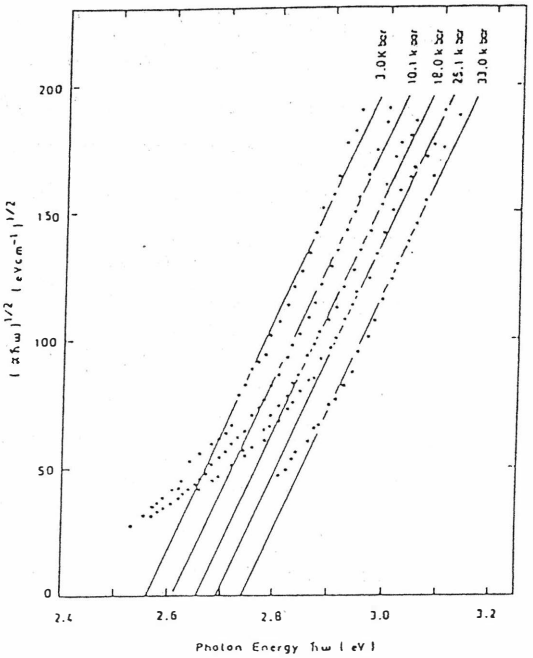

Fig.4.Variation of $(\alpha\hbar\omega)^{1/2}$ on pressure versus $\hbar\omega$.

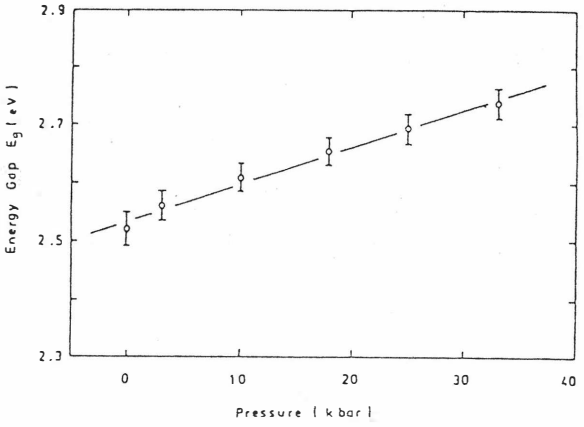

Fig.5.Dependence of the energy gap E_g on hydrostatic pressure

The thermal coefficient of energy gap E_g, dE_g/dT, is related to electron-phonon interaction and changes in lattice constant by thermal expansion according to the expression

$$(\partial E_g/\partial T)_P=(\partial E_g/\partial T)_V - (3\alpha_e/K)(\partial E_g/\partial P)_T \qquad (1)$$

where K is compressibility and α_e is the linear thermal expansion coefficient, respectively. The first and second terms correspond to the thermal coefficient by electron-phonon interaction and that by changes in lattice constant, respectively. Using the values of $(\partial E_g/\partial T)_P$, $(\partial E_g/\partial P)_T$ and room temperature value of α_e by Toyoda et al./7/ and elementary calcualtion of K for $CdInGaS_4$, our calculation suggests that the value of second term in equation (1) is approximately -2×10^{-4} eV/K. The result suggests that the first term in equation (1) is larger than the second one, and the electron-phonon interaction is

dominant in the temperature dependence of the energy gap E_g of $CdInGaS_4$.

REFERENCES

1. G.B.Abdullaev,N.D.Dzhuraev,V.B.Antonov,R.Kh.Nani and E.Yu.Salaev, Sov.Phys.Semicond. 7(1974)1428.
2. G.B.Abdullaev,N.V.Bozhovskaya,N.D.Dzhuraev,D.B.Kushev,T.R.Mekhitiev and R.Kh.Nani, Sov.Phys.Semicond. 8(1975)1417.
3. G.B.Abdullaev,V.G.Agaev,N.D.Mamedov,R.Kh.Nani and E.Yu.Salaev, Sov.Phys.Semicond. 11(1977)7.
4. W.A.Shand, Phys.Status Solidi (a) 3(1970)K77.
5. T.Irie,H.Miyashta and S.Endo, Nuovo Cimento 2D(1983)2002.
6. T.Irie,H.Nakanishi,S.Endo,H.Kurogane and T.Toyoda, Japan.J.Appl. Phys. 24(1985)881.
7. T.Toyoda,T.Irie,S.Endo and H.Nakanishi, J.Appl.Phys. 62(1987)732.
8. N.A.Moldovyan,S.I.Radautsan,V.Ya.Raylyan,V.F.Zhitar and E.D.Arama, Solar Energy Mater. 15(1987)37.
9. H.Haeuseler, J.Solid State Chem. 29(1979)121.
10. C.Razzetti,P.P.Lottici,L.Tarricone and L.Zanotti, Prog.Cryst.Growth Char. 10(1985)353.
11. S.Shionoya and Y.Tamoto, J.Phys.Soc.Japan 19(1964)1142, 1150.
12. A.G.Abdullayev and M.G.Kyasimov, Thin Solid Films 100(1983)175.
13. H.Nakanishi and T.Irie, Phys.Status Solidi (b) 126(1984)K145.

THE REFRACTIVE INDICES AND THE OPTICAL DISPERSION PARAMETERS IN $CdInGaS_4$

T.Toyoda[1], H.Nakanishi[2], S.Endo[3] and T.Irie[3]

1.Department of Applied Physics and Chemistry, The University of Electro-Communications, Chofu, Tokyo 182, Japan

2.Department of Electrical Engineering, Faculty of Science and Technology, Science University of Tokyo, Noda, Chiba 278, Japan

3.Department of Electrical Engineering, Faculty of Engineering, Science University of Tokyo, Tokyo 162, Japan

The refractive indices of $CdInGaS_4$ have been measured at wavelength from 480nm to 1300nm by interference pattern measurements. The single-oscillator energy E_0 and dispersion energy E_d were calculated from those values, and are compared with those of $CdIn_2S_4$ and $CdIn_2S_2Se_2$.

The compound $CdInGaS_4$ is a high-resistivity n-type semiconductor, which is of interest as a new photoconducting material sensitive in the visible part of the spectrum /1-3/. It shows an intense red photoluminescence, even at room temperature /4/, and therefore has significant potential for applications in light emitting devices. Recently, a new green emission band of $CdInGaS_4$ has been found at low temperatures /5, 6/. Also, it is a good candidate for applications as photovoltaic detector in the ultraviolet spectral region /7/. It belengs to the $Cd-(Ga_xIn_{1-x})_2S_4$ system in which end members $CdGa_2S_4$ and $CdIn_2S_4$ have the defect chalcopyrite and cubic spinel structure, respectively. This system has a finite homogeneity range over which rhombohedral crystals grow, and for x=0.5 it crystallizes in the same layered structure as $ZnIn_2S_4$ /8-10/. A recent electron-diffraction measurement shows the following lattice parameters for $CdInGaS_4$ at room temperature : a=b= 6.62 Å and c=24.7 Å /11/. Although several investigations have been carried out recently to study the optical properties /12-15/, there are few investigations of the refractive index of $CdInGaS_4$ except the work by Allakhverdiev et al/12/.They measured the refractive indices of CdIn-

GaS_4 (ordinary and extraordinary rays) by measuring the Brewster angle and the conoscopic pattern along the optical axis only at 0.63μm, 1.15 μm and 3.39μm wavelengths. In this paper, we report a detailed study of refractive indices at wavelength from 480nm to 1300nm performed on $CdInGaS_4$. The refractive index is not only one of the fundamental properties of materials but also it is useful for a wide variety of optics applications such as optical waveguides and formation of heterojunctions in light emitting or laser diodes. It is closely related to the electronic polalizability of ions and the local field inside materials.

$CdInGaS_4$ single crystals were grown by the normal freezing method using high purity (99.999%) starting materials in an evacuated quartz tube ($\sim 10^{-6}$Torr). The X-ray measurements exhibited a six-fold symmetric Laue pattern. In general, refractive indices of ordinary and extraordinary rays of solid in the spectrum regions concerned are measured by the angle of minimum deviation in a prism made of the materials. Because of the high anisotropy of mechanical properties, measurements of refractive indices of uniaxial crystals with layered structures present a severe problems. To obtain the refractive indices of $CdInGaS_4$, the transmission spectra of thin specimens were measured over the wavelength range 480-1300nm. Refractive indices were calculated from the interference patterns using a specimen with a thickness of 21.8μm. Since the c-axis of $CdInGaS_4$ is oriented perpendicular to the surface of the specimen, the refractive index obtained here is that for the ordinary ray. The thin specimen with very good parallel surfaces shows regular spacing and very distinct interference patterns up to the order of interference of more than one hundred in the wavelength range considered.

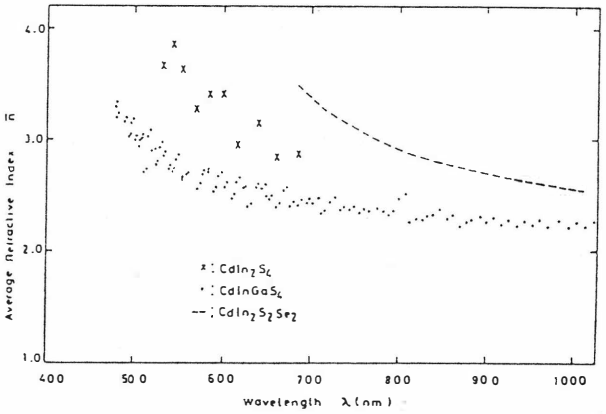

Fig.1.Refractive index $\bar{n}$ of $CdInGaS_4$ as a function of wavelength.

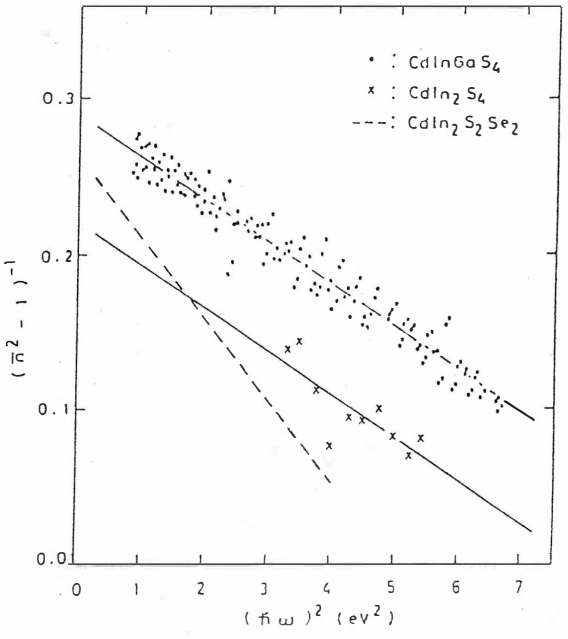

Fig.2.Plot of refractive index factor $(\bar{n}^2-1)^{-1}$ versus $(\hbar\omega)^2$.

Fig.1 shows the refractive index $\bar{n}$ as a function of wavelength together with data for $CdIn_2S_4$, derived from the transmission results of Nakanishi /16/,

and for $CdIn_2S_2Se_2$ which belongs to the same crystal structure as $CdInGaS_4$, reported by Tarricone and Lottici /15/. The value of refractive index at $\lambda=0.63\mu m$ agrees with the ordinary ray result reported by Allakhverdiev et al /12/. The values of $\bar{n}$ in $CdIn_2S_4$ and $CdIn_2S_2Se_2$ are larger than those in $CdInGaS_4$. This result suggests that the $\bar{n}$ difference between $CdInGaS_4$ and $CdIn_2S_4$ might be related to their different crystal structure and/or to Ga substitution for In. Also, we cannot explain the refractive index difference between $CdInGaS_4$ and $CdIn_2S_2Se_2$ by crystal structure alone because they belong to the same crystal structure. Wemple and DiDominico /17/ and Wemple /18/ developed the concept of the single oscillator dispersion of the electronic dielectric constant. They introduced an energy parameter E_d to describe the dispersion of the refractive index. In terms of this dispersion energy E_d and a single-oscillator energy E_0, the refractive index at frequency ω can be expressed in the form

$$n^2(\omega)-1 = E_dE_0/(E_0^2-(\hbar\omega)^2) . \qquad (1)$$

The single-oscillator energy E_0 and the dispersion energy E_d can be obtained from equation (1) by plotting $(n^2-1)^{-1}$ against $(\hbar\omega)^2$. This has been done in Fig.2 for $CdInGaS_4$, $CdIn_2S_4$ and $CdIn_2S_2Se_2$. The derived values of E_0 for their compound semiconductors are plotted in Fig.3 along with their energy gaps. Fig.3 shows that the single-oscillator energy E_0 is simply related to the energy gaps. Values of dispersion energy E_d are plotted in Fig.4. It shows a smaller E_d value for $CdInGaS_4$ than for $CdIn_2S_4$. This result may reflect crystal structure and charge distribution differences in those semiconductors. Although the crystal structure of $CdInGaS_4$ is the same as that of $CdIn_2S_2Se_2$, the dispersion energy of $CdInGaS_4$ is larger than that of $CdIn_2S_2Se_2$, and also that is

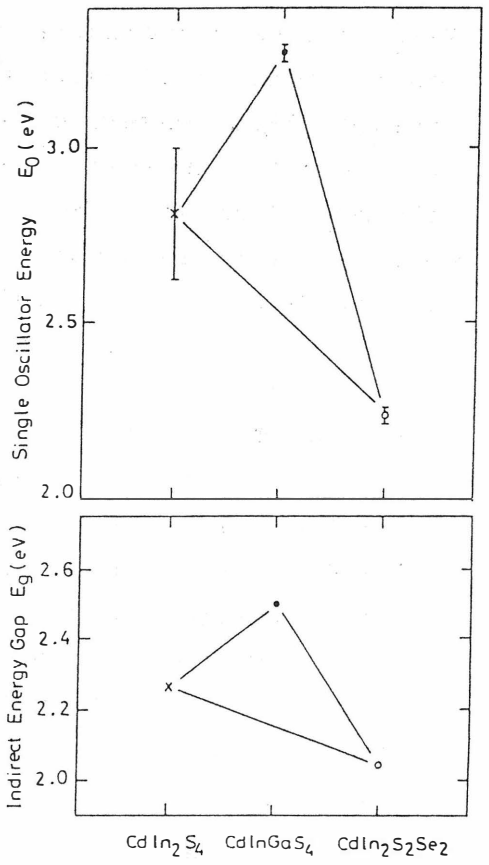

Fig.3. The single oscillator energy E_0 together with those of indirect energy gap

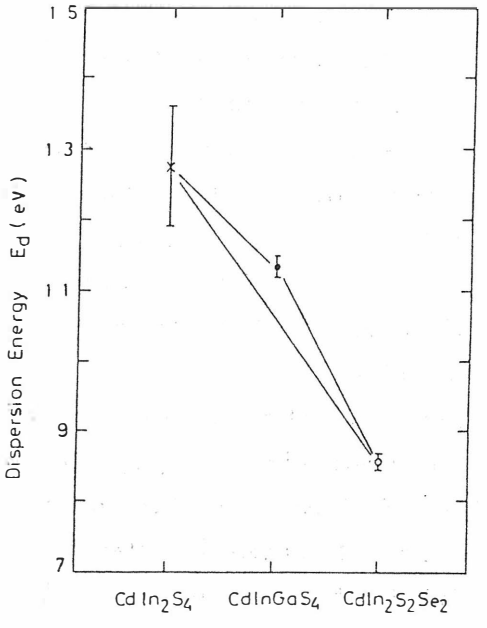

Fig.4. The dispersion energy E_d.

smaller than that of $ZnIn_2S_4$ (E_d=18.7eV) derived from the refractive index results of Shionoya and Tamoto /10/. The dispersion energy E_d is related to the charge distribution within each unit cell and is a quantity closely related to chemical bonding /17,18/. Therefore, Fig.4 shows that reduction of Sulphur ($CdInGaS_4 \rightarrow CdIn_2S_2Se_2$) causes larger variation of charge distribution than reduction of Indium ($CdIn_2S_4 \rightarrow CdInGaS_4$).

REFERENCES

1.G.B.Abdullaev,N.D.Dzhuraev,V.B.Antonov,R.Kh.Nani and E.Yu.Salaev, Sov.Phys.Semicond. 7(1974)1428.

2.G.B.Abdullaev,N.V.Bozhovskaya,N.D.Dzhuraev,D.B.Kushev,T.R.Mekhtiev and R.Kh.Nani, Sov.Phys.Semicond. 8(1975)1417.

3.G.B.Abdullaev,V.G.Agaev,N.D.Mamedov,R.Kh.Nani and E.Yu.Salaev, Sov.Phys.Semicond. 11(1977)7.

4.W.A.Shand, Phys.Status Solidi (a) 3(1970)K77.

5.T.Irie,H.Miyashita and S.Endo, Nuovo Cimento 2D(1983)2002.

6.T.Irie,H.Nakanishi,S.Endo,H.Kurogane and T.Toyoda, Japan.J.Appl. Phys. 24(1985)881.

7.N.A.Moldovyan,S.I.Radautsan,V.Ya.Raylyan,V.F.Zhitar and E.D.Arama, Solar Energy Mater. 15(1987)37.

8.H.Haeuseler, J.Solid State Chem. 29(1979)121.

9.C.Razzetti,P.P.Lottici,L.Tarricone and L.Zanotti, Prog.Cryst.Growth Char. 10(1985)353.

10.S.Shionoya and Y.Tamoto, J.Phys.Soc.Japan 19(1964)1142, 1150.

11.A.G.Abdullayev and M.G.Kyasimov, Thin Solid Films 100(1983)175.

12.K.R.Allakhverdiev,R.I.Guliev,L.A.Kulevskii,A.D.Savelev,E.Yu.Salaev and V.V.Smirnov, Phys.Status Solidi (a) 60(1980)309.

13.T.Toyoda,H.Nakanishi,S.Endo and T.Irie, J.Phys.D:Appl.Phys. 18(1985) 747.

14.L.Tarricone and P.P.Lottici, Ternary and Multinary Compounds (Materials Research Society, U.S.A., 1987) p.301.

15.T.Irie,S.Endo,S.Nomura,K.Igarashi and T.Toyoda, Ternary and Multinary Compounds (Materials Research Society, U.S.A.,1987) p.537.

16.H.Nakanishi, Japan.J.Appl.Phys. 19(1980)103.

17.S.H.Weple and M.DiDomenico,Jr,,Phys.Rev.B 3(1971)1338.

18.S.H.Wemple, J.Chem.Phys.67(1977)2151.

APPLICATION OF $AgGaSe_2$ FILTER TO EASY RAMAN SPECTROSCOPY

N. Yamamoto, H. Horinaka and H. Mineguchi
College of Engineering, University of
Osaka Prefecture, Mozu, Sakai, Osaka 591, JAPAN

An unique $AgGaSe_2$ band elimination filter is utilized for Raman scattering spectroscopy to suppress the Rayleigh scattering. Combined with AlGaAs diode laser as an exciter, a new easy Raman scattering measurement is achieved.

The importance of Raman scattering spectroscopy is recently expanding to many fields as a superior means of material characterization. A standard apparatus of Raman spectroscopy consists of a high output (typically 100 mW or more) Ar^+ ion laser, a double monochromator (with a stray light level less than 10^{-10}), and a suitable computerized light detection system. This type of system is well operated but still expensive and occupy rather a wide space. Therefore, development of an inexpensive and compact desktop apparatus of Raman spectroscopy is expected, especially for personal or field use.

In this work, a new type of easy Raman spectroscopy apparatus is constructed using a single mode AlGaAs diode laser and a unique optical band elimination filter (OBEF) made of $AgGaSe_2$ crystal /1/. An example of simultaneous measurement of both Stokes and anti-Stokes Raman scattering spectra of the sample, CCl_4 are demonstrated.

First approach to design a compact system is to substitute a single mode diode laser for Ar^+ laser as a Raman exciter. Commercially available AlGaAs diode laser can cover a wide range of wavelength from 780 nm to 830 nm. Among these, an 810 nm laser of 40 mW single mode, developed for YAG excitation, was selected in this work. The laser output was controlled by current controller with a slow start circuit to stabilize the output light intensity. Because a precise single mode wavelength varies with temperature the selection of single mode wavelength could be made by

controlling temperature using Peltier element and Pt resistance wire temperature senser. Precise temperature tuning, without changing the light output, of single mode wavelength between 805 nm and 815 nm, could be easily achieved. The assembly of laser diode Raman exciter, thus constructed, is less expensive and occupy much less space than a usual Ar^+ laser exciter.

The second approach to small and easy Raman spectroscopy system is to replace a double monochromator by a simple single monochromator. In order to realize this, however, an effective OBEF to suppress the Rayleigh scattering light should be necessary to minimize the stray light level. As such OBEF, up to now, the iodine filter /2/, the crystalline colloidal filter /3/ and the J- filter /4/ were suggested and utilized. As an alternative, a unique $AgGaSe_2$ crystal OBEF, which is constructed by two parallelly arranged Glan-Thompson prism polarizers and a single crystal plate of (100) $AgGaSe_2$ of 0.763 mm in thickness, was recently developed by the Authors /1/. $AgGaSe_2$ crystal OBEF, which was first suggested as an optical band pass filter (OBPF) /5,6/, can act, here, as OBEF by only just changing from the crossed Nicols mode to the parallel Nicols mode of the arrangement of two Glan-Thompson prisms. This OBEF acts near 811 nm at room temperature /7/.

A typical optical transmission characteristic of the $AgGaSe_2$ crystal OBEF is shown (Fig. 1). The short wavelength cut off near 700 nm is, of course, due to the direct band edge absorption (E_g) of semiconducting material of $AgGaSe_2$ and transmission range of longer wavelength expands over 17 um for this crystal (although not shown in the figure). As can be seen from the figure, a good band elimination ratio over 100 can be easily achieved at near 811 nm. If necessary, two cascade combination of this filter can achieved an elimination ratio over 5×10^3 /8/. Thus, a combination of $AgGaSe_2$ crystal OBEF and a standard single monochromator can replace a double monochromator.

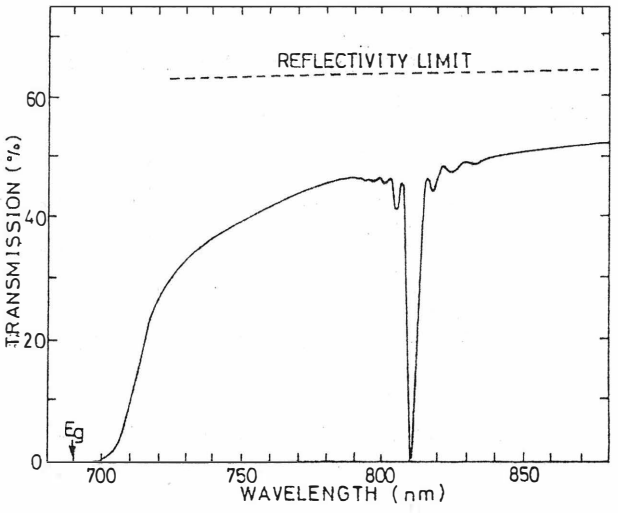

Fig.1 Transmission spectrum of $AgGaSe_2$ crystal OBEF

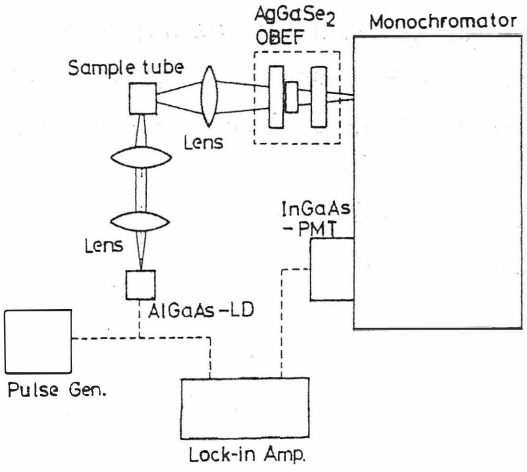

Fig.2 A compact Raman measurement system

Using the diode laser exciter and $AgGaSe_2$ crystal OBEF just described, a small desktop Raman spectrometer was constructed (Fig. 2). A 40 mW single mode laser beam of 811 nm is focused to CCl_4 sample in a quartz cell from the bottom side. A step form pulse drive of laser current was used for convenience of the measurement with a lock-in amplifier detection. Scattering light from the sample was collected by a lens and passed through the $AgGaSe_2$ crystal OBEF. Single monochromator (Jasco, CT-50) loaded with an InGaAs photocathode photomultiplier (Hamamatsu, R-2658) was used.

Typical Raman scattering spectra of CCl_4 were measured by this system by a single scan (continuously both Stokes and anti-Stokes Raman scattering peaks) (Fig.3). The Rayleigh scattering light is suppressed to a comparable order of Raman scattering spectra.

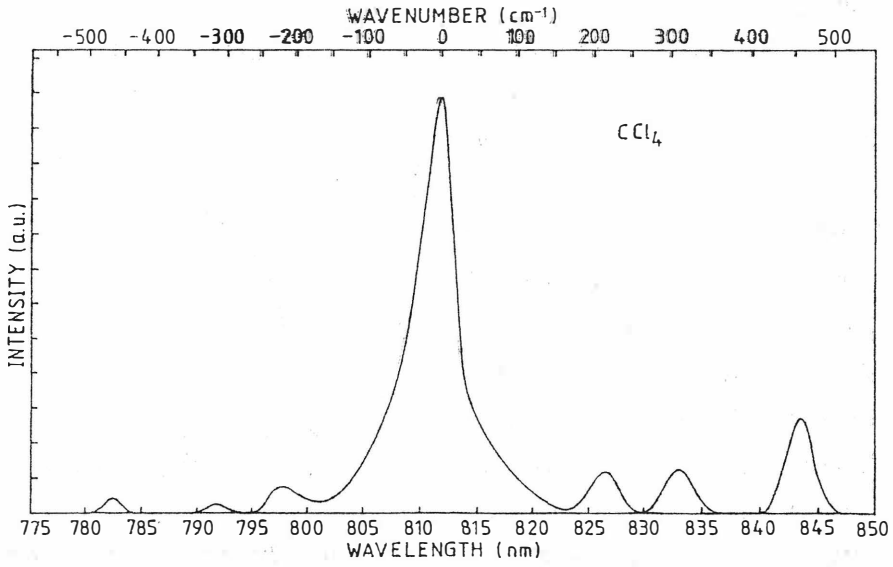

Fig.3 An example of Raman spectra including both Stokes and anti-Stokes scattering peaks of CCl_4

An additional advantage of this system, which uses single monochromator, is a possibility of loading optical multichannel

analyser (OMA). Although the result with a single scan is satisfactory, however, a use of optical multichannel analyser (OMA) with a fast multi-scan detection system would speed up the measurement and diminish a noise level. Throughout this work, a period of simple, inexpensive, high speed desktop Raman spectrometer system is just opened.

REFERENCES

1. H. Horinaka and N. Yamamoto, in: Proceedings of the 15th Congress of International Commission for Optics (ICO-15), (Aug., 1990), p. 592.
2. G. E. Devlin, J. L. Davis, L. Chase and S. Geshwind, Appl. Phys. Lett. 19 (1971) 138.
3. P. L. Flaugh, S. E. O'Donnel and S. A. Asher, Appl. Spectrosc. 38 (1984) 847.
4. H. Hamaguchi and K. Kumagawa, Appl. Spectrosc. 40 (1986) 564.
5. H. Horinaka, H. Sonomura and T. Miyauchi, Jpn. J. Appl. Phys. 24 (1985) 463.
6. T. Yamamoto, H. Takehara, H. Horinaka and T. Miyauchi, Jpn. J. Appl. Phys. 25 (1986) 1397.
7. H. Horinaka, T. Okudo and N. Yamamoto, Jpn. J. Appl. Phys. 28 (1989) 1328.
8. Our recent data of $AgGaSe_2$ OBEF (to be submitted).

CHARACTERIZATION OF $CuInSe_2$ THIN FILMS PREPARED BY ICB(IONIZED CLUSTER BEAM) TECHNIQUE

Katsuaki Sato, Seisuke Matsuda, Yuki Kudo
Faculty of Technology, Tokyo University of Agriculture and Technology, Koganei, Tokyo 184, Japan

Thin films of $CuInSe_2$ were prepared by ionized cluster beam (ICB) deposition technique on glass substrates with simultaneous deposition of Cu, Se and In clusters, of which only In was ionized and accelerated. It was found both the resistivity and the In/Cu ratio can be controlled by changing the acceleration voltage.

1. INTRODUCTION

The chalcopyrite-type semiconductor copper-indium-diselenide ($CuInSe_2$) has been attracting considerable attention for thin-film solar sell application, due to its direct energy gap around 1.0 eV and an absorption coefficient which is the highest reported to date for any semiconductors/1/. Various preparation techniques of $CuInSe_2$ films have been reported; e.g. the single-source or the two-source vacuum evaporation, the sputtering, the electrodeposition, and the selenization. Recently, a conversion efficiency of over 14 % was achieved with $CuInSe_2$ single junction solar sells/2/. The electrical properties of $CuInSe_2$ is strongly dependent on the film composition, especially on the In/Cu ratio as shown in Fig. 1, which has been obtained in our system without ionization and acceleration. The control of the In/Cu ration in this experiment has been attained by changing the source temperature of In. However, since the accurate control the In/Cu ratio by the temperature is rather difficult, an alternative method for the composition control has been required. We, then, sought a possibility of the control by the ICB(ionized cluster beam) technique, which has been known to provide an excellent controllability of film composition.

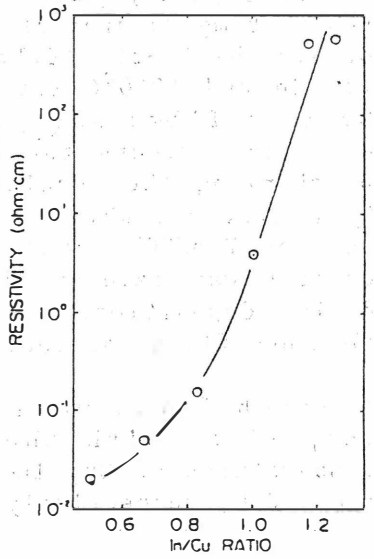

Fig. 1 Resistivity vs. In/Cu ratio curve measured by changing the source temperature

The ionized cluster beam (ICB) technique/3,4/ is an ion assisted film deposition method for forming high quality thin films by utilizing the effects of ion beam bombardment and the influence of the charge of ionized particles. At first, the clusters which contain 500-2000 atoms loosely coupled together are produced by adiabatic expansion caused by ejection of the vaporized atoms through a small nozzle in the lid of the crucible. Next, they are ionized by an electron bombardment and are accelerated towards a substrate by the application of a negative acceleration voltage Va. (Fig. 2) When these clusters arrive at the substrate they break up and migrate on the substrate with a kinetic energy obtained by the acceleration. The attractive features of the ICB technique are described as follows: (1) When the clusters are broken up on their arrival at the

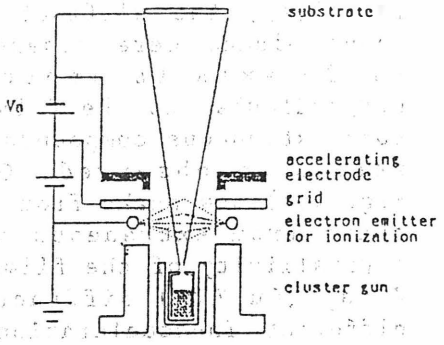

Fig. 2 Schematic diagram of an ICB gun used in our system

substrate, the incident momentum of the clusters is transformed into the surface diffusion energy. (2)The migration effect contributes to making good quality films at lower temperature of substrate. (3)By controlling the Va, it is possible to provide enough energy for surface diffusion,surface cleaning and improvement of adhesion.

2. PREPARATION

The $CuInSe_2$ films were prepared on the glass substrates by ICB deposition technique with one ionized cluster gun (for In source) and two evaporation sources(for Cu and Se) as shown schematically in Fig. 3.

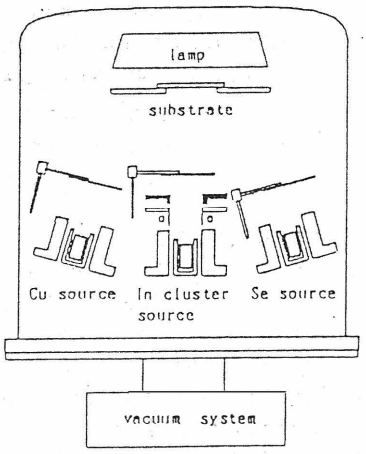

Fig. 3 Schematic diagram of the ICB deposition system

Source materials employed were Cu and Se of 99.999 % purity and In of 99.9999 % purity. The source temperatures of the three crucibles used to obtain the Cu-rich films are 1170°C for Cu, 260°C for Se and 1060°C for In. The deposition of the Cu-rich films was performed by keeping the electron currents for ionization I_e=100 mA and by changing the acceleration voltage of In V_a=0, 0.5, 1.0, 1.5 kV. The substrate temperature was kept at Ts=380°C, and the pressure in the vacuum chamber was maintained at less than $1*10^{-5}$ Torr during deposition. The typical thickness of the obtained films was approximately 5000 A.

In-rich films were also prepared for the comparison with the Cu-rich films. Source temperatures of Cu, In and Se were 1170°C, 1120°C and 260°C, respectively.

3. RESULT AND DISCUSSION

The X-ray (Cu Kα) diffraction patterns of Cu-rich $CuInSe_2$ films prepared under different In-acceleration voltages Va are shown in Fig. 4. In Fig. 4(a), the diffraction peaks from (112) and (336) planes were observed, suggesting that the <112> axis is preferentially oriented perpendicular to the film surface. The peaks from some extraneous compounds such as In_6Se_7 and Cu_2Se were also observed. On the other hand, in Fig. 4(c) new peaks from (220) or (204) and (116) or (312) were observed whereas the peaks from extraneous compounds were not observed. Thus it is found that the crystallinity of the films can be varied by changing the In-acceleration voltage. The X-ray (Cu Kα) diffraction patterns of In-rich $CuInSe_2$ films deposited under different In-acceleration voltages V_a are shown in Fig. 5. Figs. 5(a) and 5(b) represent the X-ray patters for films prepared without and with the acceleration voltage, respectively. Peaks (101) and (103) characteristic to the chalcopyrite phase were observed in both films, in addition to the peak from (112), (220) or (204), (116) or (312), (316) or (332) and (424) planes. Therefore, we observe no prominent effect of the acceleration voltage on the film crystallinity in In-rich films.

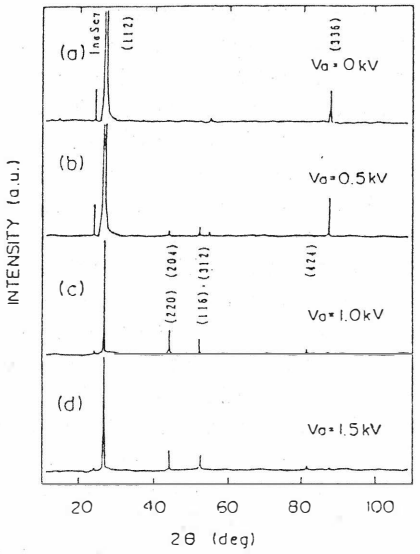

Fig. 4 The X-ray diffraction patterns in Cu-rich films

Morphologic l observations for the Cu-rich films were performed using an optical microscope and a scanning electron microscope(SEM). Increased number of bright spots with high reflectance in the films prepared with increased acceleration voltages were observed by the optical microscope studies. The quality of the films seems to be improved by increasing the acceleration voltage. The SEM observation manifests that the grain size of crystals in the films is about 0.5 μm, which becomes smaller by an application of acceleration voltage.

For In-rich films, the surface of the film prepared without acceleration voltage (V_a=0 kV) was flat and mirror-like. On the other hand, crater-like holes were observed on the surface of the film with V_a=1.0 kV. Such holes have often been observed in ICB films and have been considered to be caused by so-called spitting; the film surface is attacked by a lump of source material ejected from the hole at a burst. According to the compositional analysis by ICP (inductively coupled plasma) technique, the In/Cu ratio of the Cu-rich films increased from 0.80 for Va=0 kV to 0.99 for Va=1.0kV and was saturated to 0.99 with the increase in acceleration voltage of In as shown by a solid curve in Fig. 6. In the same figure the Se/metal(=Cu+In) ratio is also plotted by a dotted curve.

In addition, the dot-dashed curve in Fig. 6 represents the acceleration voltage dependence of the resistivity for Cu-rich films. The resistivity varied from $7.4*10^{-2}\,\Omega$ cm to $2.1\,\Omega$ cm corresponding to the change of acceleration voltage from zero to 1.5 kV. This result indicates that composition of the films reached at near stoichiometry by higher incorporation of In into the films. Though the resistivity curve seems not to agree with the analyzed In/Cu ratio curve, we can find a good correspondence between the two curves, if we take into account the fact that even the small variation in the In/Cu ratio causes a large change of resistivity amounting to several orders of magnitude at the nearly stoichiometric composition.

Figure 7 shows absorption spectra of both Cu-rich and In-rich films of $CuInSe_2$. Cu-rich films(solid curve) seem to have a considerably large absorption coefficient below the band gap. It may be due to the optical scattering by the rough surface of the Cu-rich films. The below-gap absorption coefficient was considerably reduced by

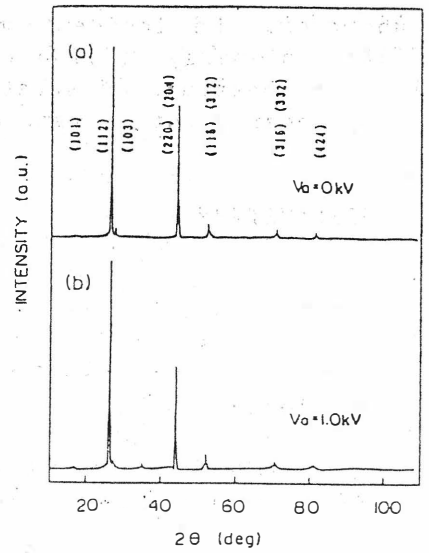

Fig. 5 The X-ray diffraction patterns in In-rich films

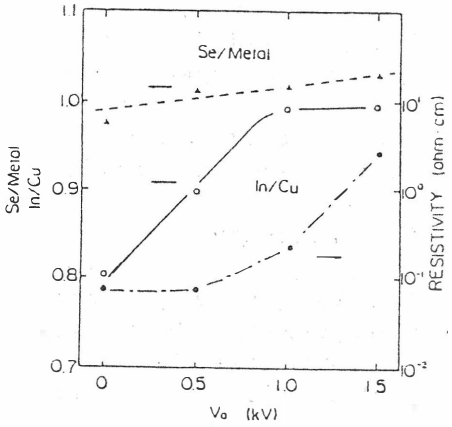

Fig. 6 Acceleration voltage dependence of In/Cu ratio (solid) and Se/Metal ratio (dotted) and resistivity (dot-dashed) for Cu-rich films

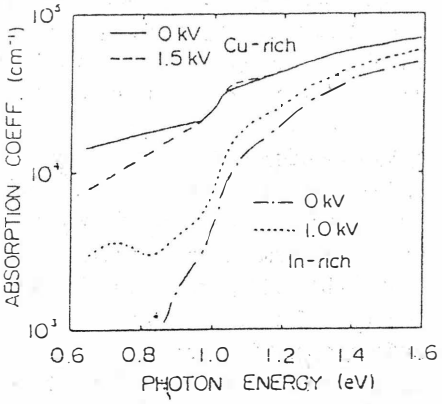

Fig. 7 Absorption spectra of Cu-rich and In-rich films with different acceleration voltages

increasing the acceleration voltage as shown by a dashed curve in Fig. 7. From the absorption spectrum the direct energy gap of the Cu-rich film was determined as 0.97 eV. No prominent shift of the energy gap by the acceleration was observed.

On the other hand, absorption spectra in In-rich high resistivity films show a well defined absorption edge and a small absorption coefficient for photon energies below the energy gap as shown by the dot-dashed curve in Fig. 7. However, the acceleration introduces additional absorption to the below-gap spectrum as shown by the dotted curve. It may be caused by the scattering due to the craters produced by spitting.

Figure 8 shows photoconductivity (PC) spectra of typical Cu-rich and In-rich films measured at room temperature. The rises of the photoconduction at the absorption edge in both films are steep. The photoresponse of the Cu-rich film decreases rapidly towards the higher energy region as described in ref. 5. The maximum of the PC is 1.05 eV and a shoulder-like structure is observed at 1.25 eV for the Cu-rich films. For the In-rich film, the photoresponse is approximately constant for energy region from 1 to 2 eV with two peaks at 1.07 eV and 1.27 eV. The photoconductivity in $CuInSe_2$ has been known to be proportional to n-th power of the light intensity. The exponent n in our films is determined to be about 0.9 for both Cu-rich and In-rich films.

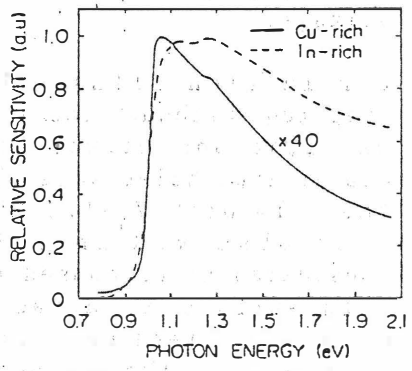

Fig. 8 Photoconductivity spectra in typical Cu-rich and In-rich films

4. Conclusion

The electrical, optical and crystallographic properties of thin $CuInSe_2$ films prepared by ICB technique were studied. Preparation of these films was made by simultaneous deposition of Cu, In and Se clusters. Films with the <112> axis preferentially oriented perpendicular to the surface were obtained. For Cu-rich films the composition ratio of In to Cu was able to be controlled by changing the acceleration voltage for the ionized cluster of In. Simultaneously, the resistivity was found to be varied by 2 orders of magnitude by the acceleration. The observation by an optical microscope revealed that the reflectivity increases with the acceleration. The below-gap absorption coefficient in the absorption spectrum was found to be considerably reduced by the acceleration, indicating the improvement of the film properties. On the other hand, the acceleration brought about a damaged surface for the In-rich high resistivity films. No improvement of the film properties were observed in the In-rich case.

Acknowledgment
This work has been partially supported by Hoso-Bunka Foundation. A support from the Sunshine Project from the Ministry of International Trade and Industry is also acknowledged. We express deep gratitude for Fuji Electric Corporate Research and Development Ltd. for compositional analysis by ICP technique.

References
1. Solar Cells **16** (1986)[Special issue for $CuInSe_2$].
2. K.Mitchell, C.Eberspacher, J.Ermer, D.Pier, Proc. 20th IEEE PVSC, (1989) p1384.
3. T Takagi, K.Matsubara, H.Takaoka and I.Yamada, Thin Solid Films **63**, 41 (1979).
4. T.Takagi, Thin Solid Films **92**, 1 (1982).
5. V.Ramanathan, T.Datta and R.Noufi, Appl. Phys. Lett. **51**, 746 (1987).

PROCEEDINGS

OF THE 8th INTERNATIONAL CONFERENCE

ON TERNARY AND MULTINARY COMPOUNDS

Kishinev, USSR, September 11-14, 1990

Vol.1. Diamond like semiconductors;
defect and layered compounds;
magnetic and semimagnetic
semiconductors

Edited by

S.I.RADAUTSAN and C.SCHWAB

Institute of Applied Physics

"Shtiintsa" Press

Kishinev 1990

Vol.2 High Temperature Superconductors;
Amorphous (noncrystalline)
Semiconductors; Multinary Solid Solutions

三元および多元化合物に関する研究会
代表幹事　入　江　泰　三
事 務 局　〒162 東京都新宿区神楽坂1-3
東京理科大学工学部電気工学科
入江・遠藤研究室
Tel.(03)260-4271　内3326・3397